ge of

Oceanic and Atmospheric Sciences

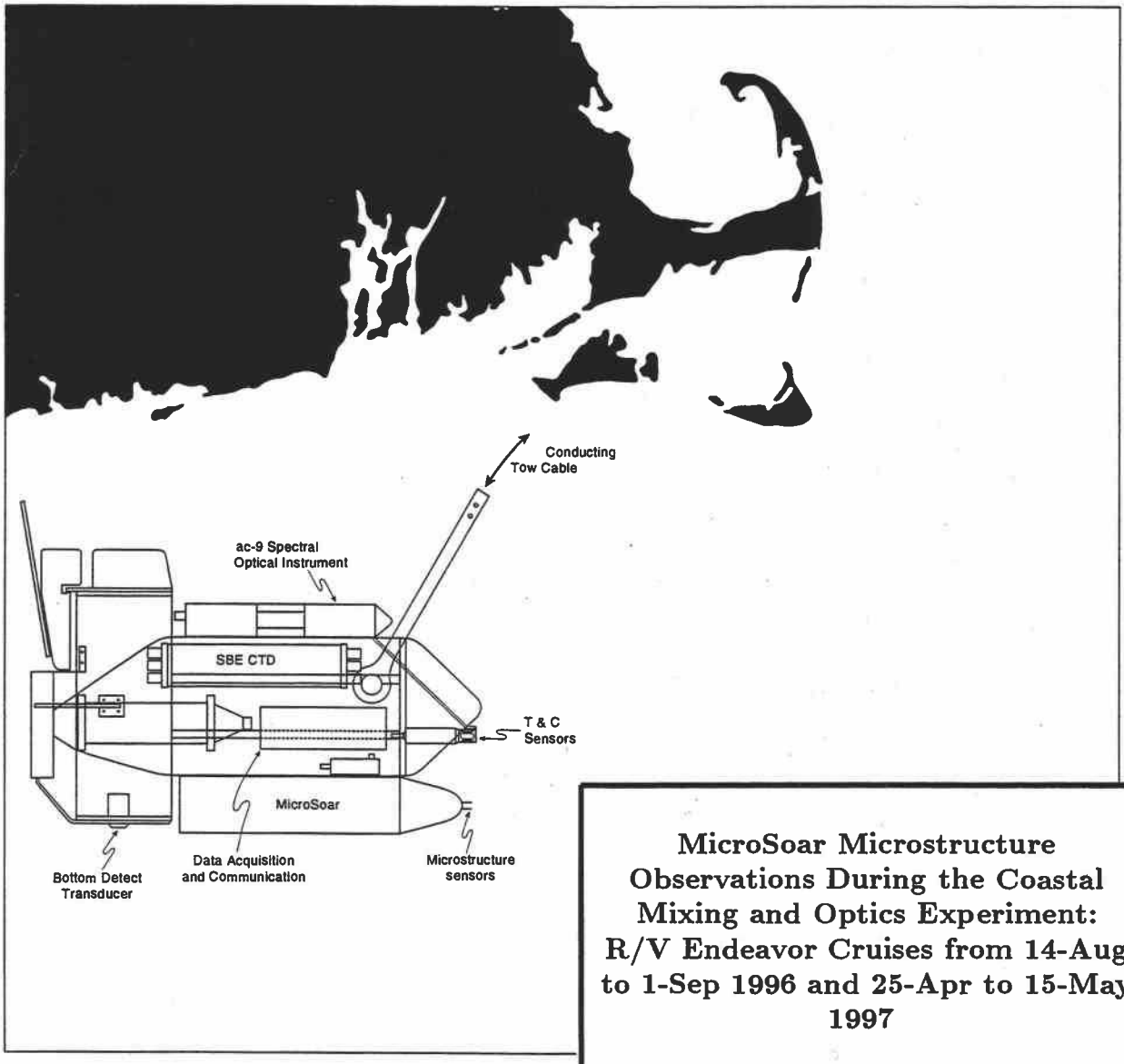

MicroSoar Microstructure Observations During the Coastal Mixing and Optics Experiment: R/V Endeavor Cruises from 14-Aug to 1-Sep 1996 and 25-Apr to 15-May 1997

by

A. Y. Erofeev, T. M. Dillon, J. A. Barth and G. H. May

College of Oceanic & Atmospheric Sciences
Oregon State University
Corvallis, OR 97331–5503

Data Report 170
Reference 98-3
September 1998

Oregon State University

MicroSoar Microstructure Observations During the Coastal Mixing and Optics Experiment

R/V Endeavor Cruises from 14-Aug to 1-Sep 1996 and from 25-Apr to 15-May 1997

A.Y. Erofeev, T.M. Dillon, J.A. Barth and G.H. May

Oregon State University
College of Oceanic and Atmospheric Sciences
104 Ocean Admin Bldg
Corvallis, OR 97331-5503

Data Report 170
Reference 98-3
October 1998

http://diana.oce.orst.edu/cmoweb/micro/main.html

College of Oceanic and Atmospheric Sciences
Oregon State University

Table of Contents

MicroSoar Microstructure Observations During the Coastal Mixing and Optics Experiment

R/V Endeavor Cruises from 14-Aug to 1-Sep 1996 and from 25-Apr to 15-May 1997

Introduction

Small-scale turbulence is a random phenomenon, and theoretical relationships about turbulent processes are often only crude approximations. There are relatively few accurate statements that can be made about a turbulent flow without recourse to experimental evidence from flow itself (Tennekes and Lumley, 1972). In the atmosphere, turbulent flows are relatively easy to observe. In the ocean, however, it is very difficult to directly visualize small-scale turbulence. Satellite remote sensing images allow visualizations of large scale turbulent motions, such as eddies and river plumes entering the ocean. Below the water's surface however, it is difficult and expensive to obtain information about the details of fluid motion. Wind speed at the water's surface has been used to estimate mixed-layer turbulence. This is because the mixing layer developed by wind stress is known to be a principle source of turbulent mixing in the waters above the thermocline. It is usually assumed that the energy available for mixing, and the dissipation, are both proportional to the cube of the wind speed (Dillon and Caldwell, 1980).

Often low resolution (on the order of one sample per meter) measurements of the vertical gradients of properties, such as temperature, salinity and density, are used to estimate the extent of the mixed layer. Brainerd and Gregg (1995) calculated mixing layers and mixed layers on data sets for which microstructure data were available. This allowed the depths estimated from the density difference and the density gradient methods to be compared with appropriate microstructure data. It appears the best way to find mixing layers is from measurements that resolve the turbulent overturns within the mixing layer (Brainerd and Gregg, 1995). Moum et al. (1989) measured diurnal turbulent kinetic energy dissipation rate fluctuations well below the depth of the mixed layer, as defined by density gradient criteria, near the equator.

Many investigators need to know more than how deep the mixing is occurring. They need to calculate vertical heat, momentum, chemical and biological fluxes through the water column.

Turbulence is the dominant contributing process for diapycnal transport of these water properties. Turbulent mixing events in the ocean are extremely intermittent, and basin-scale averages of transport are dominated by rare, energetic events. Samples of mixing must be intensively collected over large space and time scales to obtain a meaningful average.

SeaSoaring during The Coastal Mixing and Optics Experiment

Two physical oceanography cruises on the R/V Endeavor were conducted by the co-PIs Jack Barth and Mike Kosro as part of the ONR-sponsored Coastal Mixing and Optics (CMO) Accelerated Research Initiative. The objective was to rapidly survey a region around 40.5°N, 70.5°W where a set of moorings and a stationary vessel conducting profiling operations were located (Figure 1). The first cruise took place during a period of strong summer stratification (14 August to 01 September 1996); the second cruise was conducted in the following spring (25 April to 15 May 1997) as water over the shelf restratified after mixing by winter storms. The water column was sampled by towing the undulating vehicle SeaSoar from the surface to within 5-7 m of the bottom (Figure 2). The vehicle was equipped with a standard Seabird 9/11+ CTD sensor to measure conductivity, temperature, and depth; a nine-wavelength light absorption and attenuation meter (WETLabs ac-9); and a new microstructure instrument developed by OSU (MicroSoar) which measured conductivity and temperature at a very high frequency sampling rate using robust, fast-response probes (Figure 3). This report details the MicroSoar system and presents data collected with it during the CMO SeaSoar surveys.

The SeaSoar tows were concentrated in two areas: a small box pattern covering roughly 25 by 30 km centered on 40.5°N, 70.5°W (in 70 m of water on the mid-shelf) and with north-south lines separated by about 6 km; and a big box pattern covering roughly a 70 by 80 km area which included the small box region but extended out over the continental slope and with north-south lines separated by about 12 km (Figure 1). Each of these boxes was sampled repeatedly during both the summer and spring surveys. Maps and sections of hydrographic properties, water velocity (from a shipboard Acoustic Doppler Current Profiler) and optical properties were thus obtained over the continental shelf and slope. Between SeaSoar tows, CTD/rosette casts were

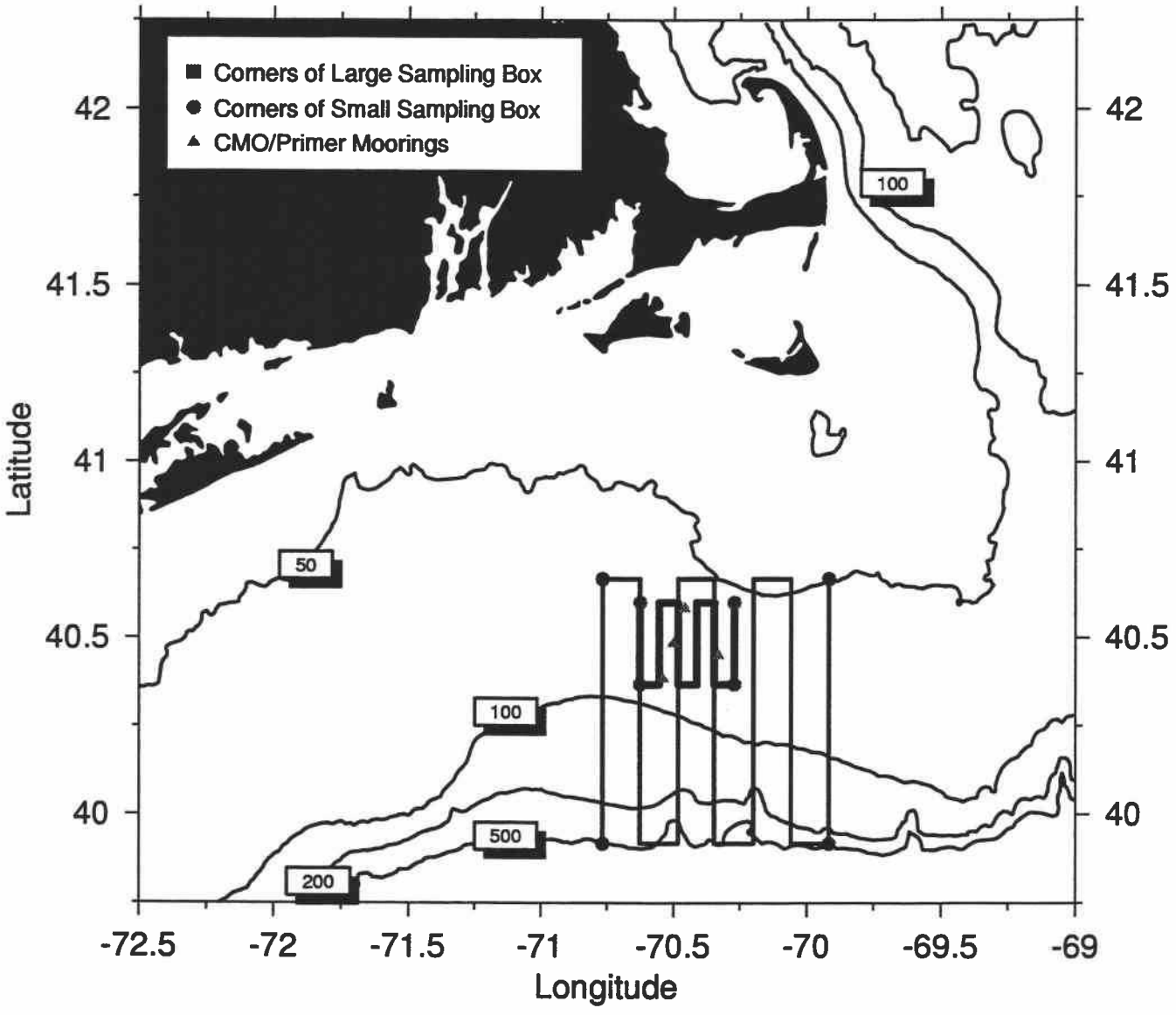

Figure 5. Map of the Coastal Mixing and Optics study, Region in the Mid-Atlantic Bight south of Cape Cod, Massachusetts. Bottom topography in meters.

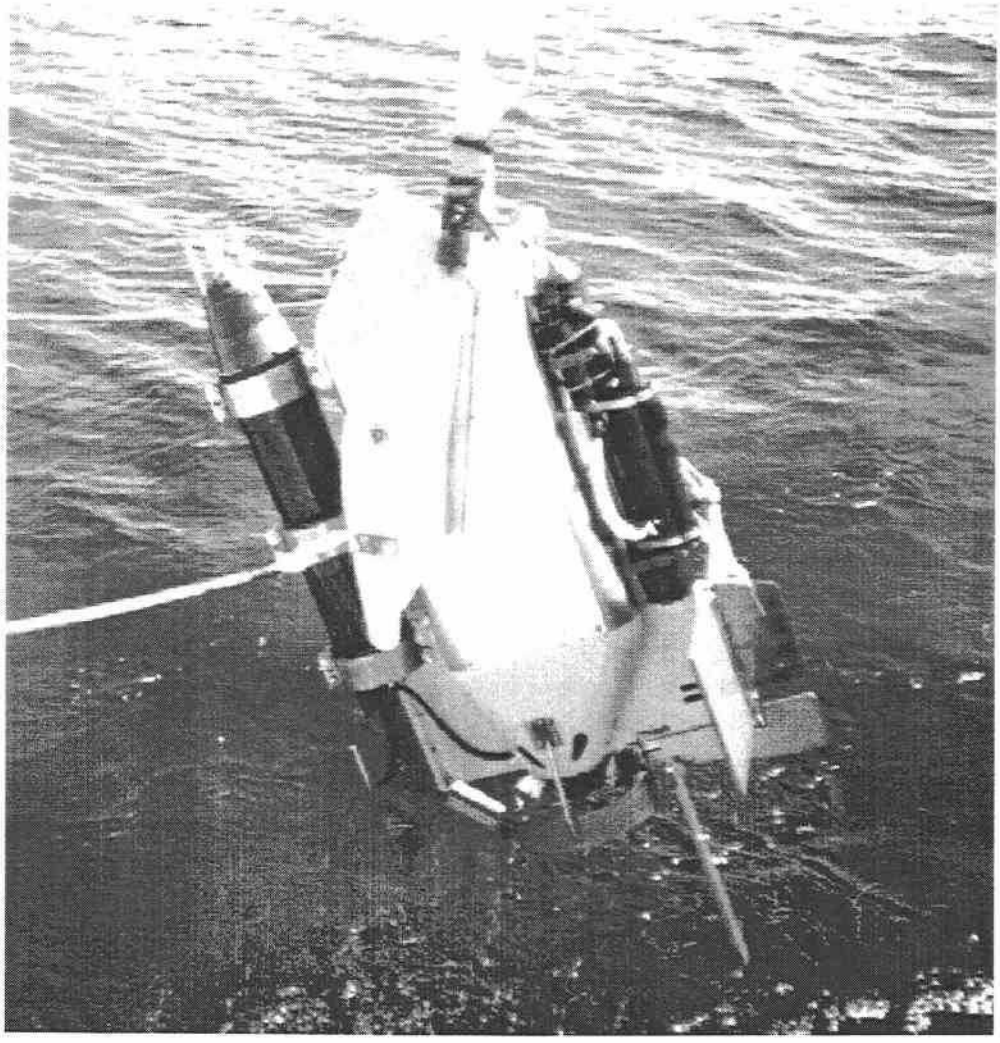

Figure 2. MicroSoar mounted underneath of SeaSoar

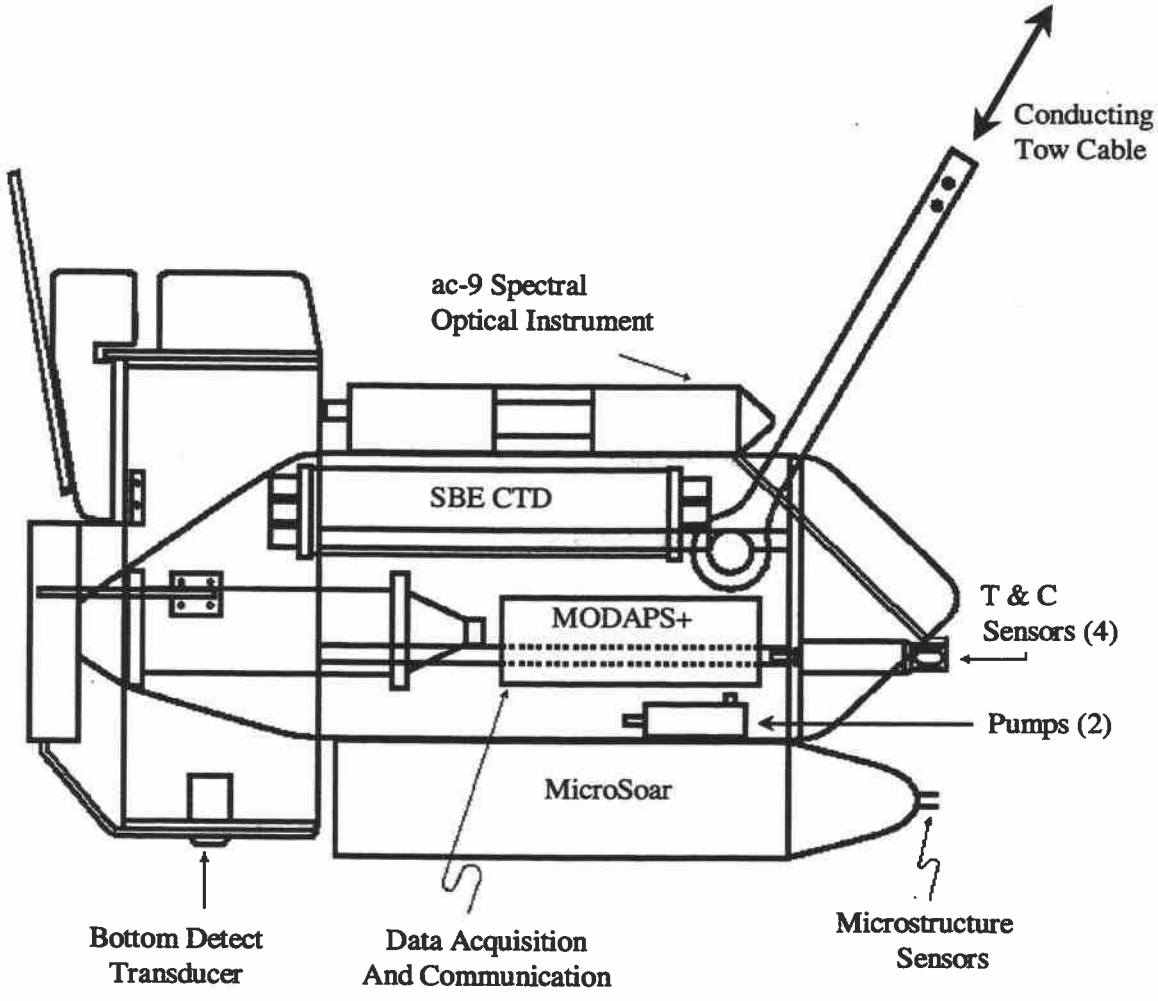

Figure 3. The SeaSoar vehicle equipped with a Seabird (SBE) 911+ CTD with its pressure case mounted inside the vehicle and dual temperature/conductivity (T/C) sensors mounted pointing forward through SeaSoar's nose. Dual SBE pumps mounted inside the vehicle ensured a steady flow past the T/C sensors. A nine-wavelength light absorption and attenuation instrument, ac-9 (WETLabs, Inc., Philomath, Oregon), was mounted on top of SeaSoar in a rigid saddle and with a streamlined nose cone to minimize drag.

also made. Underway surface temperature, salinity, and meteorological measurements were made continuously.

Along with SeaSoar profiling, the measurement of subsurface velocities using a shipboard acoustic Doppler current profiler (ADCP) was a primary activity during the R/V Endeavor CMO cruises. To achieve higher vertical resolution, Endeavor's standard 150-kHz ADCP transducer was replaced with a 300-kHz transducer from Oregon State University (OSU).Currents were measured with a resolution of every 4-m in the vertical, as compared with the 8-m bins available from the 150-kHz unit. For a full report on the ADCP data collected onboard Endeavor during the two CMO SeaSoar/ADCP cruises see Pierce et al. (1998) and *http://diana.oce.orst.edu/cmoweb/adcp/main.html.*

During the two R/V Endeavor CMO cruises, 24 days of continuous SeaSoar profiling were conducted. This resulted in approximately 34,900 vertical profiles of the water column over the continental shelf and slope.For details of the SeaSoar data acquisition system, SeaSoar CTD data calibration and processing techniques, and cross-shelf vertical sections and horizontal maps of temperature, salinity and density see O'Malley et al. (1998) and *http://diana.oce.orst.edu/cmoweb/csr/main.html.*

The SeaSoar vehicle was equipped with the pressure case of a Seabird Electronics (SBE) 9/11+ CTD mounted inside the vehicle with dual temperature and conductivity (T/C) sensors both mounted pointing forward through SeaSoar's nose (Figure 3, 4). Dual SBE pumps mounted inside the vehicle ensured a steady flow past the T/C sensors. The WETLabs ac-9 was mounted on top of SeaSoar in a rigid saddle and with a streamlined nose cone to minimize drag. For more details of the ac-9 installation, operation and data processing see Barth and Bogucki (1998); for the data report see Barth et al. (1998) and *http://diana.oce.orst.edu/cmoweb/ac9/main.html.*

The new microstructure instrument (MicroSoar) was carried on the bottom of the SeaSoar. Normally there is a streamlined lead weight in that location, so the MicroSoar pressure case had lead weights added in the form of a streamlined nose cone to match the weight it was replacing.

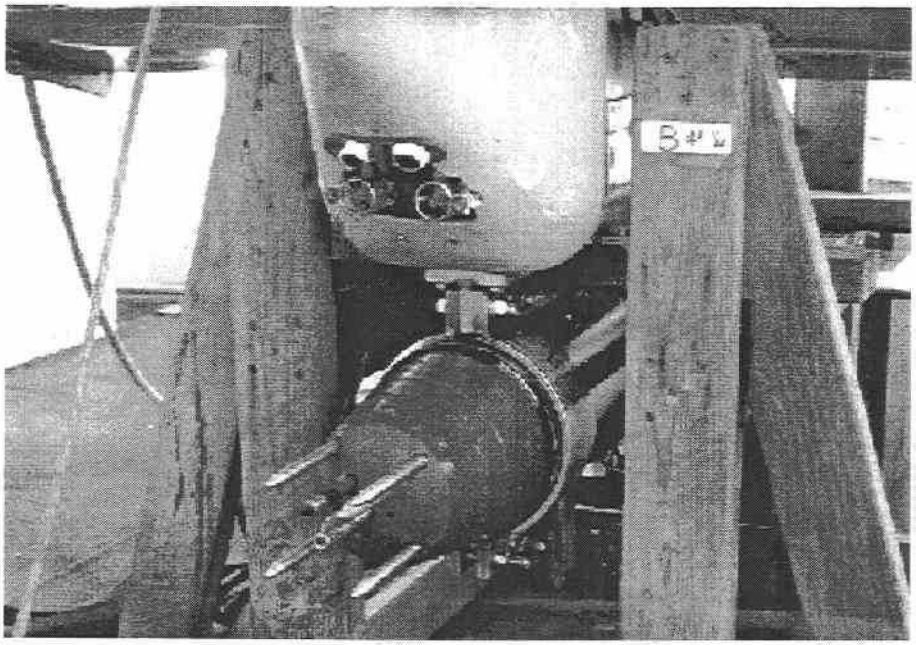

Figure 4. Closeup view of dual T/C sensors (middle), optical flow inlet and outlet (top), and microstructure sensors (bottom) on the front of SeaSoar

The MicroSoar is capable of either sending its entire data stream (~ 1 MByte per minute or 16 kBytes per second) topside or storing all the data internally on hard disks and just sending a subset of the data topside to monitor data quality. More details about the MicroSoar are contained in this report, in Dillon et al. (1998) and at *http://diana.oce.orst.edu/cmoweb/micro/main.html.*

During the CMO SeaSoar cruises, SeaSoar was towed using a bare (i.e., no streamlined fairing attached as required for deep tow profiling; see Barth et al., 1996), 5/16" armored, seven-conductor (plus ground) cable from a trawl winch aboard Endeavor. Flight characteristics were similar to previous experiments using bare-cable towing (e.g., Barth et al., 1996) with maximum depths reached of around 105 m. The vehicle profiled from the surface to 105 m and back in approximately 4 minutes at the deep ends of the north-south survey lines, and it took about 1.5 minutes to cycle down to 55 m and back at the shallow ends of the lines. The presence of the external instruments -- ac-9 on top, MicroSoar on bottom -- did not adversely impact the flight performance of the SeaSoar system in this bare cable configuration.

The SeaSoar vehicle was also equipped with an engineering package measuring wing angle, propeller rotation rate, pitch and roll. These sensors were connected to the analog-to-digital (A/D) channels of the SBE CTD. The propeller rotation rate sensor worked well throughout the cruise. The pitch and roll sensors returned good data for the majority of the cruise. The wing angle sensor was damaged almost immediately due to improper alignment of the coupling piece between the SeaSoar hydraulic unit and the wing angle potentiometer shaft. Even with perfect alignment, though, the wing angle sensor is not designed for the stresses in this environment, and a new design needs to be found. Lastly, a 200-kHz Datasonics echosounder was mounted on the lower tail fin of SeaSoar pointing down (Figure 3), to measure the distance between the vehicle and the bottom. Power to the altimeter was supplied on two of the tow cable's seven conductors, and data were returned via one of the CTD's A/D channels.

To supply power to each of the instruments onboard SeaSoar and to return a merged data stream, a prototype power supply and signal multiplexor unit was used during the August 1996 CMO SeaSoar/ADCP cruise. The Modular Ocean Data and Power System Plus (MODAPS+)

was manufactured by WETLabs, Inc., Philomath, Oregon, motivated by the need of Oregon State University scientists for a system capable of supplying more power and returning more data than possible with WETLabs' existing MODAPS (WETLabs, 1994). The MODAPS+ was installed inside the SeaSoar vehicle (Figure 3) and operated using 3 wires plus ground of the conducting tow cable. A topside power supply sent 300 volts down the cable where the subunit converted and parceled out power to the CTD, ac-9, ac-9 pump and to the MicroSoar. The data from each of these instruments was multiplexed and sent topside for storage as raw binary files on a PC. The signals were also split out by the MODAPS+ deckunit and sent to each instrument's data display computer. The CTD signal was passed through a WETLabs SBE deckunit emulator (a 286-based processor card) whose purpose was to turn the CTD signal communicated by MODAPS+ into that produced by a standard SBE 11 deckunit. The CTD data stream was then fed into data acquisition, display and flight control systems (O'Malley et al., 1998).The MicroSoar data was sent to a PC-based, LabWindows/CVI display system (see Section "The A/D Conversion and Data Acquisition Software").

For detailed cruise narratives of the two CMO SeaSoar cruises see O'Malley et al. (1998). The 14 August to 1 September 1996 cruise was R/V Endeavor EN-287, but we shall refer to it as E9608 to conform to our traditional way of naming cruises using the first letter of the ship's name, followed by the year and month. During the first part of E9608, power to and data from MicroSoar were routed through the MODAPS+. However, MODAPS+ was unable to maintain the bandwidth required to bring the full MicroSoar data stream to the surface. Therefore, data stored on MicroSoar's internal hard drives were transferred to topside computers via a direct connection while MicroSoar was on deck between tows.

At 2230 on 21 August (all times UTC), SeaSoar was recovered after the signal was lost from the MODAPS+. From late on 21 August through 22 August, a series of unsuccessful tests (on deck, in the lab, and eventually with the MODAPS+ subunit pressure case opened up) were conducted in an effort to fix the MODAPS+ data communication problem. At 2217 it was decided to remove the MODAPS+ power and communications module and to replace it with a solution based on a WETLabs MODAPS (WETLabs, 1994) which was brought along as a spare. Since the backup MODAPS was not capable of powering and communicating with

MicroSoar, the latter was reconfigured to accept 300 volts directly from topside by installing a power converter inside the MicroSoar pressure case to supply 15 volts to the instrument. A new RS-232 communications channel was also installed in the MicroSoar subunit to allow it to communicate via MODAPS (the previous MicroSoar-MODAPS+ communication was via ethernet). The CTD and ac-9 continued to run via MODAPS, and required three of the seven conducting wires plus ground; the SeaSoar control signals required two wires; and the remaining two conducting wires were being used to power the MicroSoar.

At 1240 on 24 August, SeaSoar with the new configuration based on the old MODAPS was deployed. It was found that stable CTD and ac-9 data were only obtainable with the MicroSoar turned off, presumably due to interference between the MODAPS communication lines and the MicroSoar power lines. Because of this, MicroSoar was not powered up from 1949 on 24 August to 1700 on 26 August (Small Box surveys SB4, SB5 and SB6). The next time SeaSoar was recovered and on deck, the MicroSoar was detached and moved to the lab. A capacitor was installed in the MicroSoar to isolate it from the MODAPS RS-485 communication lines and a successful deck test with stable CTD, ac-9 and MicroSoar data communication was performed. MicroSoar was reinstalled on SeaSoar and the vehicle was redeployed and reliable data from all onboard instruments was acquired.

In summary, during E9608 despite a number of instrumental challenges, a total of 11 days of SeaSoar towing were conducted yielding high-quality CTD, optical and microstructure data. Nine occupations of the small box grid, three of the big box grid, three repeats of the butterfly pattern and a day of soliton chasing were completed. The total number of water column profiles produced by SeaSoar was approximately 17,400.

The 25 April to 15 May 1997 cruise was R/V Endeavor EN-299 or E9704 using our cruise naming convention. The SeaSoar vehicle was equipped as in the August 1996 CMO cruise (E9608): SBE 9/11+ CTD; WETLabs ac-9; MicroSoar and a next-generation prototype single-channel fluorometer (WETLabs FlashPak). A major difference from E9608 was that the WETLabs MODAPS+ power and data communications module did not work when installed in SeaSoar and connected to the seven-conductor tow cable while dockside. Given that result, the

SeaSoar vehicle was loaded with the old WETLabs MODAPS as done during the second half of E9608.

After 10 days of successful SeaSoar towing, on Line 6 of SB8 the counterweight on SeaSoar's rudder fell off, which acts in concert with the rudder to keep the vehicle flying level and right-side-up. Upon recovery of the vehicle at 1945 on 7 May during rough seas, the MicroSoar microstructure probes were damaged necessitating replacement. SeaSoar with a repaired MicroSoar aboard was deployed at 0530 on 8 May and towed on the remainder of SB8.

In summary, during the Spring 1997 cruise (E9704) in excess of 13 days of continuous towing of the SeaSoar vehicle were conducted. This included 12 occupations of the small box centered around the CMO central site and 2 occupations of the big box which included sampling the shelfbreak frontal region out over the continental slope. The total number of water column profiles produced by SeaSoar was approximately 17,500. Overall, these were two very successful cruises and operation of SeaSoar in this region of considerable shipping and fishing activity could not have been accomplished without the superb efforts of the captain, mates and crew of the R/V Endeavor. In particular, the electronic charting of lobster fishing gear and the around-the-clock vigilance of the captain and mates made it possible to slalom along the survey grids.

MicroSoar on SeaSoar

MicroSoar to date has been used as a passenger instrument aboard the Oregon State University (OSU) SeaSoar towed profiling platform. MicroSoar mounts underneath, replacing the SeaSoar ballast weight, (Figure 2, 3). The SeaSoar "flies" through the water behind the towing vessel making a series of depth profiles of the water. When it approaches the surface, the wings are commanded to tilt, so that it dives rapidly. When it approaches the bottom, the wings are commanded to tilt, so that it climbs rapidly to the surface. The OSU SeaSoar is equipped with a Seabird 9/11+ CTD that samples dual temperature and conductivity sensors 24 times per second.

The CTD temperature and conductivity sensors are mounted pointing forward through a hole in SeaSoar's nose, considerably improving performance over a previous sideways-plumbed T/C configuration (Barth et al. 1996). The Seabird CTD onboard SeaSoar serves as a reference against which the low-frequency accuracy of the MicroSoar sensors can be calibrated.

MicroSoar functional description

MicroSoar is a general-purpose high-frequency computer-controlled measurement system. It uses a high performance PC/AT-compatible PC/104 100 MHz 486DX4 CPU CoreModule™ (CM/486, AMPRO Inc.™). Within just 14 square inches of space, the CM/486 includes the equivalent functions of a PC/AT motherboard and meets the demands of embedded systems, through its extreme compactness, low power consumption, +5V-only operation, wide operation temperature range and high reliability. The motherboard includes 8 Mbytes on board DRAM memory, a 16-bit expansion bus, and dual-serial and parallel controllers. It also has an enhanced embedded BIOS, Watchdog Timer and Socket for a bootable "Solid State Disk". The CM/486 is plugged into the application circuit board described in May (1997). Besides the motherboard, the Computer Electronic System (CES) includes PC/AT compatible disk drive interfaces (floppy controller and IDE hardware interface) supporting two hard disks, high resolution display controller, and an Ethernet NE2000 compatible LAN communication adapter. Two 16-bit, 8-channels 100 kHz fully differential analog to digital (A/D) converters (AIM-16, Analogic Inc.™), sampling at 2048 Hz per channel (higher or lower frequencies can be used, depending on the specifics of the experiment). Multiple modules in CES can be stacked together, or they can be mounted separately on the application circuit board. The CES also contains two Western Digital IDE hard drives with 2 GBytes each. The operating systems used were DOS-6.22 and Windows 3.11 for Work Groups™. The Intelligent Data Acquisition Software (IDAS) was developed at OSU to be executed in a DOS/Windows environment. The IDAS runs automatically after the CES has powered up and computer reboots. A typical operating mode for MicroSoar includes delivering digital data signals to the surface (at least one second averaged data for the visual analysis in real time), as well as recording all data on MicroSoar's hard disks. Windows is usually used for high speed transferring of data to the deck host computer, using the TCP/IP protocol and Ethernet interface. As a rule, it takes 2-3 days to fill

up the hard disks, depending on what sample rate is used. After that, SeaSoar and MicroSoar are pulled on deck, and MicroSoar is directly connected to the deck computer via an Ethernet twisted pair (10BaseT). The next step is downloading raw data to another storage medium, and then clearing MicroSoar's hard disks. The data transfer rate is approximately 27 Mbytes per second, and it takes usually 3 hours to move all data from the MicroSoar Submerged Computer to the Deck Unit hard disks. After that, MicroSoar is ready for next measurements.

MicroSoar sensors

MicroSoar's Analog Electronic System (AES) provides power conditioning, sensor excitation voltages, offset and gain calibration adjustments, buffering, filtering and signal routing of all analog signals. AES was configured to have 11 analog differential channels. Conductivity, conductivity derivative, and a reference ground signal, were sampled at 2048 per second. Temperature, temperature derivative, pressure, pressure derivative, three single axis accelerometers (axis X, axis Y and axis Z), and reference ground signal, are sampled 256 times per second by the second ADC board. The complete sample rate of all 11 channels is 8192 samples per second, corresponding to 131,072 bits per second. MicroSoar carries a capillary microconductivity probe, Figure 5 (Paka et al. 1998; May 1997); a temperature probe, built at OSU, utilizes a Thermometrics™ FastTip FP07 glass-coated bead thermistor. A stainless steel protective sleeve protects the thermistor probe tip during handling and deployment (see Figure 5). The pressure sensor is an Endevco™ model 8510B, 500 psig, piezoresistive pressure transducer with a sensitivity of .5 mv/psi. MicroSoar uses three IC Sensors™ model 3140-002 accelerometers, featuring approximately 1 volt/g output, with flat response up to 500 Hz, with a maximum of two gravities acceleration. MicroSoar's design details, and detailed information about the microconductivity sensor and analog and digit electronics, can be found in May (1997).

Structure of raw data

The length of one record of MicroSoar raw data is 16384 bytes (8192 samples) and is storred in a RAM double-buffer once each second. Raw data records are copied from a memory buffer to a hard disk file during the data acquisition process. Each record is supplemented by a header of 32 bytes, containing the start record label, PC time and date, record number, etc. (see Figure 6).

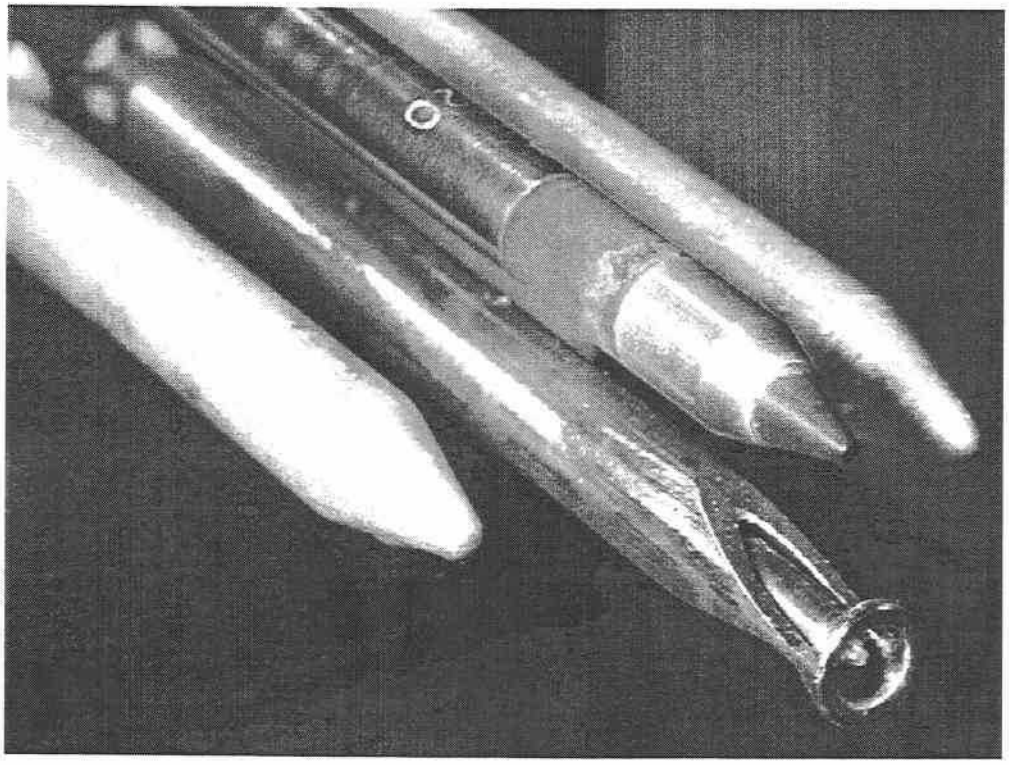

Figure 5. MicroSoar capillary microconductivity probe (top sensor); Temperature probe (bottom sensor), built at OSU, utilizes a Thermometrics™ FastTip FP07 glass-coated bead thermistor. A stainless steel protective sleeve protects the thermistor probe tip during handling and deployment

Each record in a raw data file consist of 256 scans and each scan contains $3_{channels}$ x 8_{times} = 24 samples of the fast channels, and 8 samples of the slow channels, with the sampling frequencies 2048Hz and 256Hz respectively.

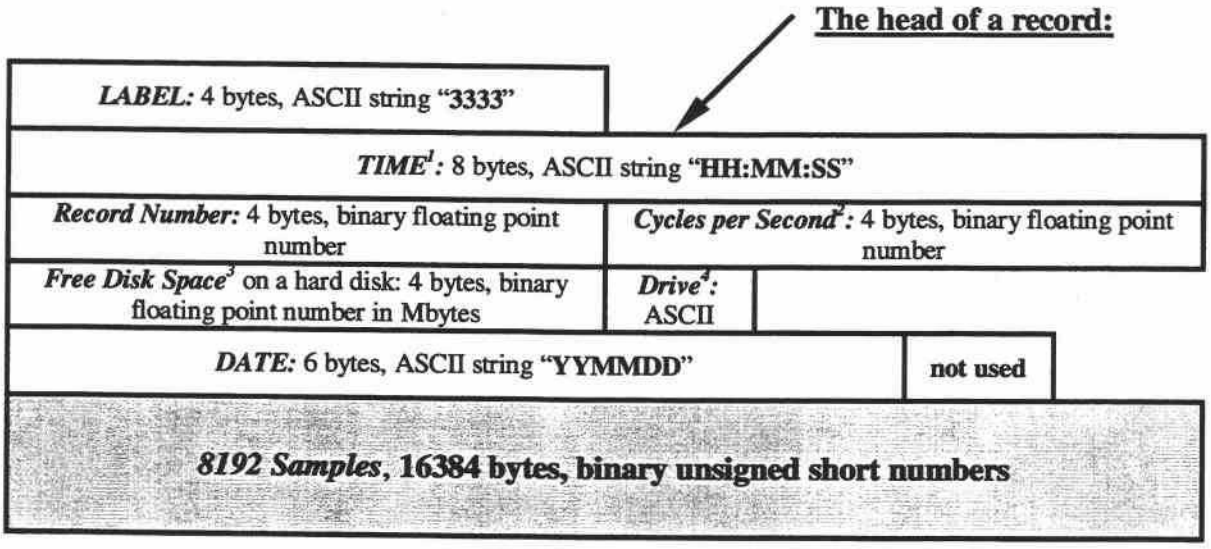

Figure 6. MicroSoar raw data record structure.

The sequence of MicroSoar channels in a scan is shown below.

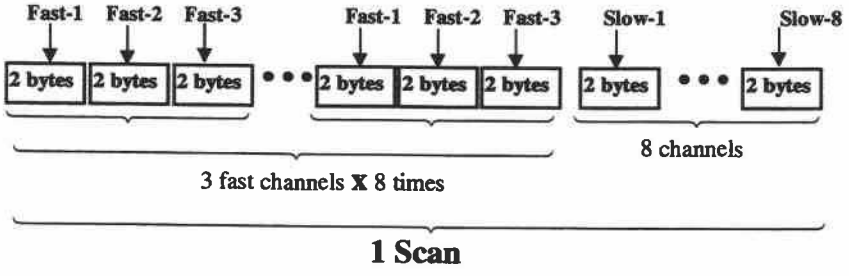

[1] Time when a record of 8192 samples is ready to be saved to a hard disk.
[2] Optional parameter is used to indicate indirectly how much time is available on MicroSoar computer for calculations during data acquisition process.
[3] How much disk space in Mbytes is available on current MicroSoar hard disk.
[4] Letter "C" or "D"

The A/D Conversion and Data Acquisition Software

The AIM16/12-1/104 A/D converters have 8 differential input channels with software programmable gains for each channel. The channel list consists of a starting channel code and an ending channel code. Data is stored in a 256x16 bit FIFO buffer and transferred to the host via programmed I/O or DMA. The converter sets a status bit "true" when the FIFO is half full.

The MicroSoar data acquisition software is based on an interrupt driven I/O routine. There are 3 modes of operation for reading data from an A/D converter. We used a procedure when the mode of operation which initiates a conversion each time that a trigger signal occurs, and a burst of conversions is taken. There are 3 functional regimes of the trigger, corresponding to an external timer, an internal timer, and a programmed register bit. The internal trigger timer counter is used in MicroSoar. In this mode, a 24 bit counter is pre-scaled with a 24 bit code and the counter is clocked by the on-board 10MHz clock. When a conversion trigger occurs, a burst of conversions takes place. A channel range is programmed in the A/D setup register and the trigger counter begins as soon as the GO bit is set true. A conversion burst begins at the start channel, and ends with the end channel Within such burst, conversions occur at a rate of 10^5 conversions per second.

MicroSoar can acquire data using up to 16 channels in differential mode, that is, 8 channels per each A/D converter. One of the A/D converters is used as a "master" board. It is programmed using an internal trigger timer counter. The second one is a "slave" board, and is programmed using a software trigger. The software trigger is set via a programmed I/O instruction; when triggered a burst of conversions occurs in the "slave" A/D converter. For example, if it is necessary to collect data from 11 channels (3 channels at the sample rate 2048Hz, and 8 channels at the slower rate 256Hz), we can use the master A/D converter for the faster channels, and the slave A/D converter for the slower channels. Schematically, the acquisition process is shown below:

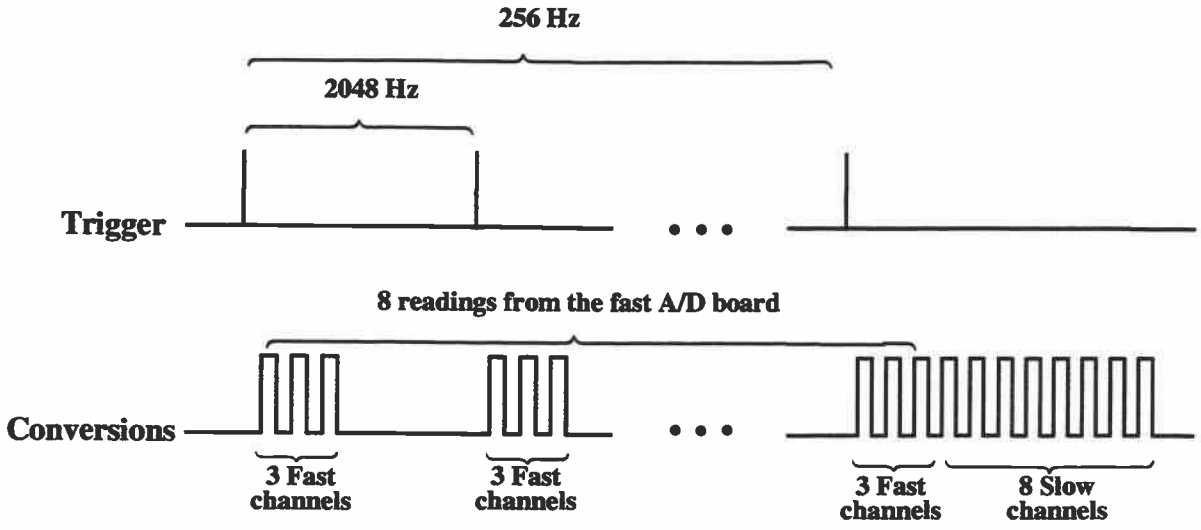

All data collected from both A/D boards are stored in a large memory FIFO buffer. When this buffer is half full, a "save to a hard disk" operation invoked by a background program. Every 5 minutes, the current raw data file is closed and new file is opened. This procedure was designed to insure that only small portion of raw data will be lost if some incidents, such as unplanned loss of power, occurs. If, for example, the MicroSoar computer "locks up", less than 5 minutes of data will be lost. This procedure also keeps raw data in sequentially stored 5 minutes data files, which is very convenient for calibrating MicroSoar's sensors.

The background software also includes the following procedures: 1) checking how many bytes are available on the hard disks; 2) one second data averaging; 3) sending the data to the Deck Unit computer via a standard RS232 interface for visual monitoring in real time. During measurements, the Deck Unit computer is used for a real time visualization of MicroSoar data. One second averaged data for 11 channels are shown on the screen simultaneously, in a strip chart display and are continuously scrolled in their windows from the right to the left (Figure 7). The following information is displayed on the screen: 1) Start time of measurements; 2) current time (GMT-time); 3) how many Mbytes have been already acquired by the MicroSoar submerged computer (MSC); 4) how many Mbytes are available on MSC. There is also an option to send complete sets of raw data to the Deck Unit Computer in real time. We used the PC/TCP OnNet Developer's Toolkit 3.1 software to develop DOS functions for transferring data using the TCP/IP communication protocol.

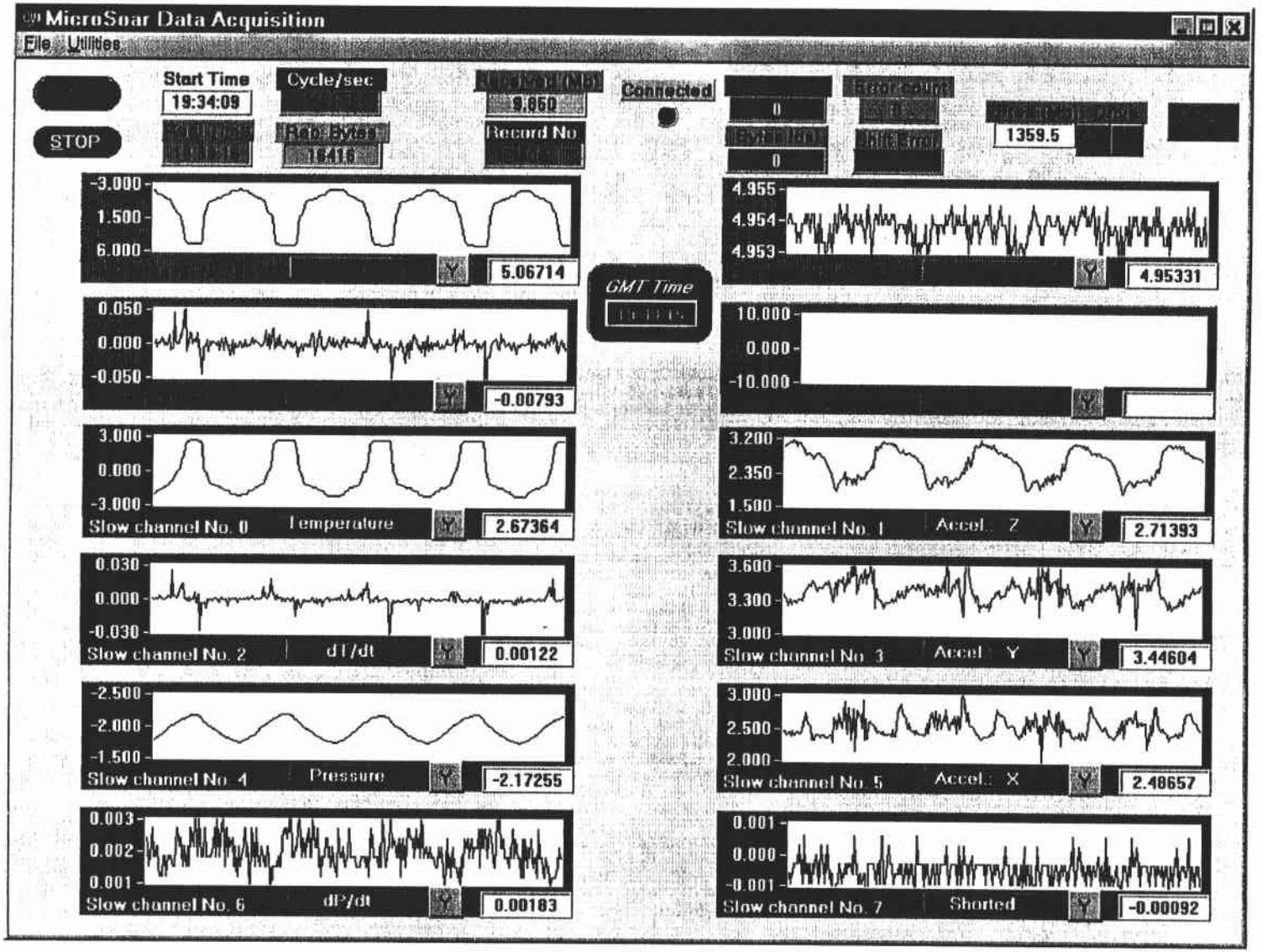

Figure 7. Realtime monitoring display for MicroSoar data showing one second averaged data

Comparison with calibrated Seabird CTD

As shown in Figure 8, SeaSoar is fitted with a Seabird 9/11 CTD, whose redundant sensors are factory calibrated. MicroSoar data can be compared at any time to these calibrated reference standards. Actual cruise data can be used to evaluate MicroSoar's performance compared to the Seabird CTDs. The Seabird temperature and conductivity sensors are designed to drift as little as possible over time. This stability is achieved at the expense of sampling speed and sensitivity, which is the goals of the microconductivity sensor design. To determine the amount of drift over time in the MicroSoar system, nine 5 minutes segments of data were selected over a 4 hour period. The CTD and MicroSoar data sets were averaged down to one second. Linear regression analysis were then performed for pressure, temperature and conductivity for each of nine 5 minute segments of data. All data sets have very good correlation. The results of linear fitting for MicroSoar and Seabird data is shown in Table 1.

Table 1. Calibration of MicroSoar sensors

File name	Time (GMT)	Linear Fitting		
		Pressure	Temperature	Conductivity
30.mcs	01:33 - 01:38	$108.3369 \times P_{volts} + 239.0149$	$2.0246 \times T_{volts} + 14.3412$	$0.1090 \times C_{volts} + 3.0297$
36.mcs	02:03 - 02:08	$108.2648 \times P_{volts} + 238.8326$	$2.0282 \times T_{volts} + 14.3552$	$0.1088 \times C_{volts} + 3.0302$
42.mcs	02:33 - 02:38	$108.1770 \times P_{volts} + 238.7387$	$2.0330 \times T_{volts} + 14.3701$	$0.1082 \times C_{volts} + 3.0321$
48.mcs	03:03 - 03:08	$108.3640 \times P_{volts} + 238.7440$	$2.0321 \times T_{volts} + 14.3725$	$0.1072 \times C_{volts} + 3.0362$
54.mcs	03:34 - 03:39	$108.0672 \times P_{volts} + 238.3823$	$2.0352 \times T_{volts} + 14.3852$	$0.1082 \times C_{volts} + 3.0326$
60.mcs	04:04 - 04:09	$108.1080 \times P_{volt} + 238.5025$	$2.0473 \times T_{volts} + 14.4257$	$0.1098 \times C_{volts} + 3.0260$
66.mcs	04:34 - 04:39	$108.0860 \times P_{volts} + 238.3773$	$2.0290 \times T_{volts} + 14.3544$	$0.1078 \times C_{volts} + 3.0340$
72.mcs	05:04 - 05:09	$108.2279 \times P_{volts} + 238.7929$	$2.0251 \times T_{volts} + 14.3504$	$0.1078 \times C_{volts} + 3.0351$
78.mcs	05:34 - 05:39	$108.1618 \times P_{volts} + 238.6329$	$2.0282 \times T_{volts} + 14.3523$	$0.1086 \times C_{volts} + 3.0311$
Summary		$\mathbf{(108.2 \pm 0.1) \times P_{volts} + (238.7 \pm 0.2)}$	$\mathbf{(2.03 \pm 0.01) \times T_{volts} + (14.37 \pm 0.03)}$	$\mathbf{(0.108 \pm 0.001) \times C_{volts} + (3.032 \pm 0.003)}$

These data were measured during a scientific cruise off the coast of Oregon in May 1996. The coefficients in the summary represent averaged calibration coefficients over period of almost 4 hours of measurements. Standard root mean square errors for the coefficients are also included.

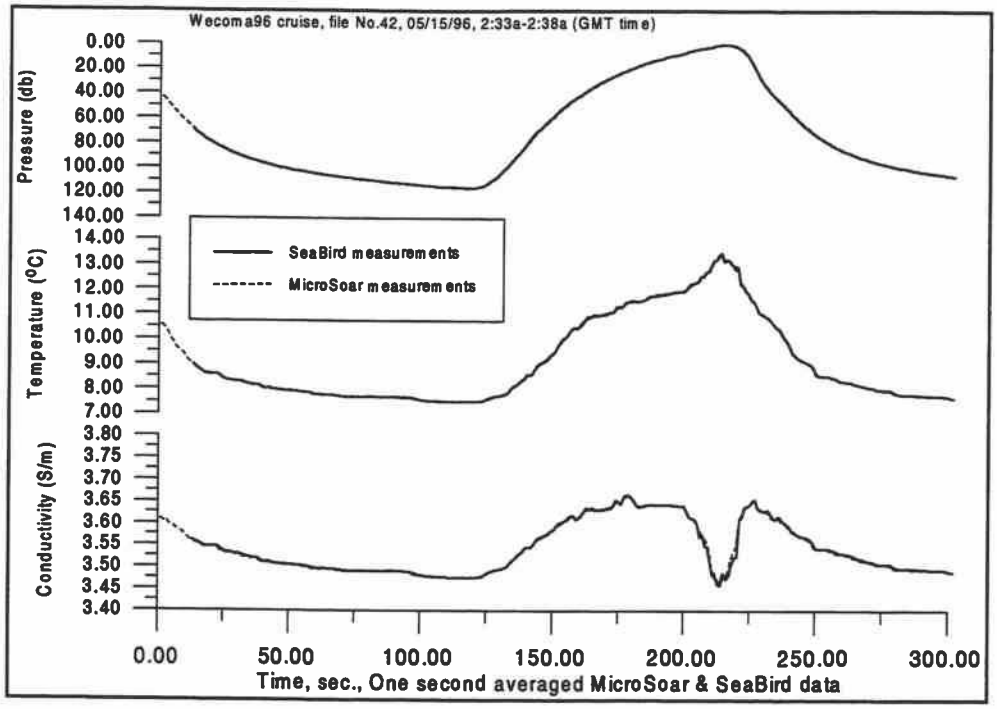

Figure 8. Comparison of MicroSoar and SeaBird CTD data. Note that the SeaBird traces (solid lines) almost always completely cover the MicroSoar data (dotted lines).

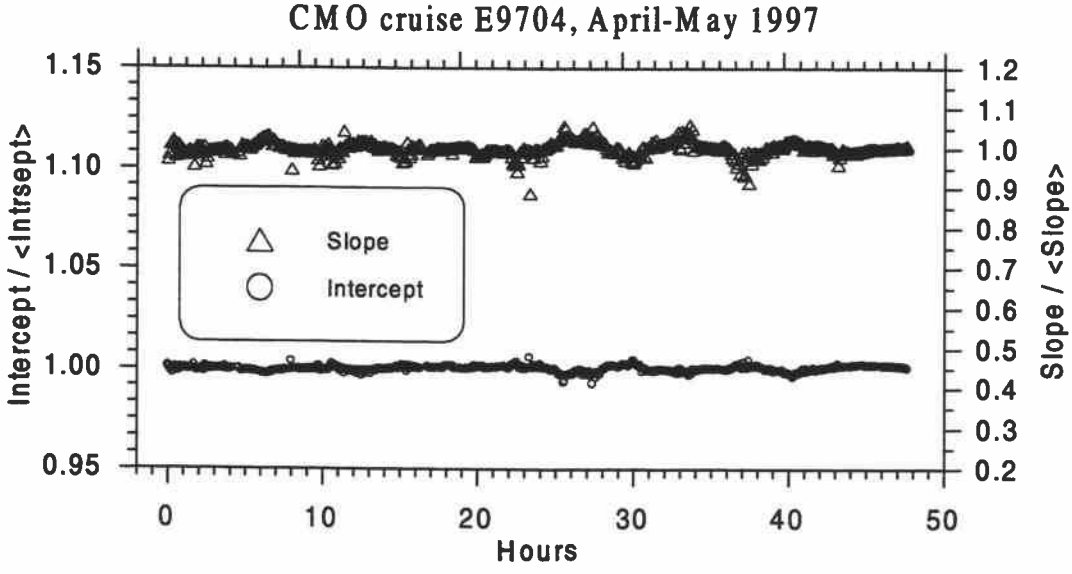

Figure 9. A time series analysis of calibration coefficients for MicroSoar microconductivity sensor

Figure 8 shows one of the 5 minutes segments of data used in the analysis above. Note that there are no significant drifts or offsets in the MicroSoar data when graphed using the calibration coefficients in Table 1.

Figure 9 shows a time series analysis of calibration coefficients for the MicroSoar microconductivity sensor for about 50 hours duration. Each point in the graph represents one pair of slope and intercept calculated for over sequential 5 minute time interval, and divided by their averaged values. Calibration of MicroSoar raw data is strait-forward, and is an automatic procedure. A time series analysis of calibration coefficients has been used for "outlier" detection for the MicroSoar microconductivity sensor. Considering the huge amount of MicroSoar raw data, this analysis is very helpful for detecting segments of raw data (if slope and/or intercept are outside of ±%5 interval) which are candidates for hand editing and calibration. Usually there are not many points outside of ±%5 interval, and mostly they are related to some intermittent problems with the MicroSoar analog electronics.

Analysis of instrument vibration using three-axis accelerometer data

It is important to insure that MicroSoar does not affect the deployment or flying characteristics of SeaSoar, and that vehicle motion is sufficiently small. "Sufficiently small" means that measurements of scalar properties, such as temperature or conductivity, are unaffected by SeaSoar vibrations. A three-axis accelerometer was used to estimate the displacement of MicroSoar in all three directions: Z-axis (straight forward), Y-axis (up and down) and X-axis (in horizontal plane).

An acceleration can be expressed as a sum of harmonics. A value of acceleration for each harmonic at a frequency ω can be estimated by the formula $\partial V / \partial t = A \cdot \sin(\omega \cdot t)$, where A is the amplitude, and $V = -A \cdot \omega^{-1} \cos(\omega \cdot t) \equiv \partial l / \partial t$. Displacement for the harmonic with the amplitude A and frequency ω can be defined as

$$d(\omega) = |l(\omega)| = A / \omega^2 . \qquad (1)$$

We estimated displacement at dominant frequency, ω_{peak}, of an acceleration power spectrum. Maximum displacement in the straight forward direction was Z_{max}= 0.06mm at the ω_{peak}=88Hz, maximum displacement in the up and down direction Y_{max}= 3mm at the ω_{peak}=22Hz, maximum

displacement in the left and right direction X_{max}=0.7mm at the ω_{peak}=20Hz. An estimation of displacement also can be calculated for a frequency range, giving an integrated estimation of displacements. If $S_A(\omega)$ is the FFT transformation of an acceleration *a*, then the variance of *a* is estimated as

$$\sigma_a^2 = \int_0^\infty S_a(f)df \,. \tag{2}$$

If the spectrum of acceleration is known, we can estimate the velocity variance as

$$\sigma_V^2 = \int_0^\infty \frac{S_a(f)}{f^2} df \,, \tag{3}$$

and the displacement variance as

$$\sigma_d^2 = \int_0^\infty \frac{S_a(f)}{f^4} df \,. \tag{4}$$

Data from MicroSoar's three-axis accelerometer, measured during CMO cruise in August 1996 (E9608), were used to examine the effect of SeaSoar vibration. MicroSoar was towed at 6 knots vessel speed in the depth range of 0-45 meters. The values of a root mean square displacement, rms_{d_x}, rms_{d_y} and rms_{d_z}, are shown on the Figure 10. The acceleration components were measured at a 256Hz sample rate, and each point on the figure is calculated using 256 raw data points (i.e., one second intervals). The *rms* of displacements on the Figure 10a, 10b, 10c and 10d were calculated for the frequency ranges 1 to 128Hz, 1 to 50Hz, 10 to 128Hz and 50 to 128Hz respectively. ($\pm 2\sigma$) for 1 second interval are shown in the Table 2.

Table 2. Estimation of vehicle displacements for different depth and frequency ranges

frequency range, (Hz)	1 to 128		1 to 50		10 to 128		50 to 128	
depth range, (m)	0 – 5	5 – 45	0 – 5	5 – 45	0 – 5	5 – 45	0 – 5	5 – 45
$2\sigma_x$, (mm) - lateral	21.6	7.4	21.6	7.4	0.12	0.16	0.007	0.03
$2\sigma_y$, (mm) - vertical	19.6	5.2	19.6	5.2	0.16	0.14	0.006	0.02
$2\sigma_z$, (mm) – forvard	42.0	24.0	41.4	23.0	0.12	0.1	0.004	0.014

The largest values of the displacements typically appear in the upper 5 meters depth range, and smaller values appear in 5-45 meters depth range. It is important that displacements, as well as

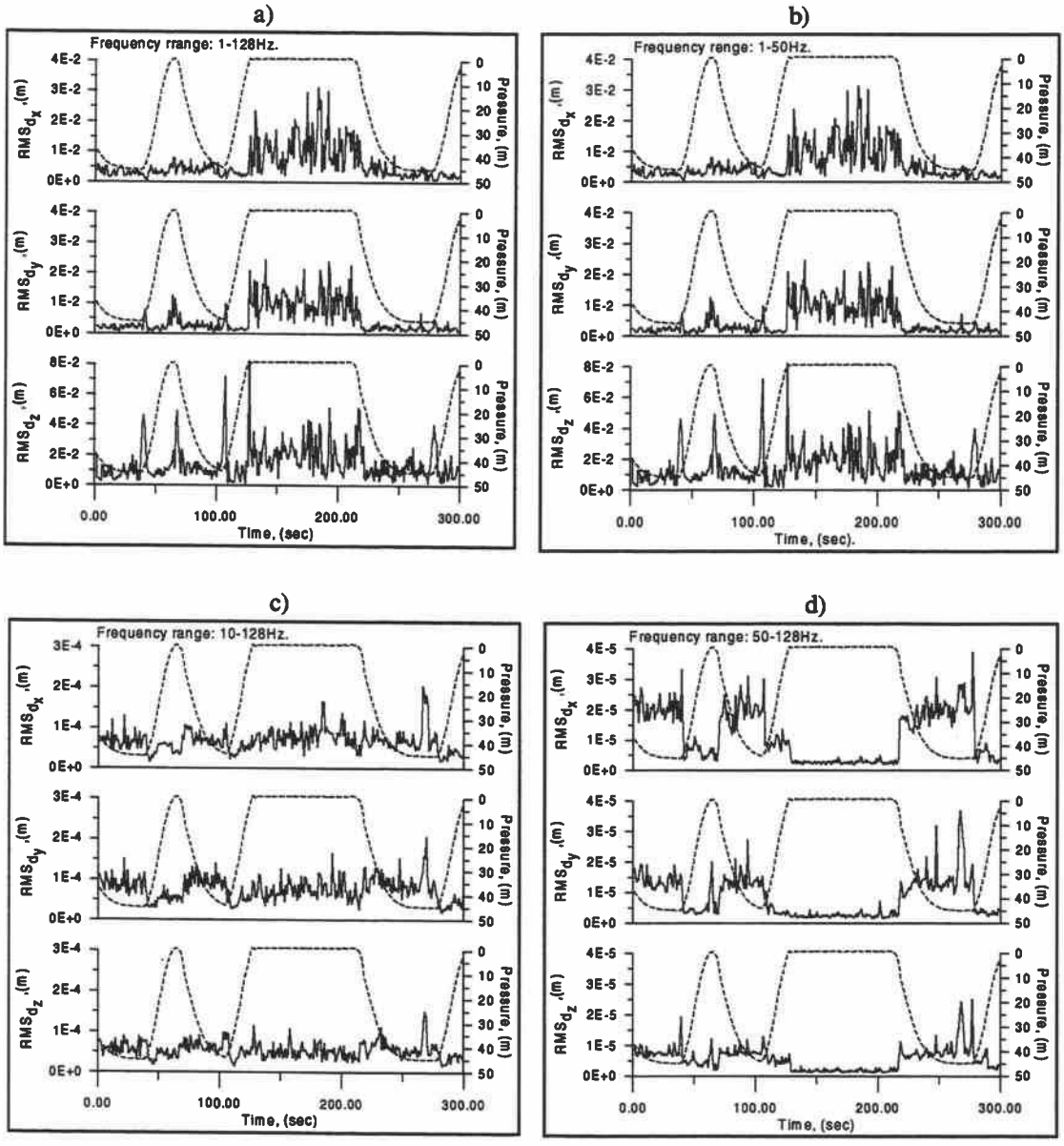

Figure 10. The *rms* of displacements calculated for the frequency ranges a) 1÷128Hz; b) 1÷50Hz; c) 10÷128Hz and d) 50÷128Hz.

vibration, have significant values only in the lower 1-10Hz frequency range, and negligible values in the 10-128Hz frequency range. Typical *rms* of displacements in the *X*, *Y* and *Z* directions have been calculated for the 10-128Hz frequency range. They are practically the same at every depth. The 2σ values in the range of 0.1-0.2mm are negligible and cannot be considered as a source of significant errors for MicroSoar small scale measurements.

Temperature variance dissipation rate calculation.

It is not easy to directly measure the flux of water properties across stratified boundaries in the ocean. In principal, if the velocity fluctuations and concentration gradient of the water property (e.g., heat, chemical composition, or density) can be precisely measured at the same point and time, the flux can be calculated. For instance, the heat flux F_H is given by $F_H=\rho C_p\langle u'_z T'\rangle$. Here , u'_z is vertical velocity fluctuations, $\langle u'_z T'\rangle$ is the correlation of u'_z and T', ρ is density and C_p is the specific heat. A problem with directly measuring a set of correlated data for u'_z and T' arises because the correlation is quite small. These measurements may include errors introduced by non-turbulent internal waves, imprecisely matched sensor response time, and movements of the measurement platform. It has proven more effective to infer fluxes from measurements of the turbulent kinetic energy dissipation rate, ε, or from the temperature variance dissipation rate, χ_T, both of which rely on the measurement of only one fluctuating quantity.

Cox Number, C_x. The Cox number, C_x, is a ratio of the variance in the temperature gradient fluctuations (a function of stirring due to turbulent mixing) to the mean temperature gradient, against which the turbulence was established. Higher Cox numbers indicate that turbulence is playing an increasingly important role in mixing the water column. The Cox number can be determined from vertical microstructure temperature measurements (Dillon and Caldwell 1980):

$$C_X = \frac{\overline{(\partial T'/\partial z)^2}}{\overline{\partial T/\partial z}^2} = \frac{\sigma^2_{T'}}{\overline{\partial T/\partial z}^2} \qquad (5)$$

Heat Flux F_H can be defined as

$$F_H = -\rho \cdot C_P \cdot D \cdot I_{SO} \cdot C_X \frac{\overline{\partial T}}{\partial z} = -\rho \cdot C_P \cdot D \cdot I_{SO} \frac{\sigma^2_{T_z}}{\overline{\partial T / \partial z}} \qquad (6)$$

where, typically, ρ = 1025 kg/m^3, C_p = 4000 J/(kg °C), D = 1.4 x 10^{-7} m^{2}s^{-1}, and I_{so} = 3. Numerically, in SI units,

$$F_H \approx \left[1.72 \cdot w \frac{m^{-2}}{^oC}\right] \frac{\sigma^2_{T'}}{\overline{\partial T / \partial z}} \qquad (7)$$

The Temperature Variance Dissipation Rate, χ_T, is

$$\chi_T = 2 \cdot D \cdot I_{SO} \cdot \sigma^2_{T'} = 2 \cdot D \cdot I_{SO} \overline{(\partial T' / \partial z)^2} = 2 \cdot D \cdot I_{SO} \cdot C_X \left(\overline{\partial T / \partial z}\right)^2 . \qquad (8)$$

Existing thermistor temperature sensors can resolve χ_T in the range of 1-20Hz, at best. A way to increase the frequency range is to use a micro conductivity sensor, which can resolve fluctuations up to 1000Hz or more. It is important to note that vertical profiles of small-scale fluctuations are not necessary, and that one-dimensional measurements in any arbitrary (say, $\vec{l}$) direction provide as much information, as long as the mean gradient is known. The temperature variance dissipation rate is given by

$$\chi_T = 6D\overline{(\partial T / \partial l)^2} = \frac{6D}{u^2}\overline{(\partial T / \partial l)^2} , \qquad (9)$$

where u is the instrument velocity.

Because temperature is well-known function of conductivity and salinity, we can write

$$dT = (\partial T / \partial C)_S \cdot dC + (\partial T / \partial S)_C \cdot dS = \alpha_{TC}(S) \cdot dC + \alpha_{TS}(C) \cdot dS , \qquad (10)$$

$$\partial T/\partial t = (\partial T/\partial C)_S \cdot \partial C/\partial t + (\partial T/\partial S)_C \cdot \partial S/\partial t\,. \tag{11}$$

We also assume that the local measured T-S relation, given by

$$\frac{\Delta S(\vec{x},t)}{\Delta T(\vec{x},t)} = \gamma_{ST}, \tag{12}$$

holds from meter scales to the smallest temperature fluctuation scales, and we can write

$$\partial T/\partial t = \alpha_{TC}(S)\cdot {}^{\partial C}\!/_{\partial t} + \alpha_{TS}(C)\cdot\gamma_{ST}\cdot {}^{\partial T}\!/_{\partial t}, \tag{13}$$

$$\frac{\partial T}{\partial t} = \frac{\alpha_{TC}(S)\cdot\left({}^{\partial C}\!/_{\partial t}\right)}{1-\alpha_{TS}(C)\cdot\gamma_{ST}} = \frac{\alpha_{TC}(S)\cdot b_C\cdot\left({}^{\partial V}\!/_{\partial t}\right)}{1-\alpha_{TS}(C)\cdot\gamma_{ST}}, \tag{14}$$

where b_C is the sensor sensitivity, and $\partial V/\partial t$ is the time derivative of voltage. The final result for the temperature variance dissipation rate is:

$$\chi_T = \frac{6D\alpha_{TS}^2\cdot b_C^2}{(1-\alpha_{TS}\cdot\gamma_{ST})^2 u^2}\overline{\left({}^{\partial V}\!/_{\partial t}\right)^2}\,. \tag{15}$$

The value of $\overline{(\partial V/\partial t)^2}$ of the variance of conductivity derivative, in voltage units, is estimated by integration of the power spectrum in a time/space domain. If $S_x(\omega)$ is the frequency domain spectrum, then

$$\sigma_X^2 = \int_0^\infty S_X(\omega)d\omega \tag{16}$$

and

$$\sigma^2_{dx'/dt} = \int_0^\infty \omega^2 S_X(\omega)d\omega\,, \tag{17}$$

where $\omega = 2\pi f$. Thus,

$$\overline{\left(\partial V/\partial t\right)^2} = \int_0^\infty \omega^2 S_v(\omega) = \int_0^\infty \omega \cdot f \cdot S_v(f) \cdot 2\pi \cdot df = \int_0^\infty (2\pi)^2 f^2 S_v(f) \cdot df \,. \quad (18)$$

The advantage of this method is that we can make a correction to the variance by excluding the noise spectral component from the conductivity derivative signal. Figure 11 shows the noise spectra of conductivity derivative as a dashed line. This model of the noise spectra is used for correcting $\overline{(\partial V/\partial t)^2}$. Instrumental velocity u, in formula (15) is calculated from approximation

$$u = \left[(dP/dt)^2 + u_{ship}^2 \right]^{\frac{1}{2}}. \quad (19)$$

If X is latitude and Y is longitude, ship velocity u_{ship} is defined as

$$u_{ship} = 111.7e3 \cdot \left[\left(\frac{\Delta X}{\Delta t} \right)^2 + \left(\frac{\Delta Y}{\Delta t} \frac{\pi X}{180} \right)^2 \right]^{0.5}. \quad (20)$$

Figure 12 shows a typical example of calculated instrument velocity and all components used for calculation.

The temperature variance dissipation rate cannot be calculated if $\alpha_{TS}\gamma_{ST} = 1$, and χ_T becomes less precise, whenever $\alpha_{TS}\gamma_{ST}$ is near unity. A "figure of merit" for the calculated χ_T can be defined as

$$M = \frac{1}{(1-\alpha_{TS}\gamma_{TS})^2}. \quad (21)$$

If M is very different from unity, we cannot trust our T-S approximation, because the spectrum may be dominated by salinity rather than by temperature fluctuations. Calculations of M for entire E9704 cruise give us next results:

Condition	% of Occurance
$0.1 \le M \le 10$	93%
$0.3 \le M \le 3$	83%
$0.5 \le M \le 2$	66%

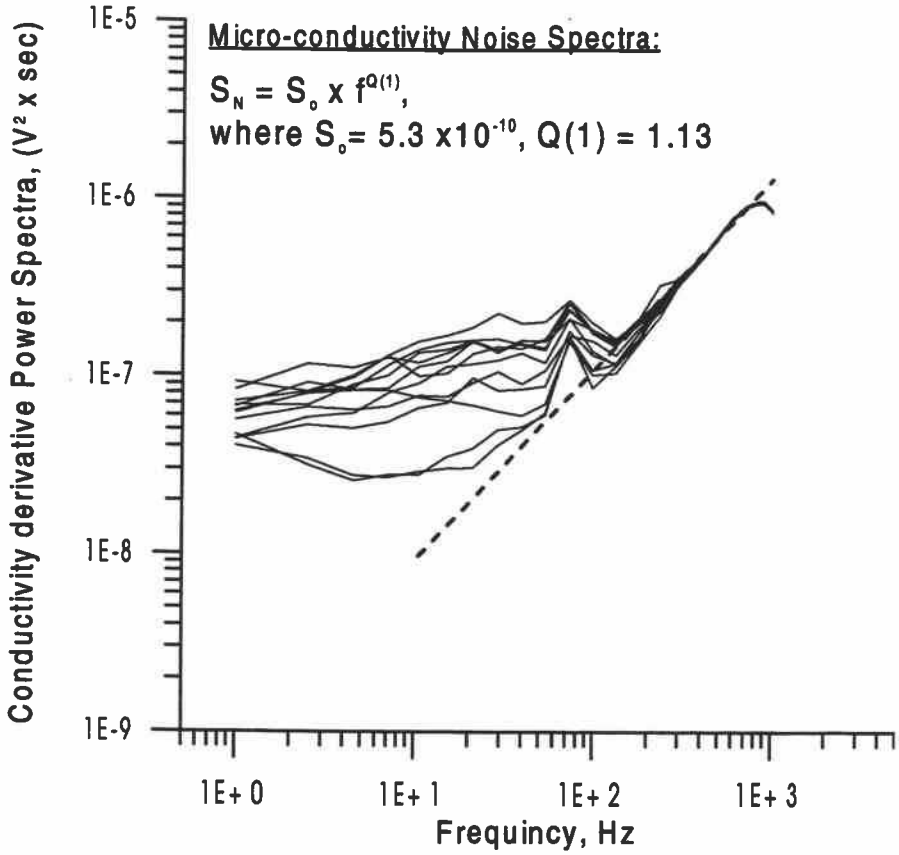

Figure 11. Band averaged spectra of conductivity derivative and conductivity noise spectra.

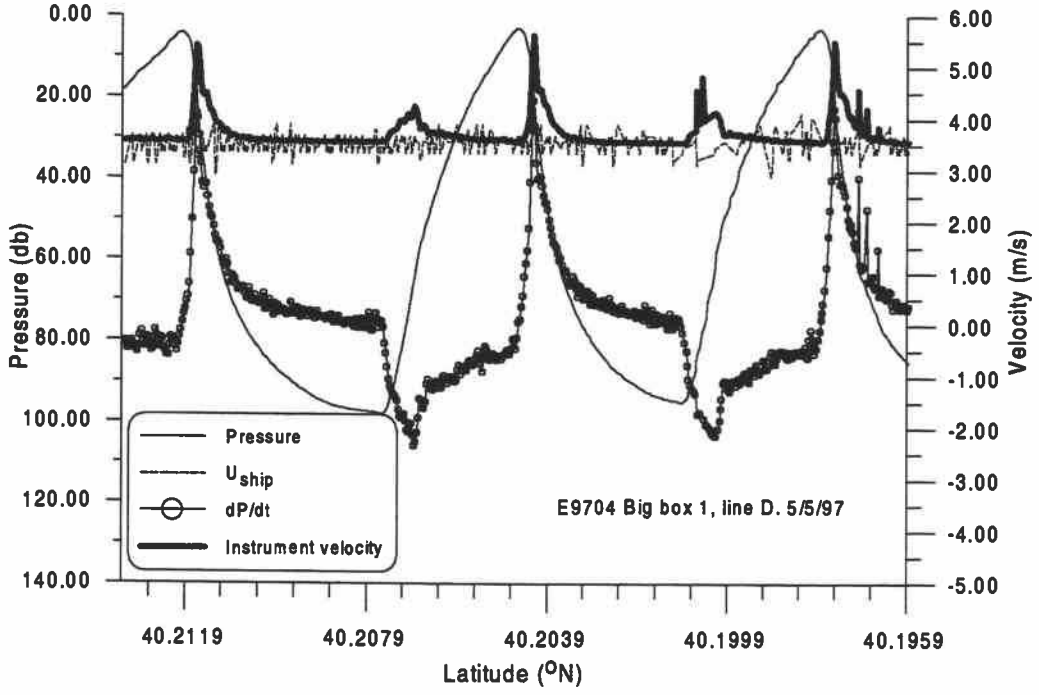

Figure 12. Calculated instrument velocity.

MicroSoar data processing steps

✓ Source: MicroSoar raw data:

C_v – conductivity ("v" mean volts), C'_v – conductivity derivative (electronically differentiated from C). Sampling frequency 2048 Hz

P_v – pressure, T_v – temperature, A_x, A_y, A_z – three axes accelerometer. Sampling frequency 256 Hz:

✓ Primary data processing (for each one second time interval):

- Remove spikes from all signals;
- Calculate $\Delta C_v = (C_v^{i+1} - C_v^{i}) / \Delta t$;
- Detrend signals and remove mean values before calculating spectra;
- Create one second averaged data set (in volts). Table 3 below shows the structure of one second averaged MicrosSoar data.

Table 3. Structure of one second averaged MicrosSoar data.

<T>	<C>	<P>	<T'>	<C'>	<ΔC/Δt>
<P'>	<Accel-X>	<Accel-Y>	<Accel-Z>	<Shorted-1>	<Shorted-2>
σ_T	σ_C	etc.	...	...	...
...	...	...	...	...	...
Skewness T	Skewness C	etc.	...	...	...
...	...	...	...	...	...
Kurtosis T	Kurtosis C	etc.	...	...	...
...	...	...	...	...	...
Fast channels frequency array, N_{fast} points					
Power spectrum of ΔC/Δt, N_{fast} points					
Power spectrum of C', N_{fast} points					
Coherence spectrum of ΔC/Δt and C', N_{fast} points					
Phase spectrum of ΔC/Δt and C', N_{fast} points					
In-Phase power spectrum of ΔC/Δt and C', N_{fast} points					
Slow channels frequency array, N_{slow} points					
Power spectrum of T', N_{slow} points					
Power spectrum of C', N_{slow} points					
Coherence spectrum of T' and C', N_{slow} points					
Phase spectrum of T' and C', N_{slow} points					
In-Phase power spectrum of T' and C', N_{slow} points					

✓ One second averaged MicroSoar data, in volts, includes these characteristics:

- Four first moments for all 11 channels, calculated over one second time interval (mean, standard deviation, skewness, kurtosis);
- Band averaged power spectra for the of $\Delta C/\Delta t$, C' and T' coherence spectra between $\Delta C/\Delta t$ and C', and between C' and T'; Phase spectra between $\Delta C/\Delta t$ and C' and between C' and T', In-Phase power spectrum between $\Delta C/\Delta t$ and C' and between C' and T'.

✓ Match MicroSoar and Seabird CTD data by pressure, correct MicroSoar time base and incorporate MicroSoar one second averaged data with navigational data.

✓ Calibration of MicroSoar data using Seabird CTD measurements. finding calibration coefficients for each 5 minutes of MicroSoar one second averaged data sets:

- $C_{ctd} = a_{\mu S} + b_{\mu S} C_v$
- $T_{ctd} = a_{\mu T} + b_{\mu T} T_v$
- $P_{ctd} = a_{\mu P} + b_{\mu P} P_v$

✓ Calculate microstructure parameters:

- Cox number;
- Heat Flux;
- Temperature variance dissipation rate;

✓ Create final MicroSoar data sets in terms of tows and lines.

Data presentation

The final 1-Hz data files contain unfiltered GPS latitude and longitude; pressure; temperature, salinity and sigma-t from the preferred sensor pair of the Seabird CTD; date and time (in both decimal day-of-year and integer year, month, day, hour, minute, second); SeaSoar velocity, Temperature Variance Dissipation rate, Cox Number and Heat Flux, an integer flag: 0 - means original CTD data are used, 1 - means there was not CTD data and MicroSoar pressure temperature, salinity and sigma-t are used.

For the SeaSoar observations, we split the tow data into the small box and big box surveys. Sections which connect one box to another were used in the maps for both boxes. Maps of Temperature Variance Dissipation rate, Cox Number and Heat Flux are shown for every ten meters between 5 and 75 meters depth for the small box surveys; the big box surveys continue that down to 105 meters. Data used in the maps were obtained by first binning the data into 2-db bins in the vertical, and 1.25 km bins in the horizontal. Then, the depth of interest was extracted from the appropriate sections for the maps. Contour maps were then created by gridding these data using "zgrid" (Crain, 1968, unpublished). The small box grid used a spacing of 0.025° longitude (2.13 km) in E-W spacing, and 0.0125° latitude (1.4 km) in N-S spacing, while the big box grids used twice that (0.05° = 4.25 km E-W and 0.025° = 2.8 km N-S spacing). Any grid point more that two grid spaces away from a data points was set to be undefined.

Vertical sections of Temperature Variance Dissipation rate, Cox Number and Heat Flux contoured using "zgrid" from the 1.25-km, 2-db averaged data are shown for each of the SeaSoar lines.

Acknowledgements

We are indebted to Robert O'Malley, who supplied the Seabird CTD data for MicroSoar sensors calibrations. We would like to thank OSU Marine Technicians Linda Fayler and Marc Willis, who were responsible for the highly successful SeaSoar operations. We also thank

Kieran O'Driscoll (summer 1996) and Andy Dale (spring 1997) who were in charge of assembling/disassembling and mounting the MicroSoar instrument to the SeaSoar vehicle. This work was funded by the Office of Naval Research Grant N0014-95-1-0382.

References

Barth, J. A. and D. J. Bogucki, 1998. Spectral light absorption and attenuation measurements from a towed undulating vehicle. *Deep-Sea Research*, submitted.

Barth, J. A., D. J. Bogucki, A. Erofeev and J. Simeon, 1998. SeaSoar spectral light absorption and attenuation observations during the Coastal Mixing and Optics experiment: R/V Endeavor cruises from 14-Aug to 1-Sep 1996 and 25-Apr to 15-May 1997. College of Oceanic and Atmospheric Sciences, Oregon State University, Corvallis , **Data Report**, in preparation.

Barth, J. A., R. O'Malley, J. Fleischbein, R. L. Smith and A. Huyer, 1996. SeaSoar and CTD observations during Coastal Jet Separation cruise W9408A August to September 1994. College of Oceanic and Atmospheric Sciences, Oregon State University, Corvallis. **Ref. 96-1, Data Report 162**, November 1996, 309 pp.

Breinerd, K.E and M.C. Gregg, 1995. Surface mixed and mixing layer depths, *Deep-Sea Research*, **42**, 1521-1543.

Dillon, T.M. and D.R. Caldwell, 1980 The Bachelor Spectrum and dissipation in the upper ocean, *Journal of Geophysical Research*, **85**, 1910-1916.

Dillon, T. M., J. A. Barth, A. Y. Erofeev and G. H. May, 1998. MicroSoar: A new instrument for measuring microscale turbulence from rapidly moving submerged platforms. *Journal of Atmospheric and Oceanic Technology.*, in preparation.

May, G.H., 1997. MicroSoar: A High-Speed Microstructure Profiling System. *M.S. Thesis*, College of Oceanic and Atmospheric Sciences, Oregon State University, Corvallis, 227 pp.

Moum, J.N., D.R. Caldwell, and C.A. Paulson, 1989. Mixing in the equatorial surface layer and thermocline, *Journal of Geophysical Research*, **94**, 2005-2021.

O'Malley, R. J. A. Barth, A. Erofeev, J. Fleischbein, P. M. Kosro and S. D. Pierce, 1998. SeaSoar CTD observations during the Coastal Mixing and Optics experiment: R/V Endeavor Cruises from 14-Aug to 1-Sep 1996 and 25-Apr to 15-May 1997. College of Oceanic and Atmospheric Sciences, Oregon State University, Corvallis. **Ref. 98-1, Data Report 168**, October 1998.

Tennekes, H. and J.L. Lumley, 1972. A First Course in Turbulence, *The MIT Press*, Cambridge, Massachusetts.

Paka, V.T., V.N. Nabatov, I.D. Lozovatsky and T.M. Dillon, 1998. Oceanic Microstructure measurements by "BAKLAN" and "GRIF", *Journal of Atmospheric and Oceanic Technology*, (in press).

Pierce, S. D., J. A. Barth and P. M. Kosro, 1998. Acoustic Doppler current profiler observations during the Coastal Mixing and Optics experiment: R/V Endeavor Cruises from 14-Aug to 1-Sep 1996 and 25-Apr to 15-May 1997. College of Oceanic and Atmospheric Sciences, Oregon State University, Corvallis. **Ref. 98-2, Data Report 169**, October 1998.

WETLabs, Inc., 1994. MODAPS User's Manual, Philomath, Oregon, 50 pp.

E9608 cruise: *Sections and Maps*

Table 4. E9608 Section Times

	Section Name	start time	stop time
Small Box 1	line1	15-Aug-96 23:20:18	16-Aug-96 01:59:54
	line1_2	16-Aug-96 01:59:55	16-Aug-96 02:23:46
	line2	16-Aug-96 02:39:56	16-Aug-96 04:19:04
	line2_3	16-Aug-96 04:19:05	16-Aug-96 04:44:54
	line3	16-Aug-96 04:44:55	16-Aug-96 07:01:37
	line3_4	16-Aug-96 07:01:38	16-Aug-96 07:30:59
	line4a	16-Aug-96 07:31:00	16-Aug-96 08:36:09
	line4b	16-Aug-96 09:39:42	16-Aug-96 10:35:54
	line4_5	16-Aug-96 10:35:55	16-Aug-96 11:13:50
	line5	16-Aug-96 11:13:51	16-Aug-96 13:10:14
	line5_6	16-Aug-96 13:10:15	16-Aug-96 13:38:06
	line6	16-Aug-96 13:38:07	16-Aug-96 15:27:16
Big Box 1	lineF	17-Aug-96 02:00:01	17-Aug-96 06:10:49
	lineE_F	17-Aug-96 06:10:50	17-Aug-96 07:00:21
	lineE	17-Aug-96 07:00:22	17-Aug-96 12:42:01
	lineD_E	17-Aug-96 12:50:43	17-Aug-96 13:42:58
	lineD	17-Aug-96 13:42:59	17-Aug-96 19:24:19
	lineC_D	17-Aug-96 19:24:20	17-Aug-96 20:11:58
	lineC	17-Aug-96 20:11:59	18-Aug-96 00:36:39
	lineB_C	18-Aug-96 00:36:40	18-Aug-96 01:28:16
	lineB	18-Aug-96 01:28:17	18-Aug-96 07:21:50
	bb1_sb2	18-Aug-96 08:28:01	18-Aug-96 09:07:44
Small Box 2	line1	18-Aug-96 09:35:18	18-Aug-96 11:31:21
	line1_2	18-Aug-96 11:31:22	18-Aug-96 11:59:06
	line2	18-Aug-96 11:59:07	18-Aug-96 13:44:25
	line2_3	18-Aug-96 13:44:26	18-Aug-96 14:12:57
	line3	18-Aug-96 14:12:58	18-Aug-96 16:06:00
	line3_4	18-Aug-96 17:07:09	18-Aug-96 17:35:17
	line4	18-Aug-96 18:02:09	18-Aug-96 19:42:21
	line4_5	18-Aug-96 19:42:22	18-Aug-96 20:06:23
	line5	18-Aug-96 21:06:45	18-Aug-96 23:12:05
	line5_6	18-Aug-96 23:12:06	18-Aug-96 23:46:51
	line6	18-Aug-96 23:46:52	19-Aug-96 01:45:26
	sb2_sb3	19-Aug-96 01:45:27	19-Aug-96 03:08:38
Small Box 3	line6	20-Aug-96 01:39:27	20-Aug-96 03:27:23
	line5_6	20-Aug-96 03:27:24	20-Aug-96 03:56:24
	line5	20-Aug-96 03:56:25	20-Aug-96 05:40:13
	line4_5	20-Aug-96 05:40:14	20-Aug-96 06:04:19
	line4	20-Aug-96 06:04:20	20-Aug-96 07:51:16
	line3_4	20-Aug-96 07:51:17	20-Aug-96 08:17:15
	line3	20-Aug-96 08:17:16	20-Aug-96 10:05:16
	line2_3	20-Aug-96 10:05:17	20-Aug-96 10:30:04
	line2	20-Aug-96 10:30:05	20-Aug-96 12:13:46
	line1_2	20-Aug-96 12:13:47	20-Aug-96 12:48:18
	line1	20-Aug-96 12:48:19	20-Aug-96 14:40:19

E9608 Section Times

	section name	start time	stop time
Big Box 2	LineA	20-Aug-96 17:03:21	20-Aug-96 22:18:46
	lineA_B	20-Aug-96 22:18:47	20-Aug-96 23:06:20
	LineB	20-Aug-96 23:06:21	21-Aug-96 04:53:03
	lineB_C	21-Aug-96 04:53:04	21-Aug-96 05:43:16
	lineC1	21-Aug-96 05:43:17	21-Aug-96 11:11:17
	lineC2	21-Aug-96 13:01:22	21-Aug-96 19:35:29
	lineC_D	21-Aug-96 19:35:30	21-Aug-96 20:23:40
	LineD	21-Aug-96 20:23:41	21-Aug-96 21:58:43
Small Box 4	line6	24-Aug-96 20:01:44	24-Aug-96 22:14:03
	line5_6	24-Aug-96 22:14:04	24-Aug-96 22:42:18
	line5	24-Aug-96 22:42:19	25-Aug-96 00:27:36
	line4_5	25-Aug-96 00:27:37	25-Aug-96 00:51:36
	line4	25-Aug-96 00:51:37	25-Aug-96 02:37:21
	line3_4	25-Aug-96 02:37:22	25-Aug-96 03:01:10
	line3	25-Aug-96 03:01:11	25-Aug-96 04:55:27
	line2_3	25-Aug-96 04:55:28	25-Aug-96 05:18:58
	line2	25-Aug-96 05:18:59	25-Aug-96 07:07:04
	line1_2	25-Aug-96 07:07:05	25-Aug-96 07:30:20
	line1	25-Aug-96 07:30:21	25-Aug-96 09:21:25
	sb4_sb5	25-Aug-96 09:21:26	25-Aug-96 11:34:55
Small Box 5	line6	25-Aug-96 11:34:56	25-Aug-96 13:31:44
	line5_6	25-Aug-96 13:31:45	25-Aug-96 13:59:09
	line5	25-Aug-96 13:59:10	25-Aug-96 15:52:39
	line4_5	25-Aug-96 15:52:40	25-Aug-96 16:17:11
	line4	25-Aug-96 16:17:12	25-Aug-96 18:14:59
	line3_4	25-Aug-96 18:15:00	25-Aug-96 18:38:20
	line3	25-Aug-96 18:38:21	25-Aug-96 20:24:41
	line2_3	25-Aug-96 20:24:42	25-Aug-96 20:51:21
	line2	25-Aug-96 20:51:22	25-Aug-96 22:48:44
	line1_2	25-Aug-96 22:48:45	25-Aug-96 23:14:43
	line1	25-Aug-96 23:14:44	26-Aug-96 01:05:56
	sb5_sb6	26-Aug-96 01:05:57	26-Aug-96 03:11:38
Small Box 6	line6	26-Aug-96 03:11:39	26-Aug-96 04:55:38
	line5_6	26-Aug-96 04:55:39	26-Aug-96 05:20:15
	line5	26-Aug-96 05:20:16	26-Aug-96 07:08:54
	line4_5	26-Aug-96 07:08:55	26-Aug-96 07:31:14
	line4	26-Aug-96 07:31:15	26-Aug-96 09:30:49
	line3_4	26-Aug-96 09:30:50	26-Aug-96 09:57:15
	line3	26-Aug-96 09:57:16	26-Aug-96 11:48:17
	line2_3	26-Aug-96 11:48:18	26-Aug-96 12:14:25
	line2	26-Aug-96 12:14:26	26-Aug-96 14:21:14
	line1_2	26-Aug-96 14:21:15	26-Aug-96 14:48:22
	line1	26-Aug-96 14:48:23	26-Aug-96 16:53:29

E9608 Section Times

	section name	start time	stop time
Butterfly 1	weA	26-Aug-96 23:59:40	27-Aug-96 00:59:48
	weB	27-Aug-96 04:05:59	27-Aug-96 05:25:22
	en	27-Aug-96 05:25:23	27-Aug-96 07:16:07
	ns	27-Aug-96 07:16:08	27-Aug-96 09:46:25
	sw	27-Aug-96 09:46:26	27-Aug-96 11:12:19
Butterfly 2	we	27-Aug-96 11:12:20	27-Aug-96 14:15:11
	en0	27-Aug-96 14:15:12	27-Aug-96 14:51:30
	en1	27-Aug-96 14:51:31	27-Aug-96 15:22:20
	en	27-Aug-96 15:22:21	27-Aug-96 17:31:05
	ns	27-Aug-96 17:31:06	27-Aug-96 20:00:15
	sw	27-Aug-96 20:00:16	27-Aug-96 21:28:56
Butterfly 3	we	27-Aug-96 23:52:14	28-Aug-96 02:36:24
	en	28-Aug-96 02:36:25	28-Aug-96 04:48:56
	ns	28-Aug-96 04:48:57	28-Aug-96 07:19:26
	sw	28-Aug-96 07:19:27	28-Aug-96 08:51:39
Butterfly 4	line1_4	28-Aug-96 09:41:28	28-Aug-96 11:09:23
	ns	28-Aug-96 11:09:24	28-Aug-96 14:53:05
	sn	28-Aug-96 14:53:06	28-Aug-96 17:09:54
Solitons	a	28-Aug-96 17:09:55	28-Aug-96 17:50:39
	b	28-Aug-96 17:50:40	28-Aug-96 18:17:37
	b_c	28-Aug-96 18:17:38	28-Aug-96 18:22:15
	c	28-Aug-96 18:22:16	28-Aug-96 18:58:20
	d	28-Aug-96 18:58:21	28-Aug-96 19:26:34
	e	28-Aug-96 19:26:35	28-Aug-96 19:50:45
	f	28-Aug-96 19:50:46	28-Aug-96 20:15:42
	g	28-Aug-96 20:15:43	28-Aug-96 21:00:00
	h	28-Aug-96 21:00:01	28-Aug-96 22:22:00
	i	28-Aug-96 22:22:01	28-Aug-96 23:36:58
	j	28-Aug-96 23:36:59	29-Aug-96 00:02:32
	k	29-Aug-96 00:02:33	29-Aug-96 00:18:30
	l	29-Aug-96 00:18:31	29-Aug-96 00:23:41
Small Box 7	line6	29-Aug-96 04:00:03	29-Aug-96 05:53:19
	line5_6	29-Aug-96 05:53:20	29-Aug-96 06:21:21
	line5	29-Aug-96 06:55:17	29-Aug-96 09:03:37
	line4_5	29-Aug-96 09:03:38	29-Aug-96 09:28:10
	line4	29-Aug-96 09:28:11	29-Aug-96 11:33:18
	line3_4	29-Aug-96 11:33:19	29-Aug-96 11:59:58
	line3	29-Aug-96 11:59:59	29-Aug-96 13:52:43
	line2_3	29-Aug-96 13:52:44	29-Aug-96 14:18:42
	line2	29-Aug-96 14:18:43	29-Aug-96 16:14:56
	line1_2	29-Aug-96 16:14:57	29-Aug-96 16:42:12
	line1	29-Aug-96 16:42:13	29-Aug-96 18:50:35
	sb7_sb8	29-Aug-96 18:50:36	29-Aug-96 21:17:35

E9608 Section Times

	section name	start time	stop time
Small Box 8	line6	29-Aug-96 21:17:36	29-Aug-96 23:24:30
	line5_6	29-Aug-96 23:24:31	29-Aug-96 23:53:13
	line5	29-Aug-96 23:53:14	30-Aug-96 01:44:01
	line4_5	30-Aug-96 01:44:02	30-Aug-96 02:09:33
	line4	30-Aug-96 02:09:34	30-Aug-96 04:10:58
	line3_4	30-Aug-96 04:10:59	30-Aug-96 04:38:14
	line3	30-Aug-96 04:38:15	30-Aug-96 06:52:04
	line2_3	30-Aug-96 06:52:05	30-Aug-96 07:19:44
	line2	30-Aug-96 07:19:45	30-Aug-96 09:16:53
	line1_2	30-Aug-96 09:16:54	30-Aug-96 09:43:08
	line1	30-Aug-96 10:06:17	30-Aug-96 12:10:57
Small Box 9	line6	30-Aug-96 14:52:14	30-Aug-96 16:51:13
	line5_6	30-Aug-96 16:51:14	30-Aug-96 17:19:02
	line5	30-Aug-96 17:19:03	30-Aug-96 19:23:28
	line4_5	30-Aug-96 19:23:29	30-Aug-96 19:53:05
	line4	30-Aug-96 19:53:06	30-Aug-96 21:45:12
	line3_4	30-Aug-96 21:45:13	30-Aug-96 22:08:56
	line3	30-Aug-96 22:08:57	30-Aug-96 23:59:22
	line2_3	30-Aug-96 23:59:23	31-Aug-96 00:26:12
	line2	31-Aug-96 00:26:13	31-Aug-96 02:29:09
	line1_2	31-Aug-96 02:29:10	31-Aug-96 02:57:00
	line1	31-Aug-96 02:57:01	31-Aug-96 04:53:39
	sb9_bb3	31-Aug-96 04:53:40	31-Aug-96 05:49:02
Big Box 3	lineC0	31-Aug-96 05:49:03	31-Aug-96 08:02:39
	lineC1	31-Aug-96 09:00:40	31-Aug-96 14:28:56
	lineC_Ds	31-Aug-96 14:28:57	31-Aug-96 15:19:51
	LineDs	31-Aug-96 15:23:45	31-Aug-96 19:00:59
	lineD_Es	31-Aug-96 19:01:00	31-Aug-96 20:06:29
	LineEs	31-Aug-96 20:06:30	31-Aug-96 23:29:47
	lineE_Fs	31-Aug-96 23:29:48	01-Sep-96 00:21:49
	LineF	01-Sep-96 00:21:50	01-Sep-96 04:46:06
	lineE_Fn	01-Sep-96 04:46:07	01-Sep-96 05:37:24
	LineEn	01-Sep-96 05:37:25	01-Sep-96 06:13:59
	lineD_En	01-Sep-96 06:14:00	01-Sep-96 07:05:38
	LineDn	01-Sep-96 07:05:39	01-Sep-96 07:45:11
	lineC_Dn	01-Sep-96 07:45:12	01-Sep-96 08:32:33
	lineC2	01-Sep-96 08:32:34	01-Sep-96 11:08:14

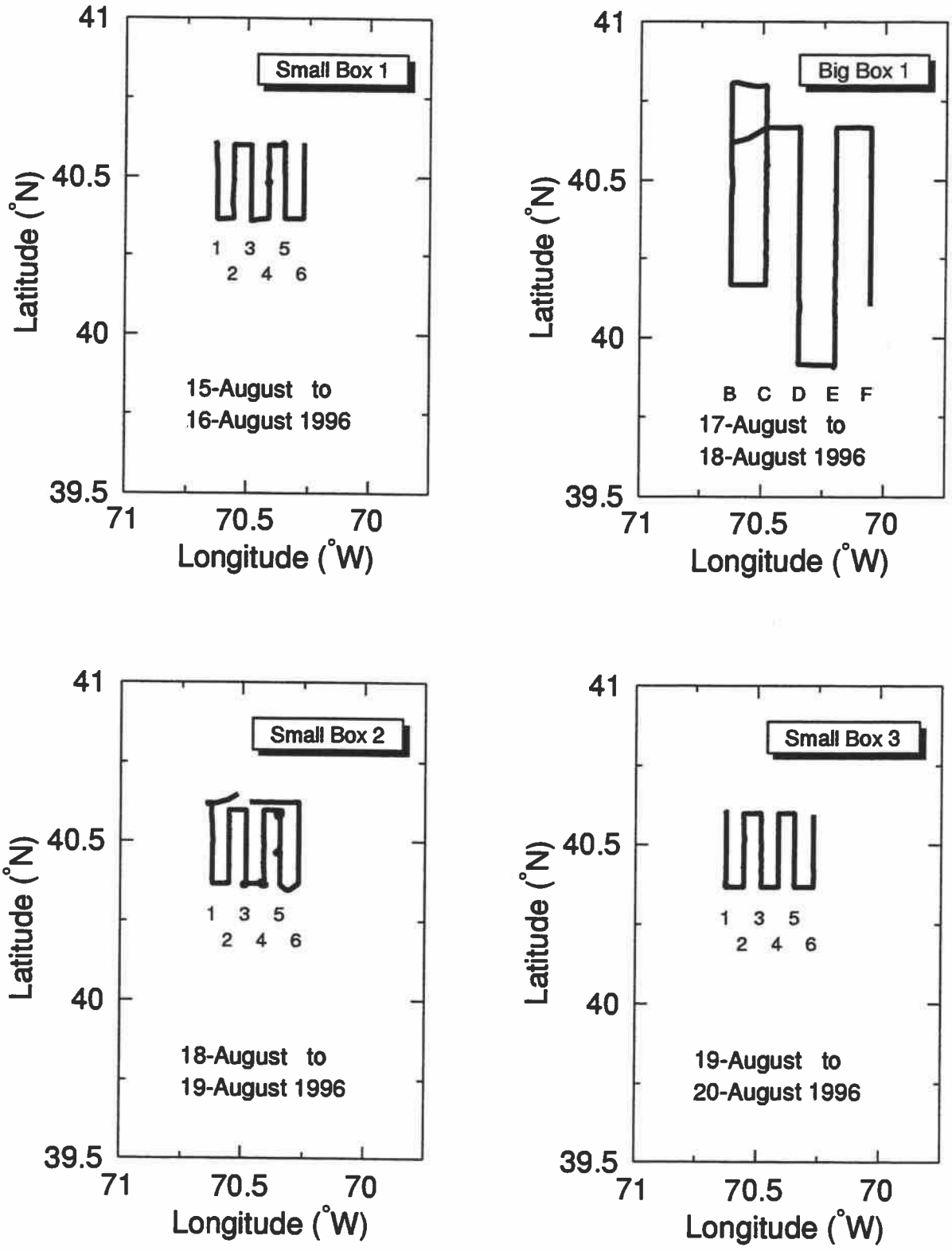

Figure 13 a. Cruise tracks during the E9608 SeaSoar surveys. See Table 4 for individual line start and stop times.

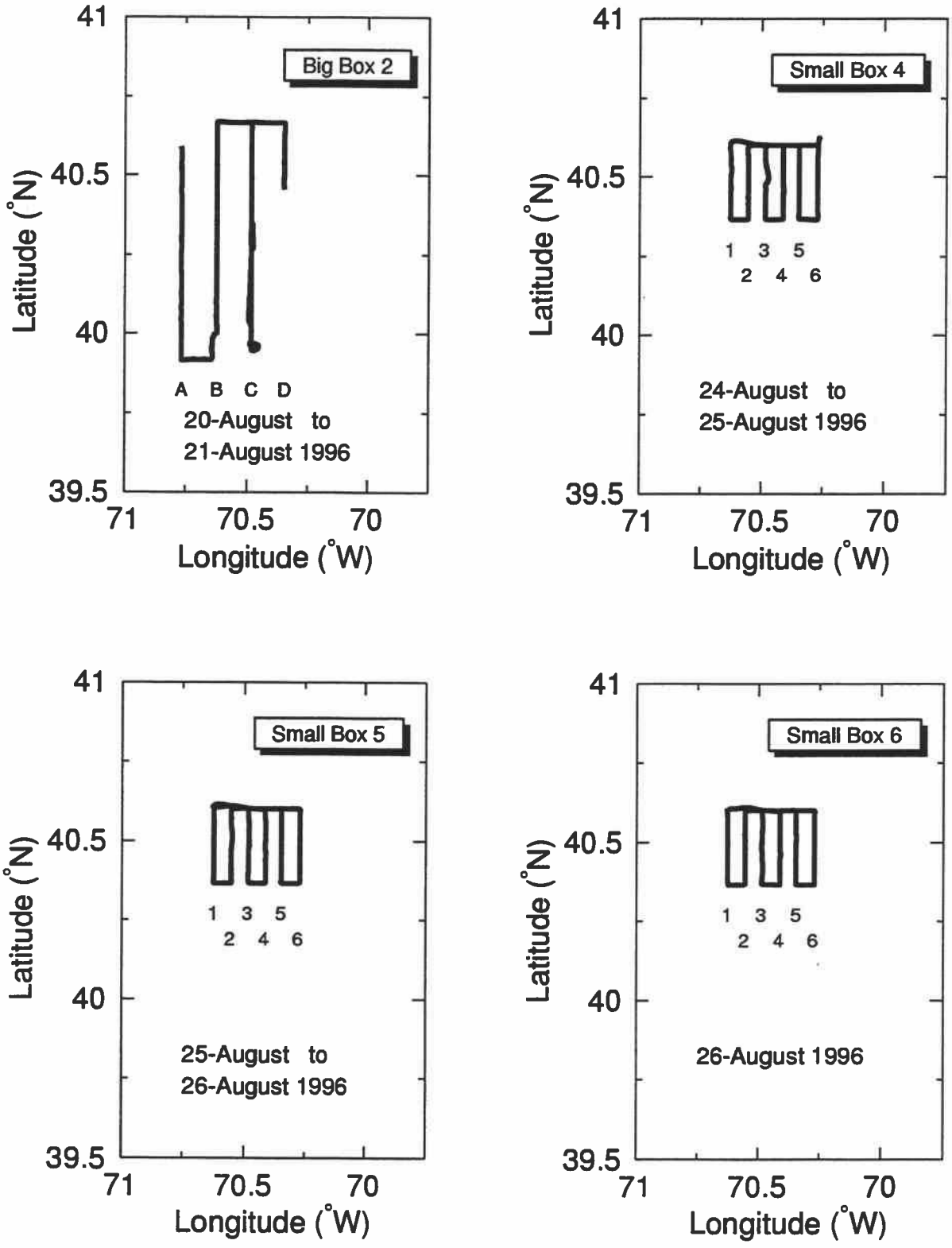
Big Box 2
A B C D
20-August to
21-August 1996
Small Box 4
1 3 5
2 4 6
24-August to
25-August 1996
Small Box 5
1 3 5
2 4 6
25-August to
26-August 1996
Small Box 6
1 3 5
2 4 6
26-August 1996
41
40.5
40
39.5
71
70.5
70
Latitude (°N)
Longitude (°W)

Figure 13 b.

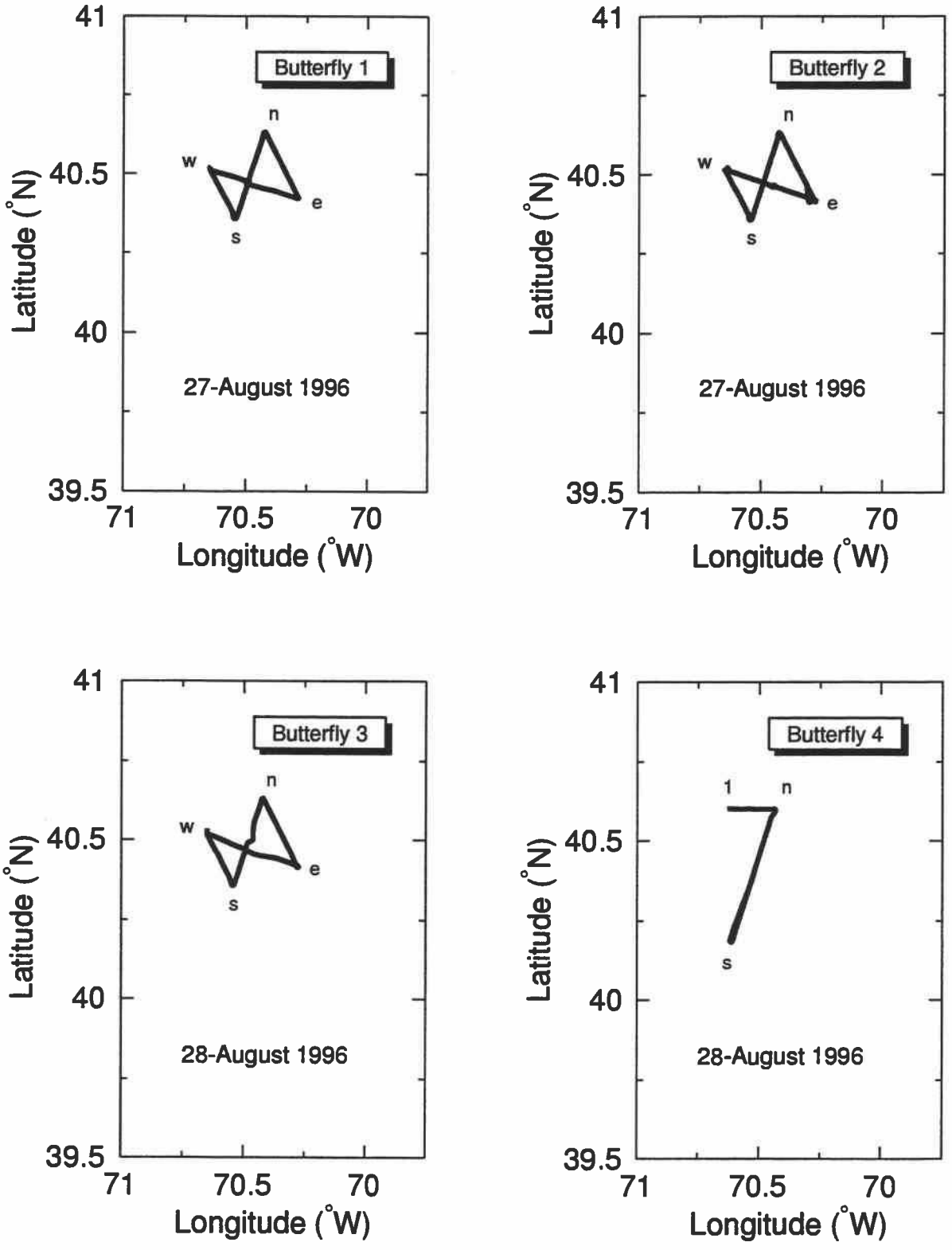
Butterfly 1
n
w
e
s
27-August 1996
Butterfly 2
n
w
e
s
27-August 1996
Butterfly 3
n
w
e
s
28-August 1996
Butterfly 4
1
n
s
28-August 1996
41
40.5
40
39.5
71
70.5
70
Latitude (°N)
Longitude (°W)

Figure 13 c.

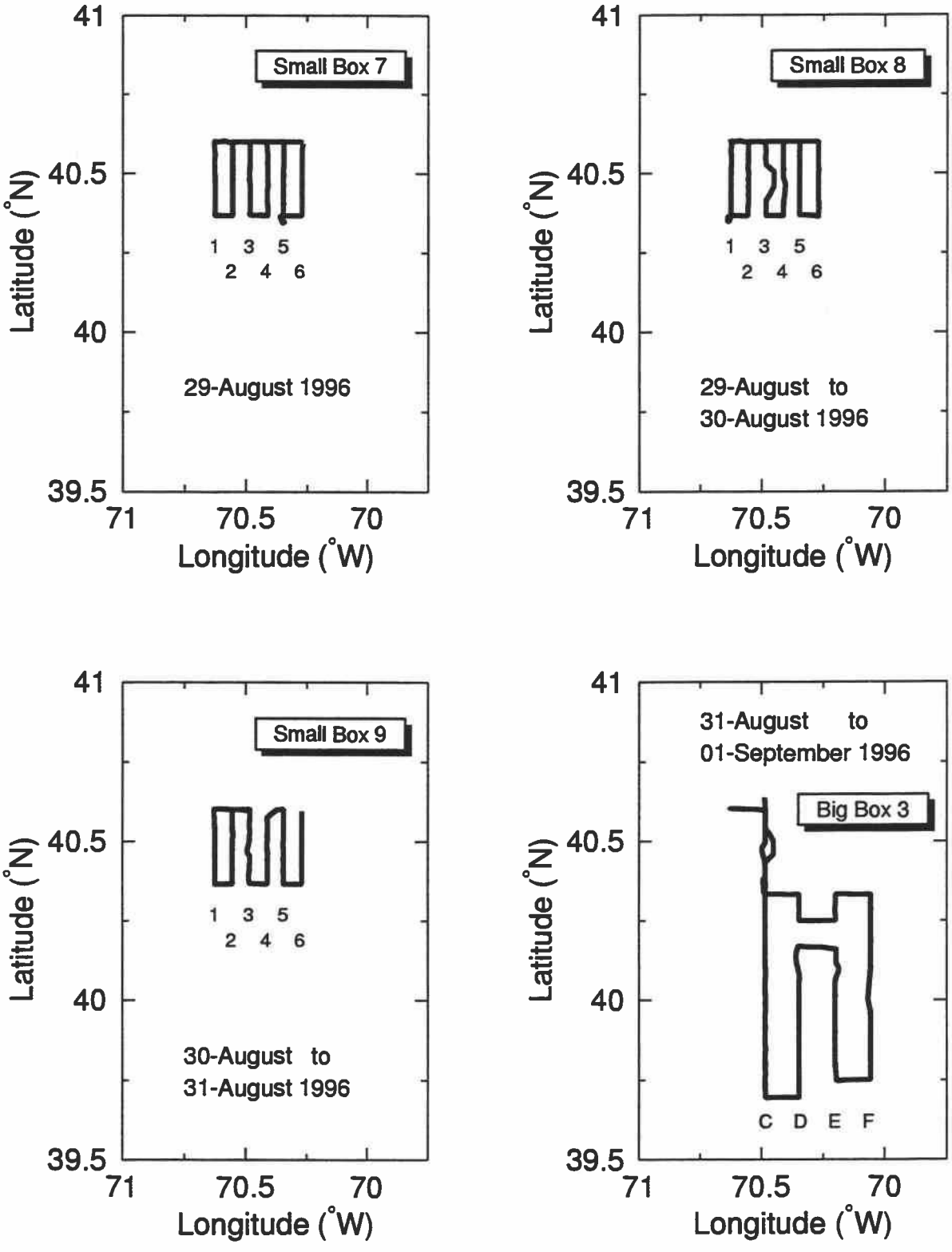
Small Box 7
1 3 5
2 4 6
29-August 1996
Small Box 8
1 3 5
2 4 6
29-August to
30-August 1996
Small Box 9
1 3 5
2 4 6
30-August to
31-August 1996
31-August to
01-September 1996
Big Box 3
C D E F
41
40.5
40
39.5
71
70.5
70
Latitude (°N)
Longitude (°W)

Figure 13 d.

Vertical sections of Temperature Variance Dissipation Rate, Cox number and Heat Flux

e9608 Big Box 1

18-Aug-96 01:29 - 18-Aug-96 06:21

Line B

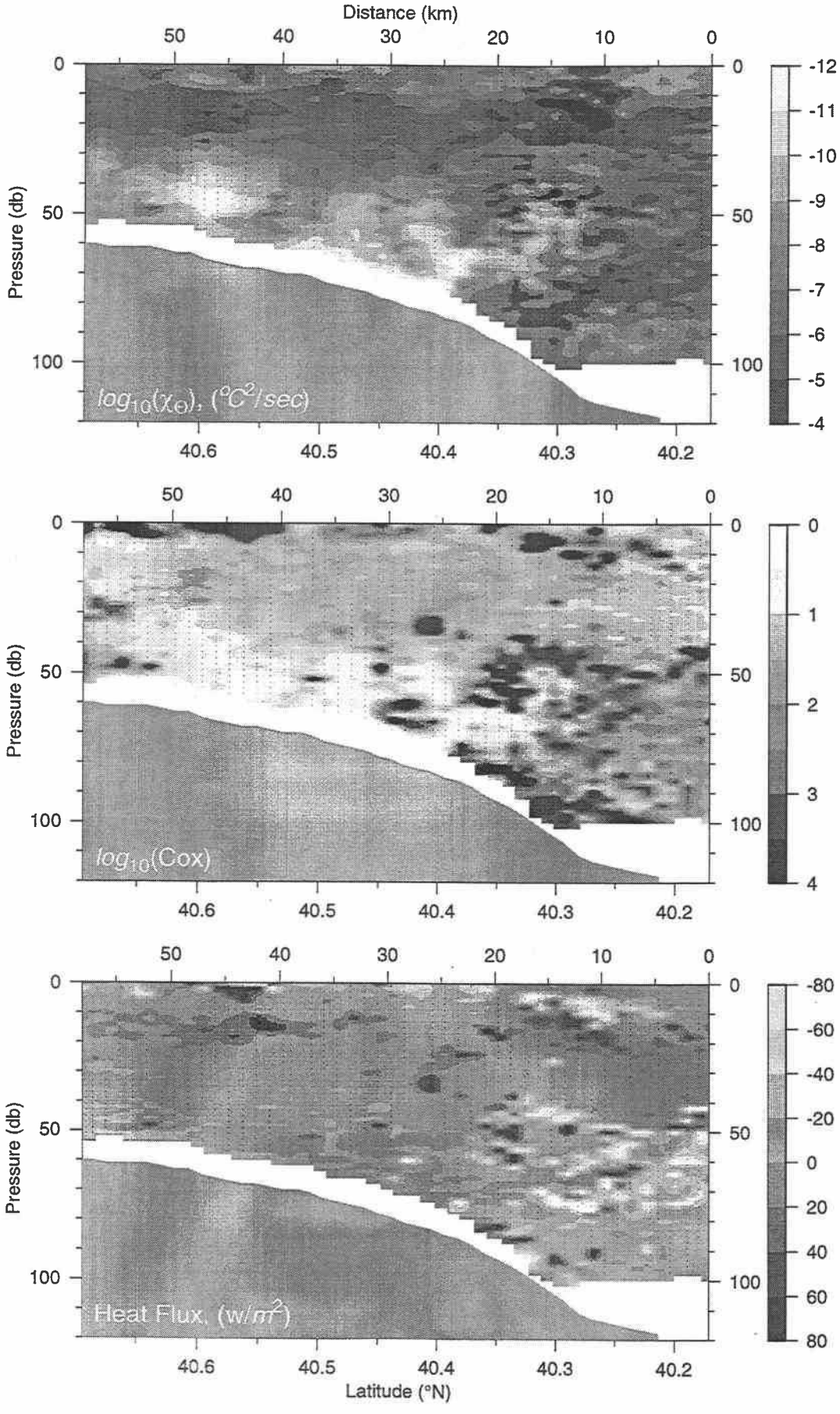

e9608 Big Box 1

17-Aug-96 20:13 - 18-Aug-96 00:34

Line C

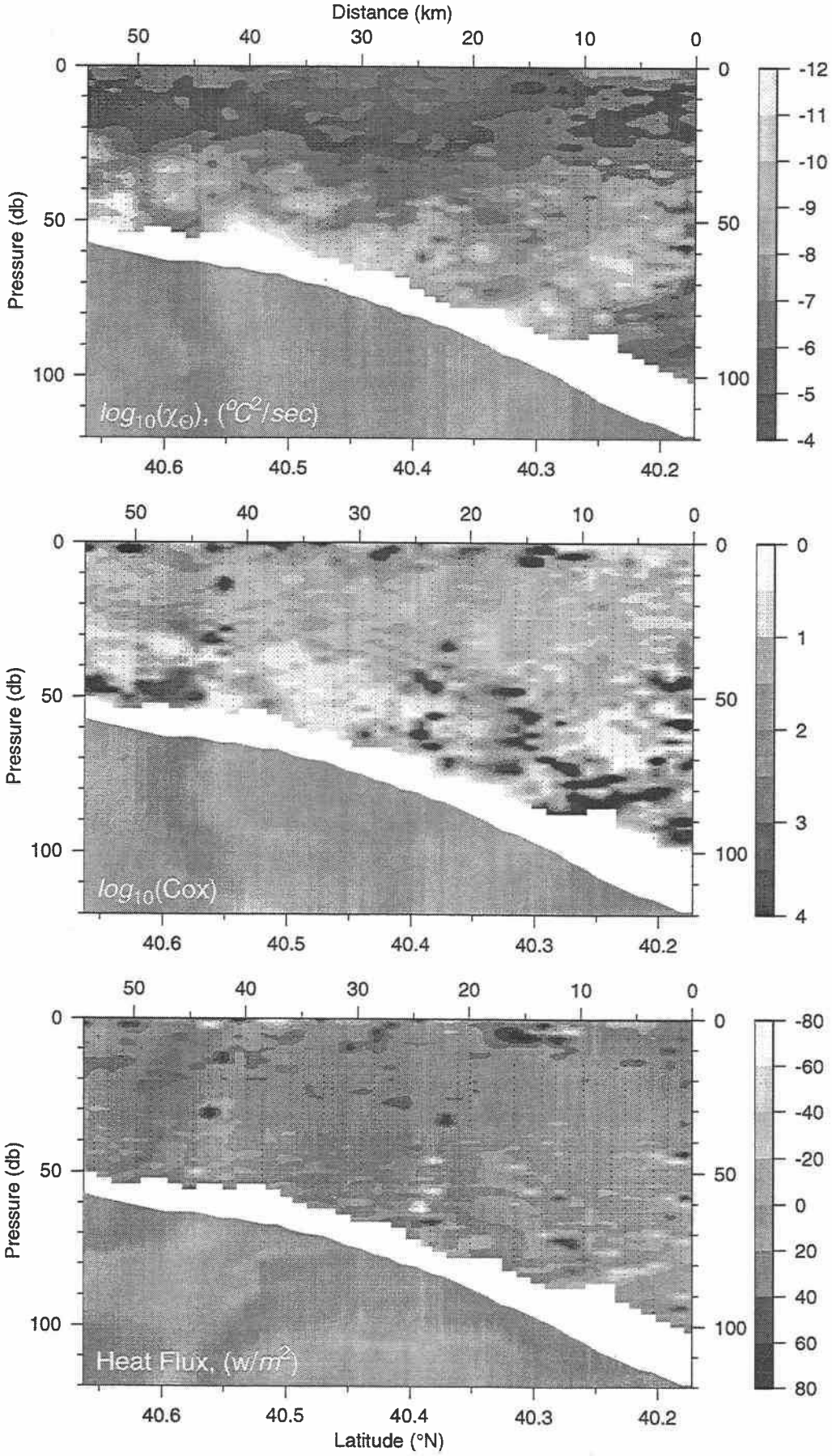

e9608 Big Box 1

17-Aug-96 13:44 - 17-Aug-96 19:22

Line D

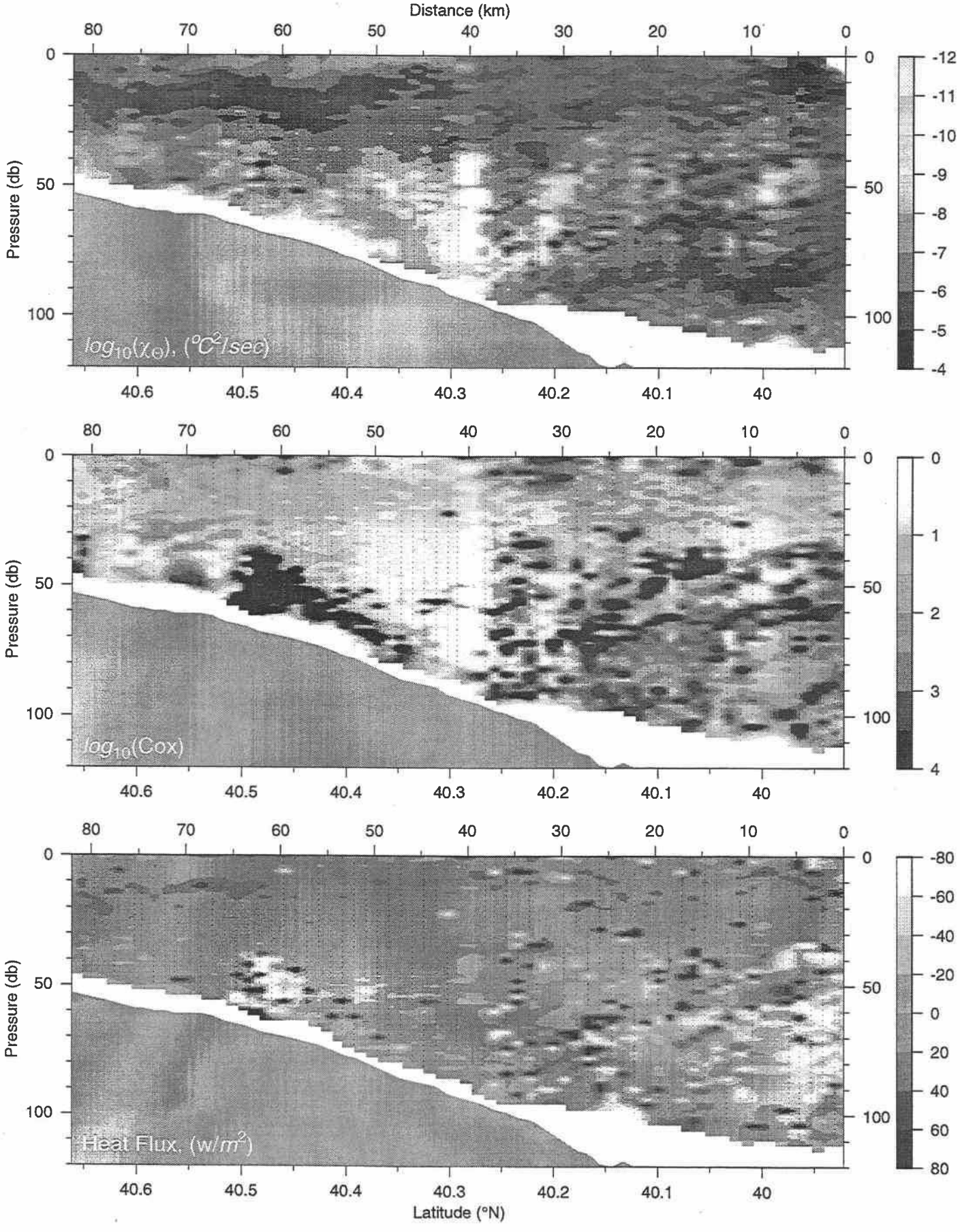

e9608 Big Box 1

17-Aug-96 07:01 - 17-Aug-96 12:39

Line E1

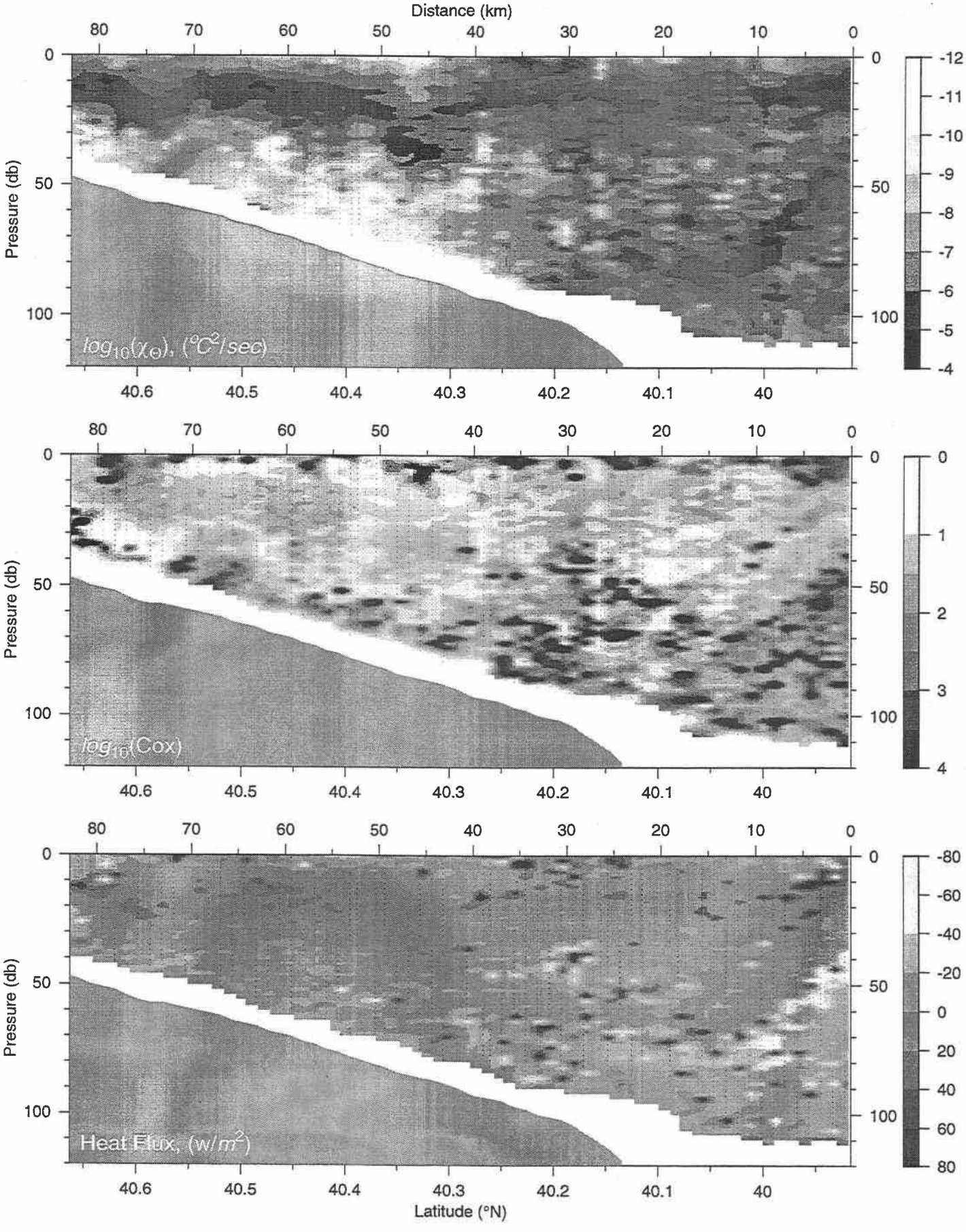

e9608 Big Box 1

17-Aug-96 02:09 - 17-Aug-96 06:08

Line F

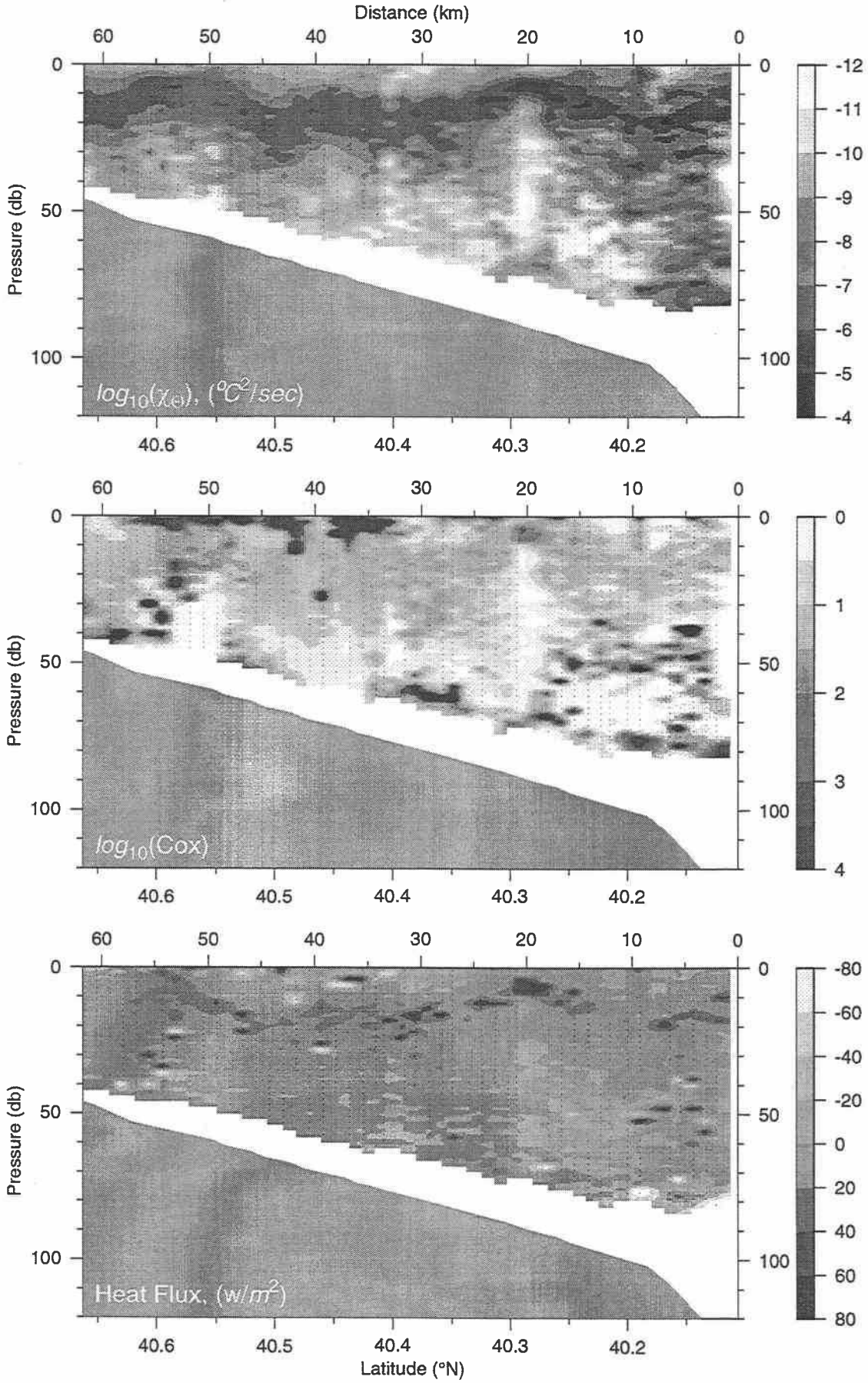

E9608 Big Box 2

20-Aug-96 17:05 - 20-Aug-96 22:16

Line A

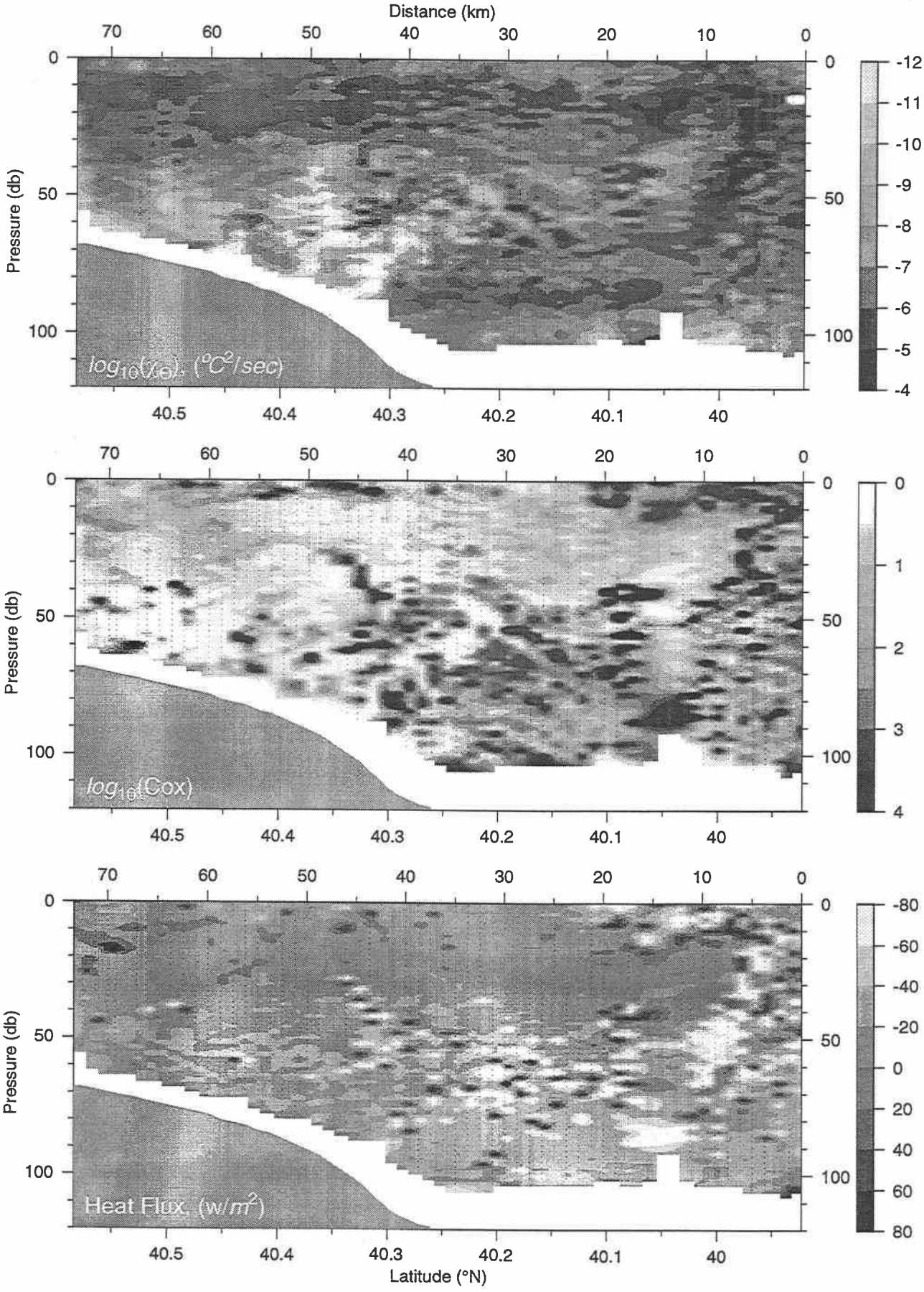

E9608 Big Box 2

20-Aug-96 23:13 - 21-Aug-96 04:55

Line B

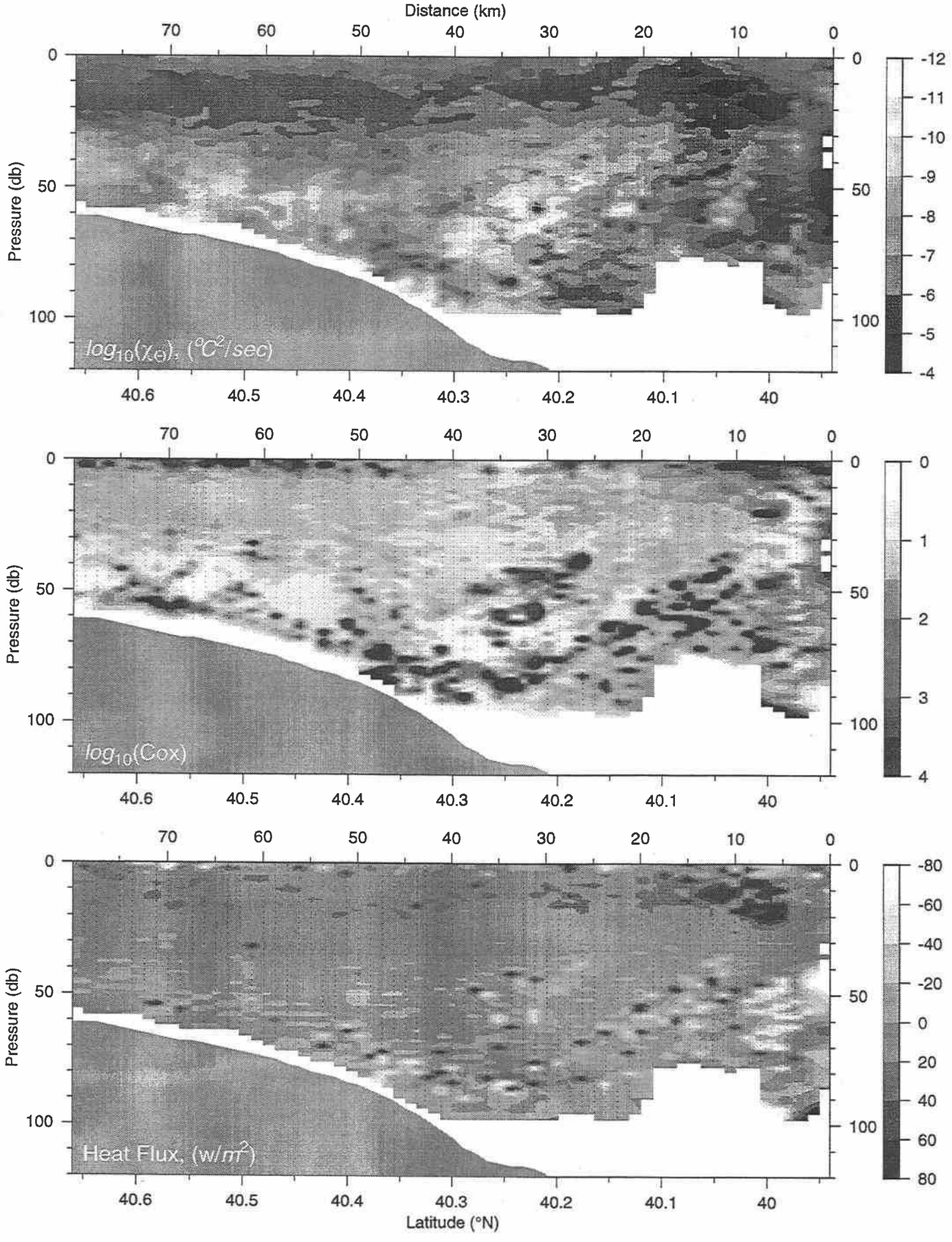

E9608 Big Box 2

21-Aug-96 13:08 - 21-Aug-96 19:34

Line C2

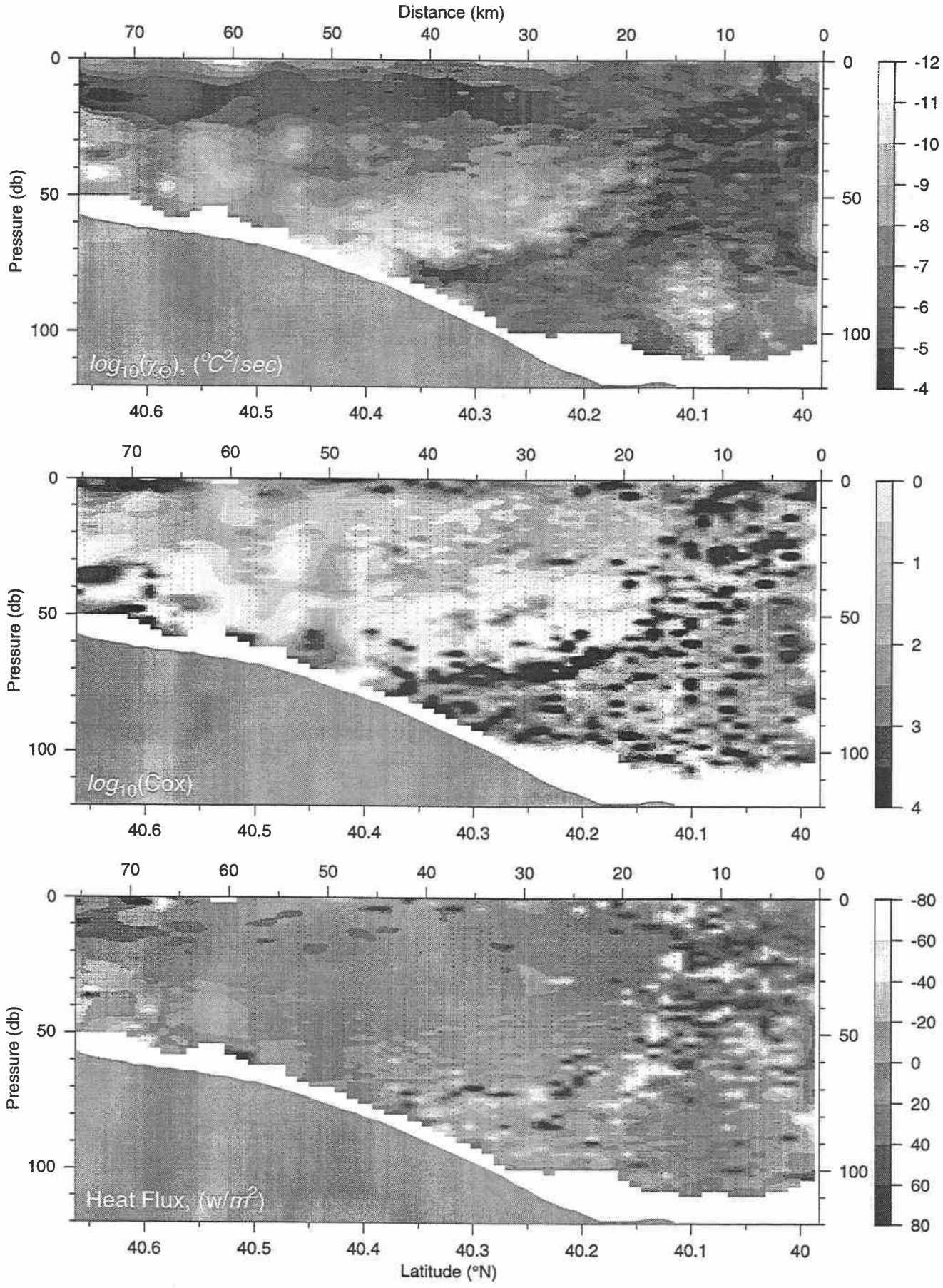

E9608 Big Box 2

21-Aug-96 20:25 - 21-Aug-96 21:39

Line D

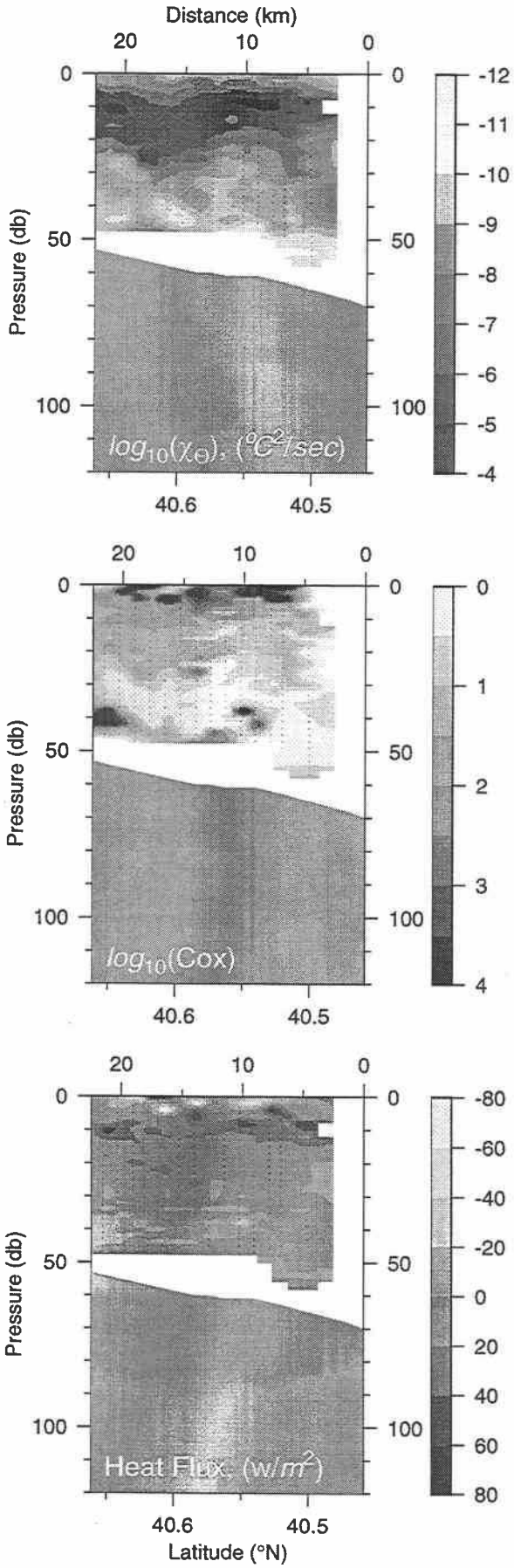

E9608 Big Box 3

31-Aug-96 05:49 - 31-Aug-96 07:58

Line C0

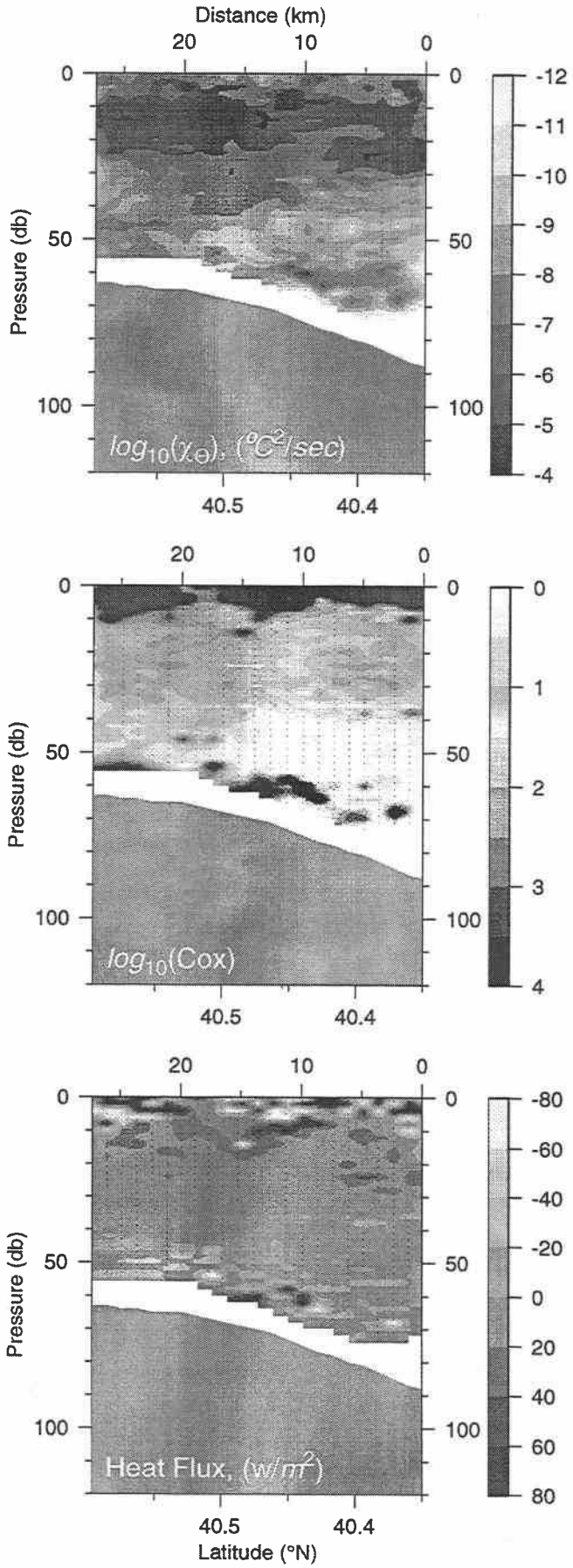

E9608 Big Box 3

31-Aug-96 09:03 - 31-Aug-96 14:27

Line C1

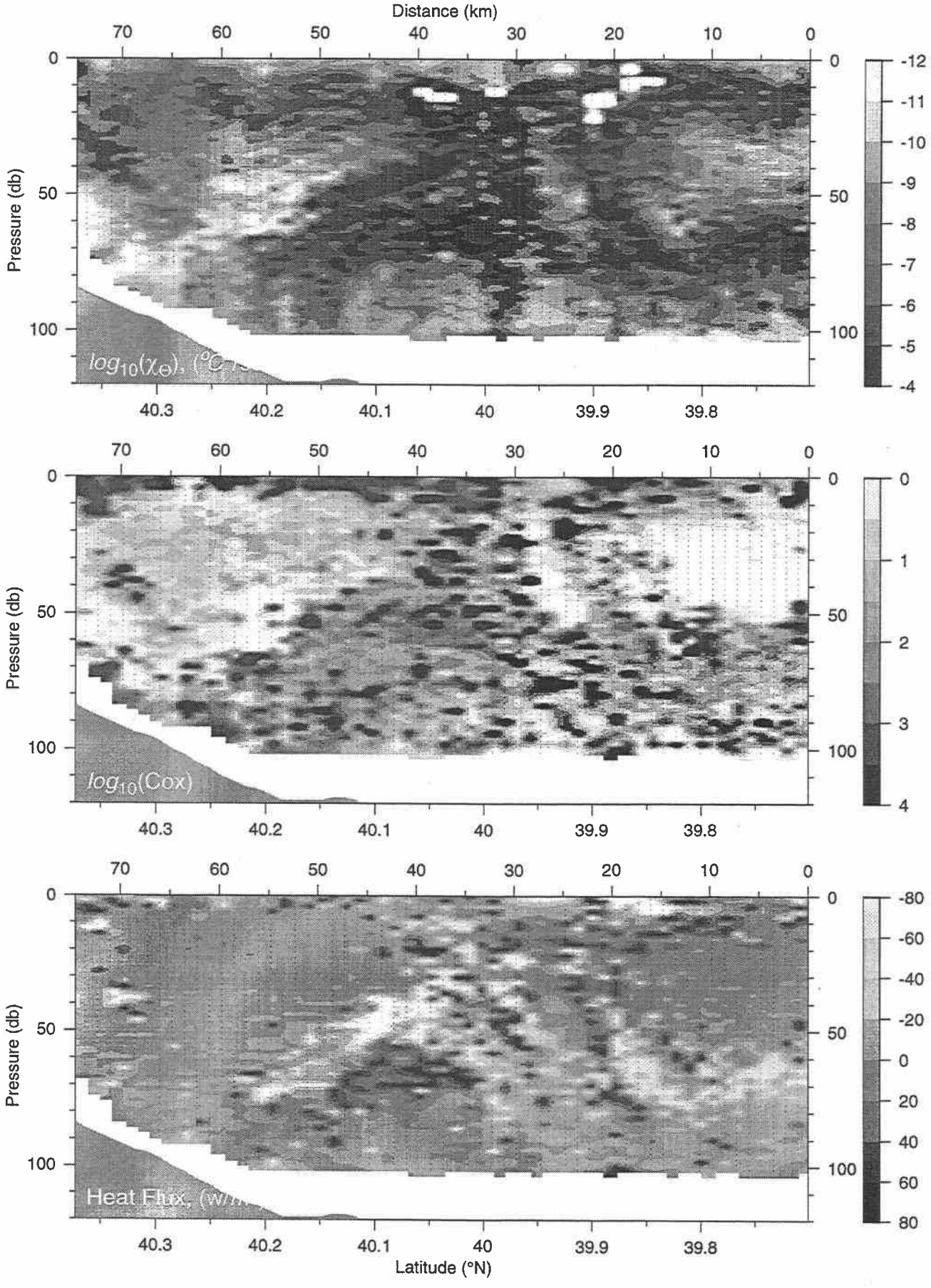

E9608 Big Box 3

01-Sep-96 08:34 - 01-Sep-96 11:03

Line C2

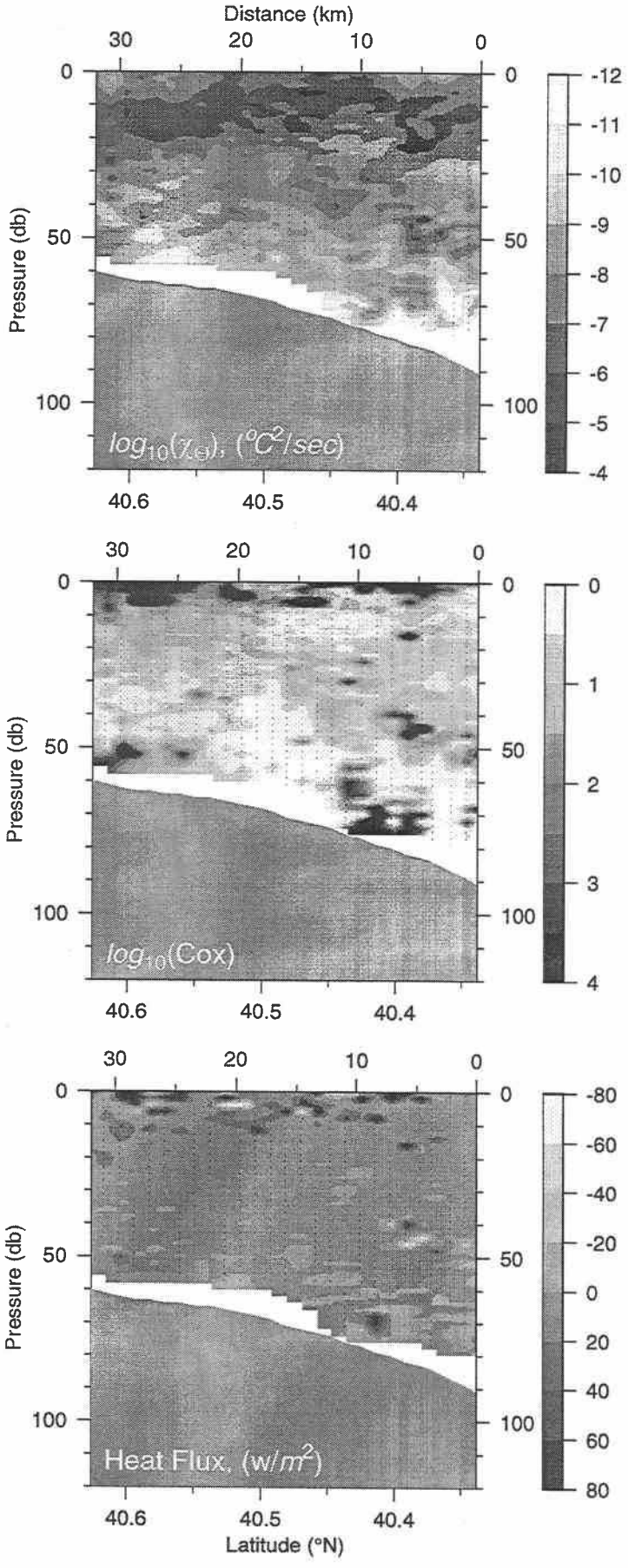

E9608 Big Box 3

31-Aug-96 15:26 - 31-Aug-96 19:00

Line Ds

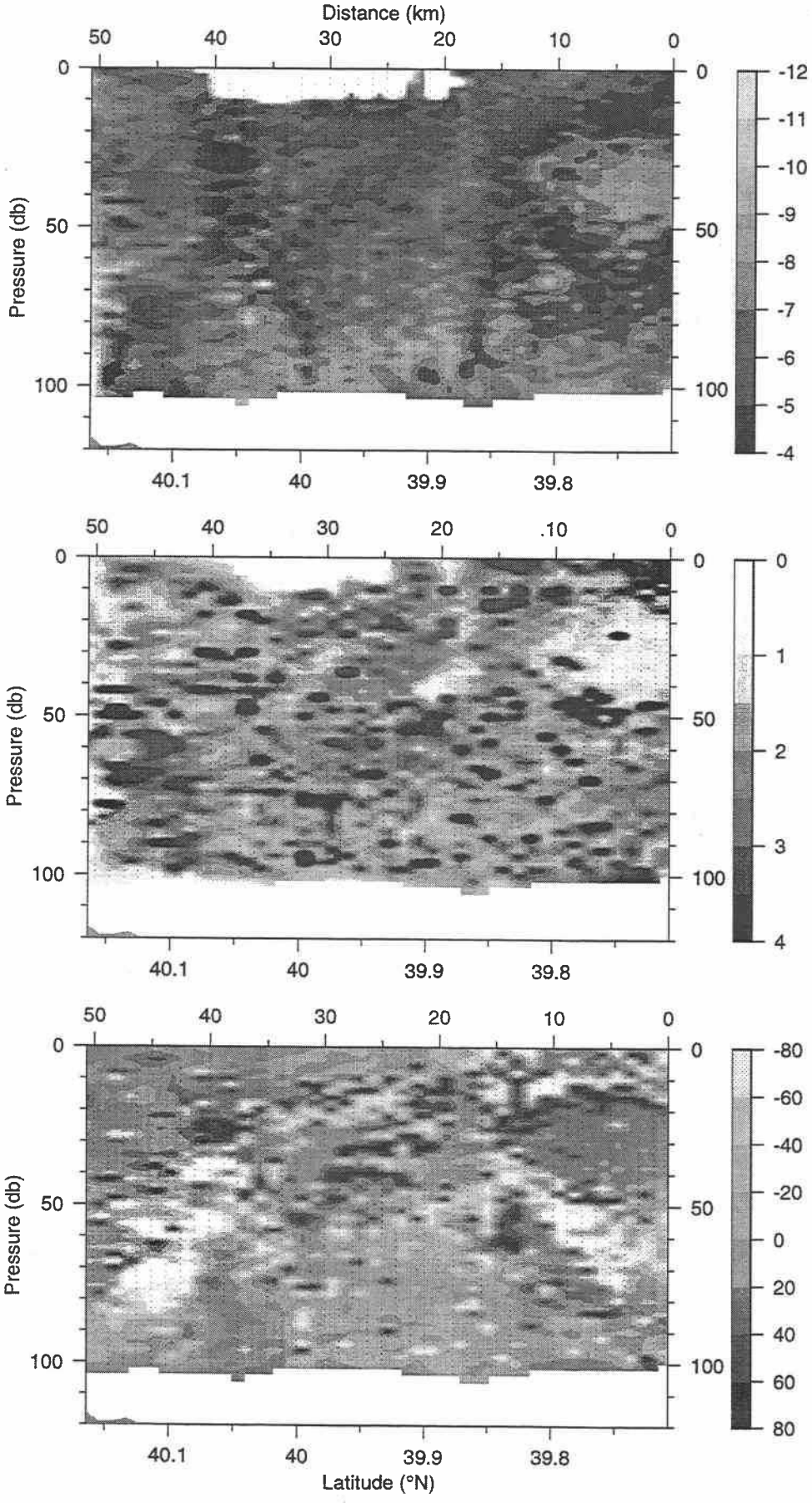

E9608 Big Box 3

31-Aug-96 20:07 - 31-Aug-96 23:27

Line Es

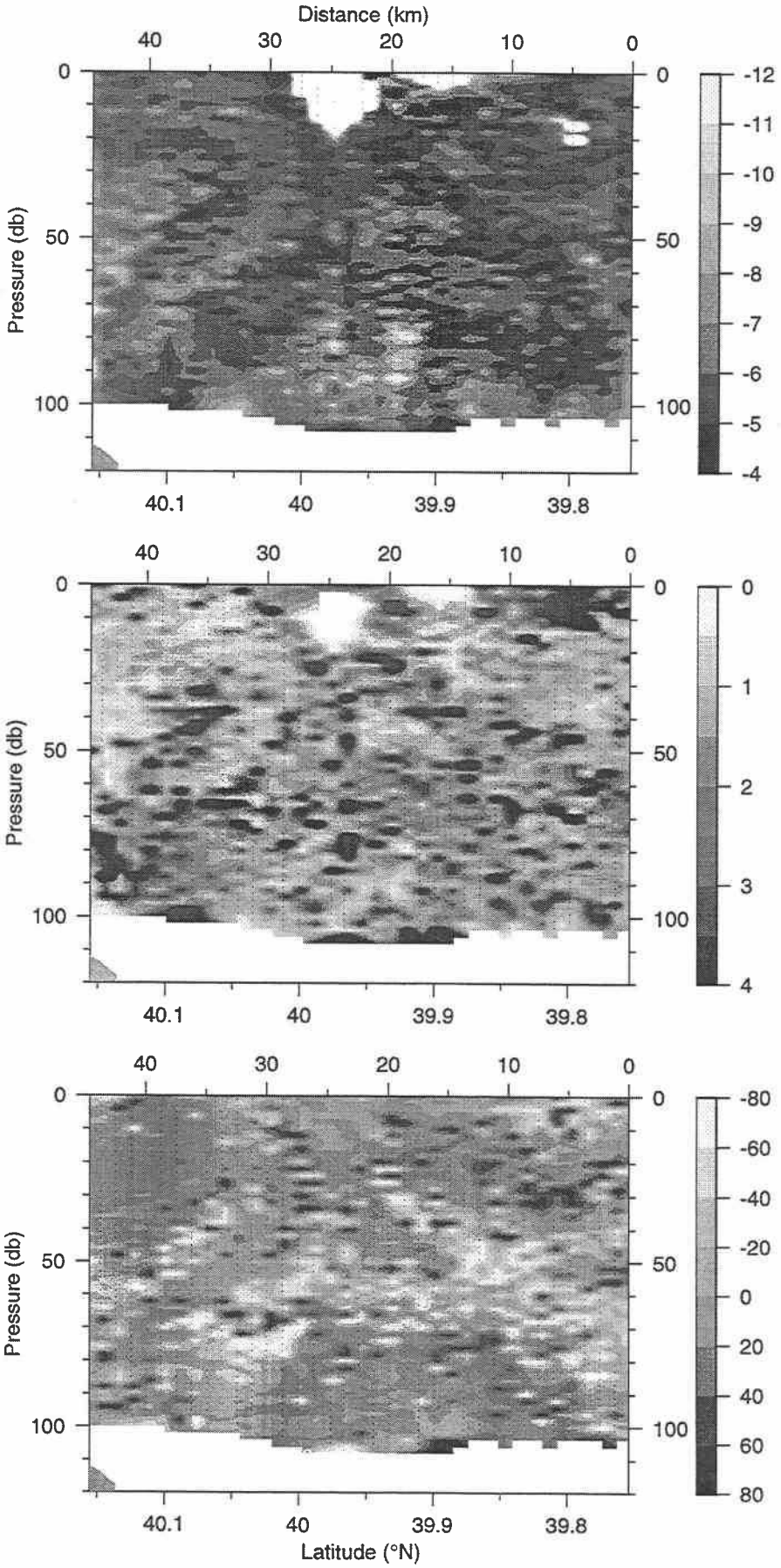

E9608 Big Box 3

01-Sep-96 00:23 - 01-Sep-96 04:44

Line F

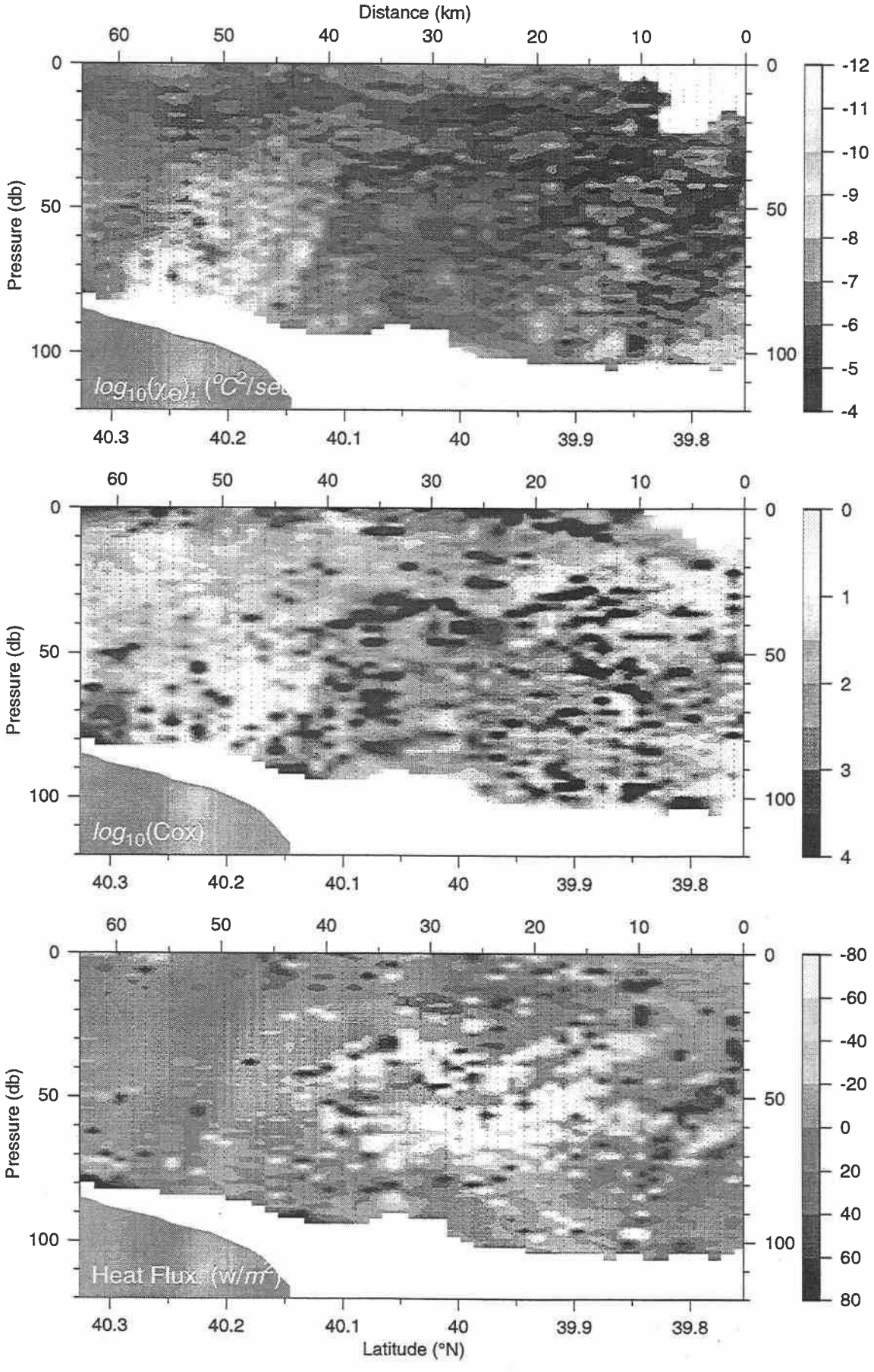

e9608 Butterfly 1

27-Aug-96 07:17 - 27-Aug-96 09:45

Line bf1ns

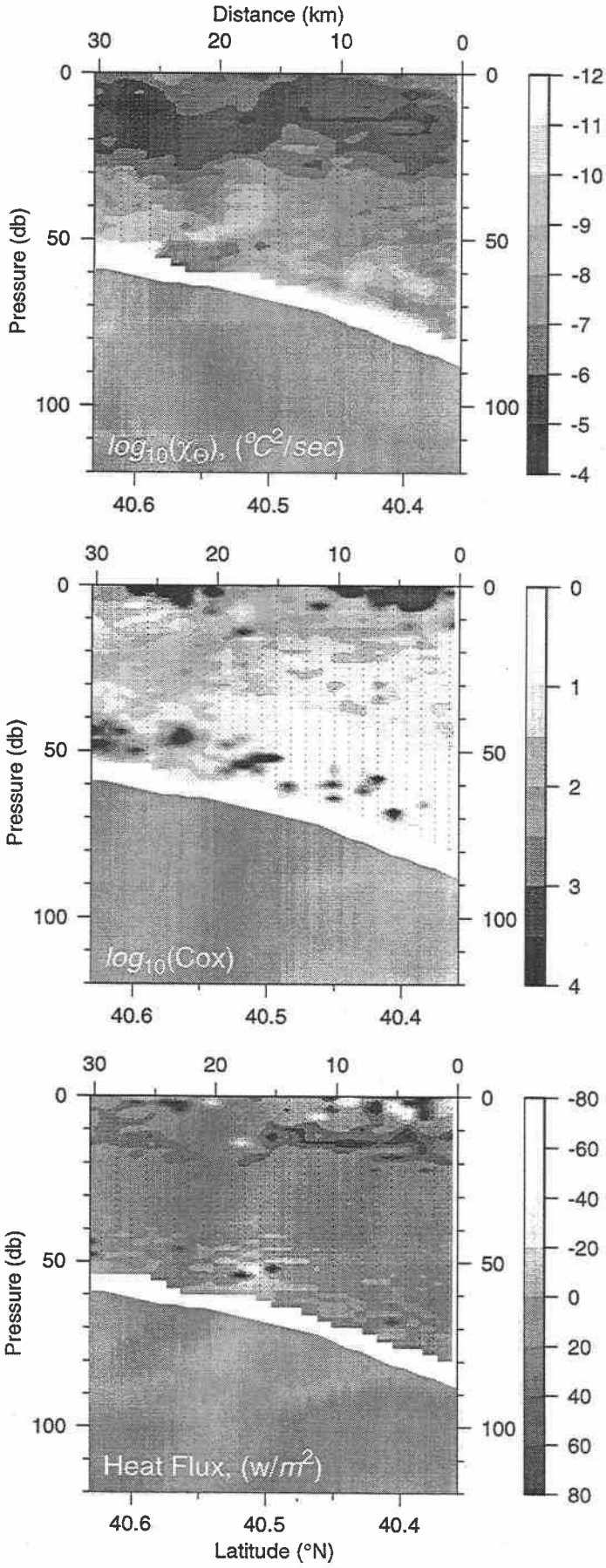

E9608 Butterfly 1

27-Aug-96 04:07 - 27-Aug-96 05:22

Line bf1we

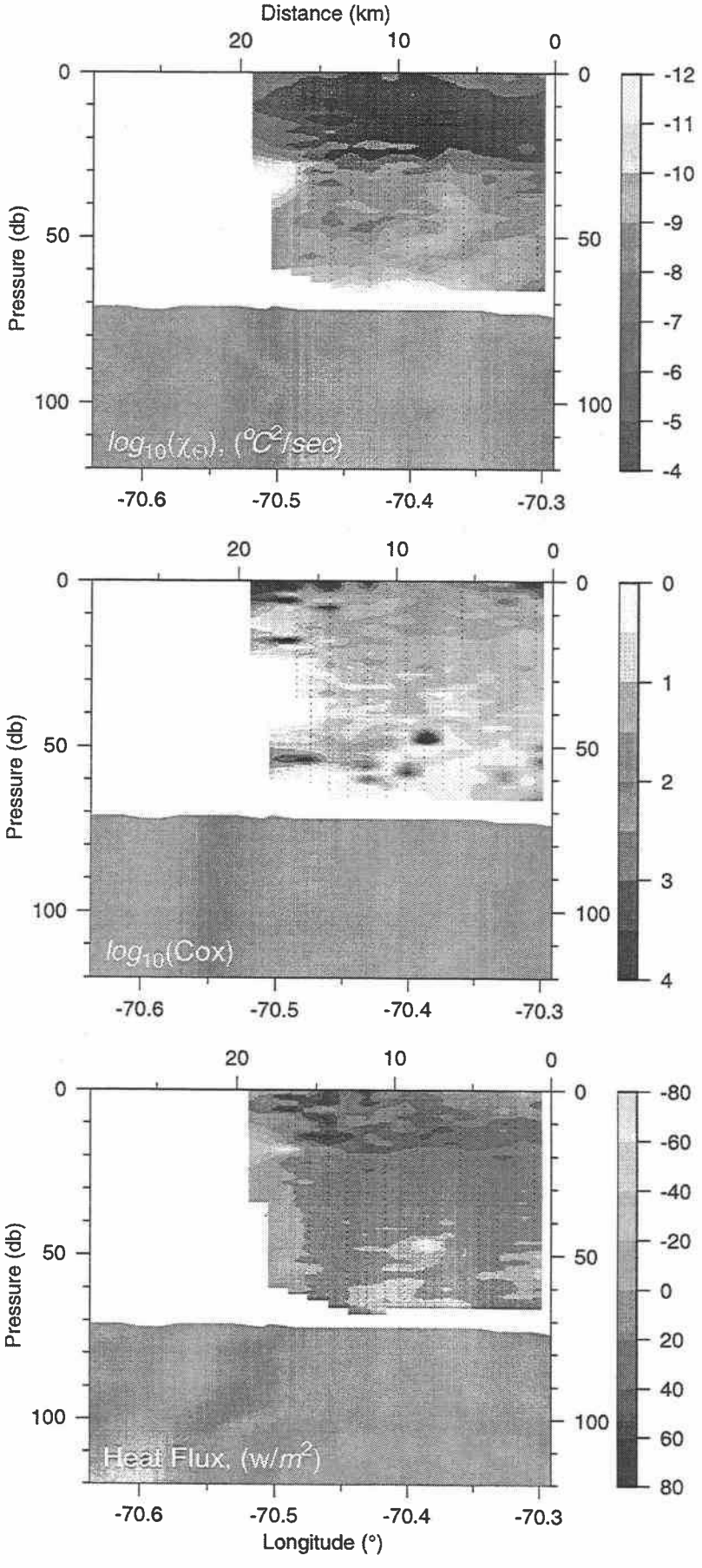

e9608 Butterfly 2

27-Aug-96 17:32 - 27-Aug-96 19:58

Line bf2ns

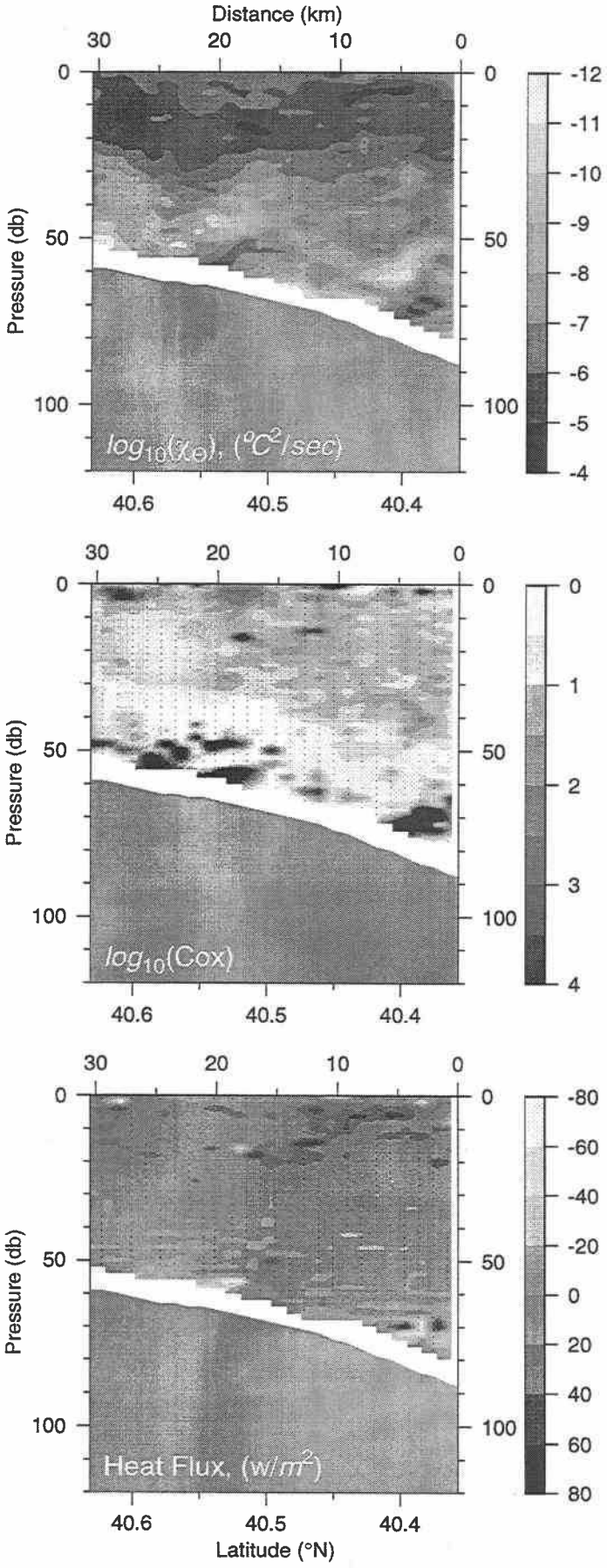

E9608 Butterfly 2

27-Aug-96 11:13 - 27-Aug-96 14:13

Line bf2we

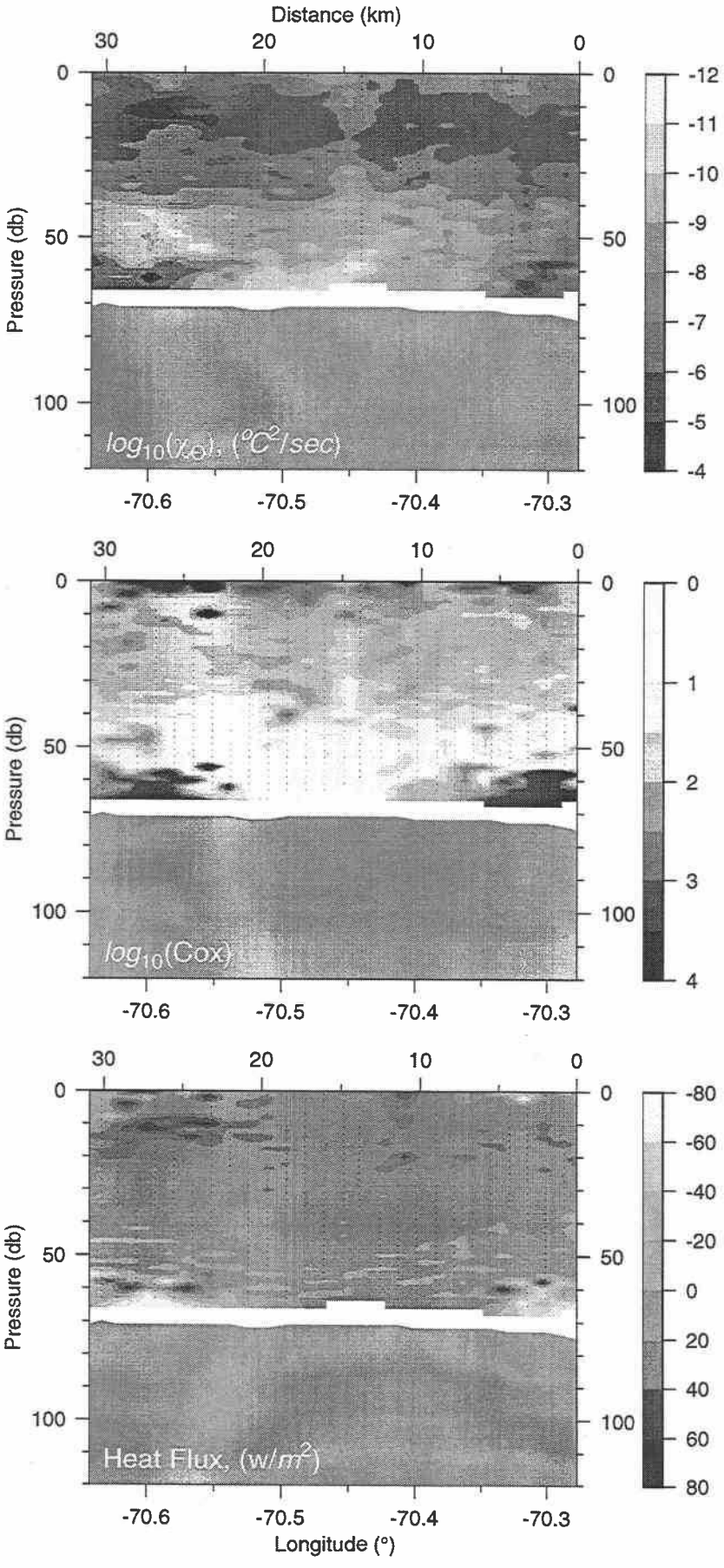

e9608 Butterfly 3

28-Aug-96 04:50 - 28-Aug-96 07:18

Line bf3ns

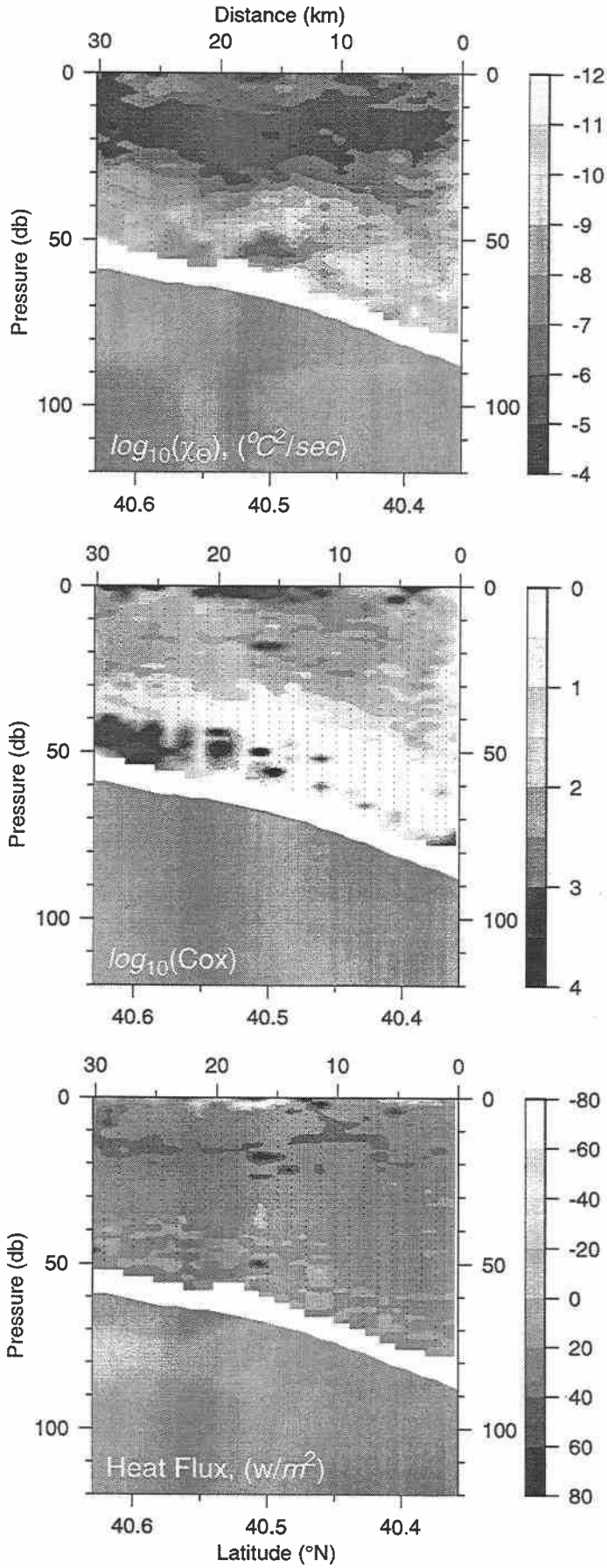

E9608 Butterfly 3

27-Aug-96 23:53 - 28-Aug-96 02:35

Line bf3we

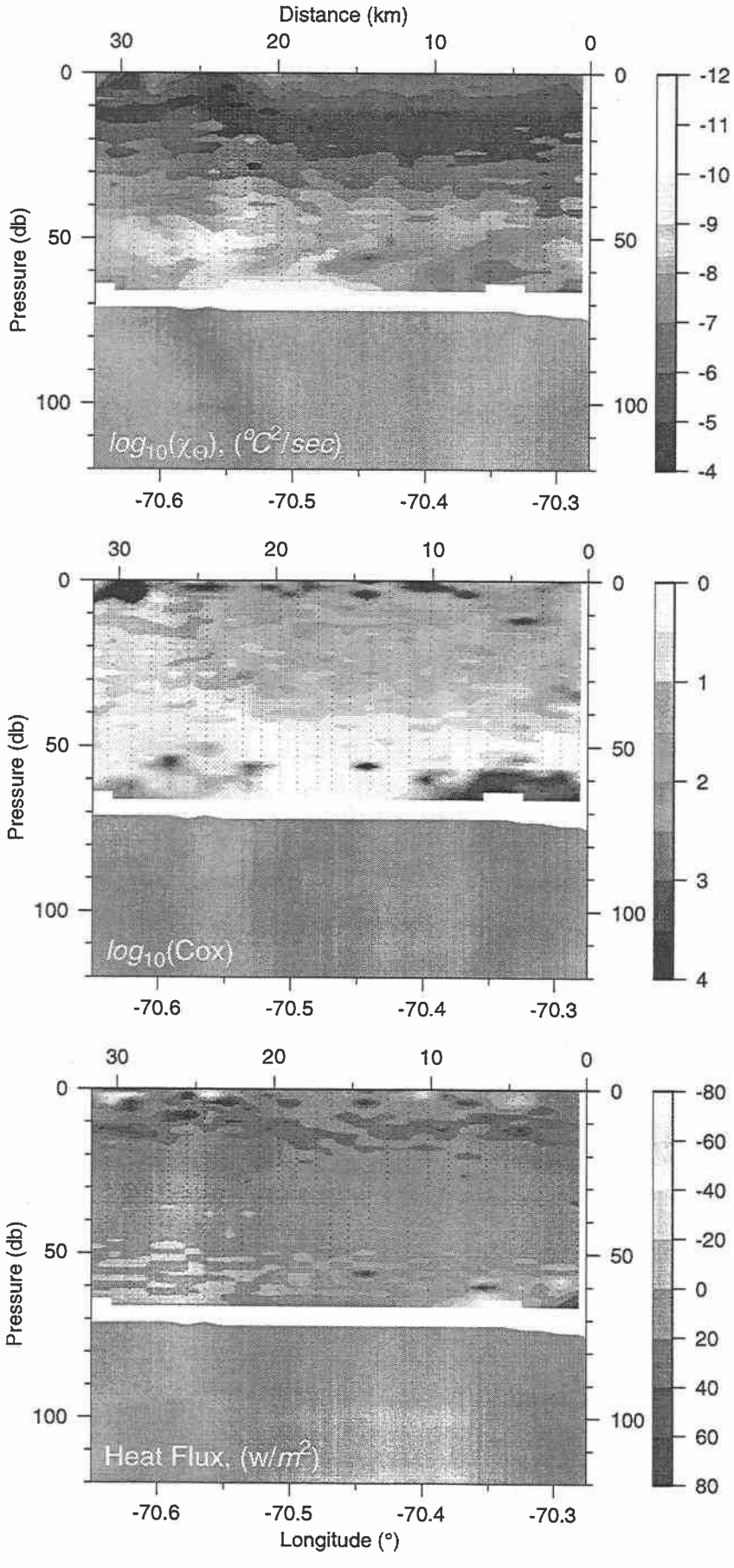

e9608 Butterfly 4

28-Aug-96 11:10 - 28-Aug-96 14:51

Line bf4ns

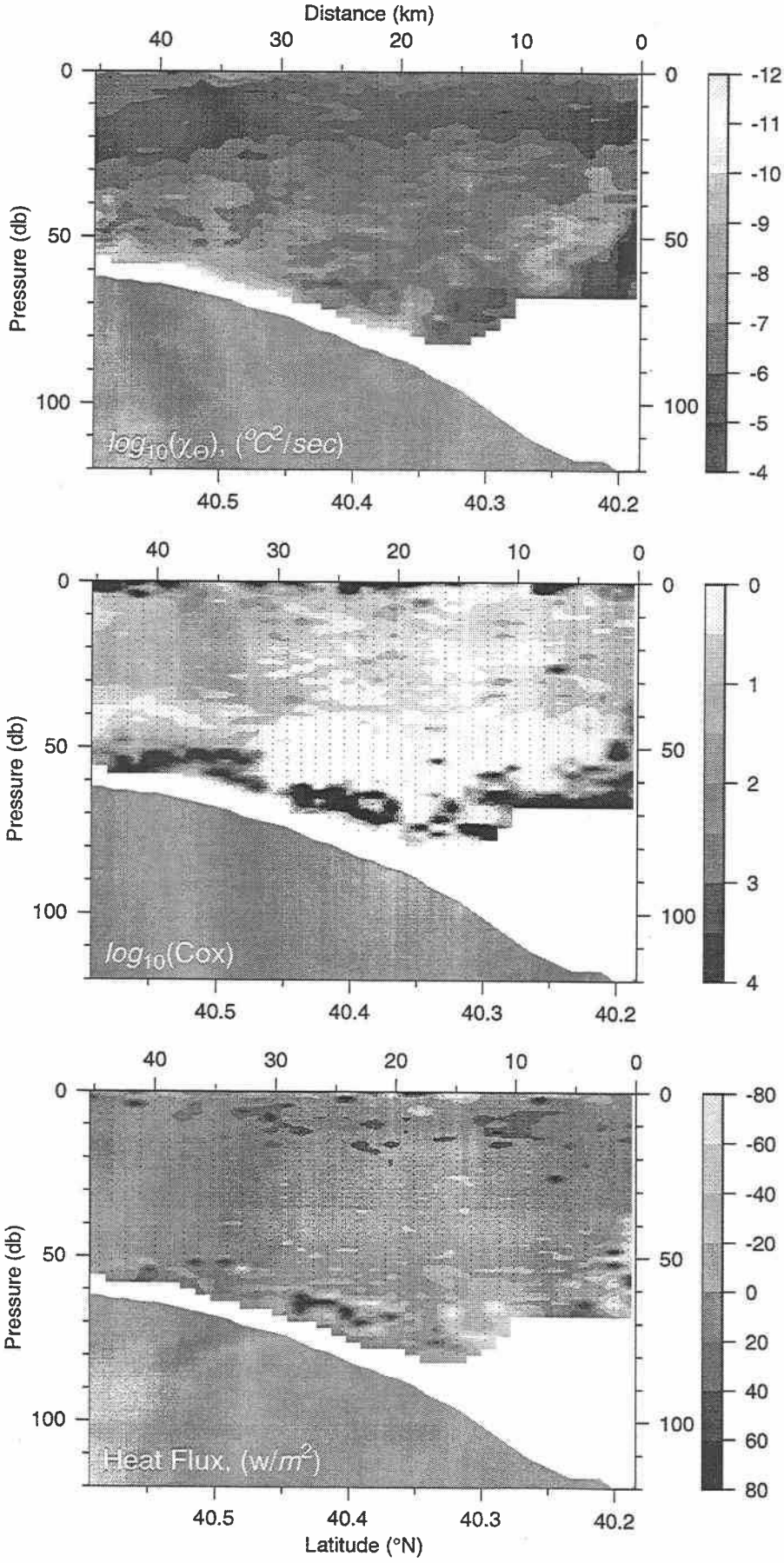

e9608 Butterfly 4

28-Aug-96 14:54 - 28-Aug-96 17:08

Line bf4sn

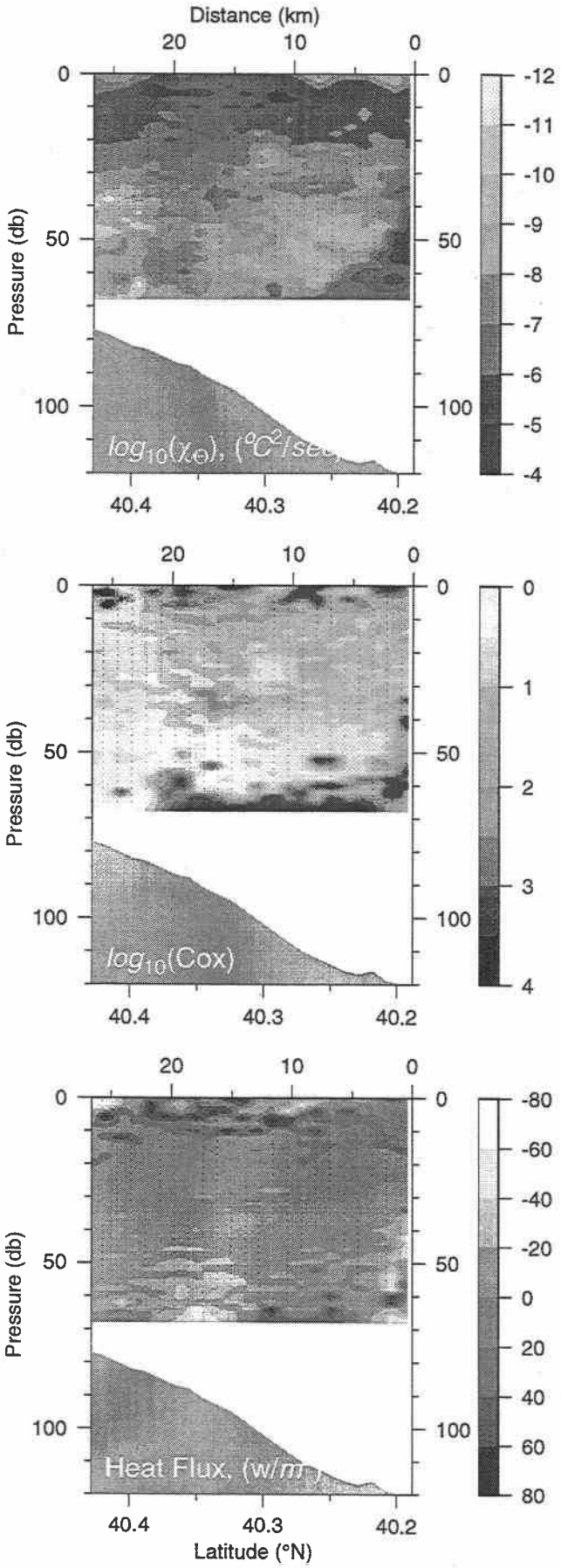

E9608 Small Box 1

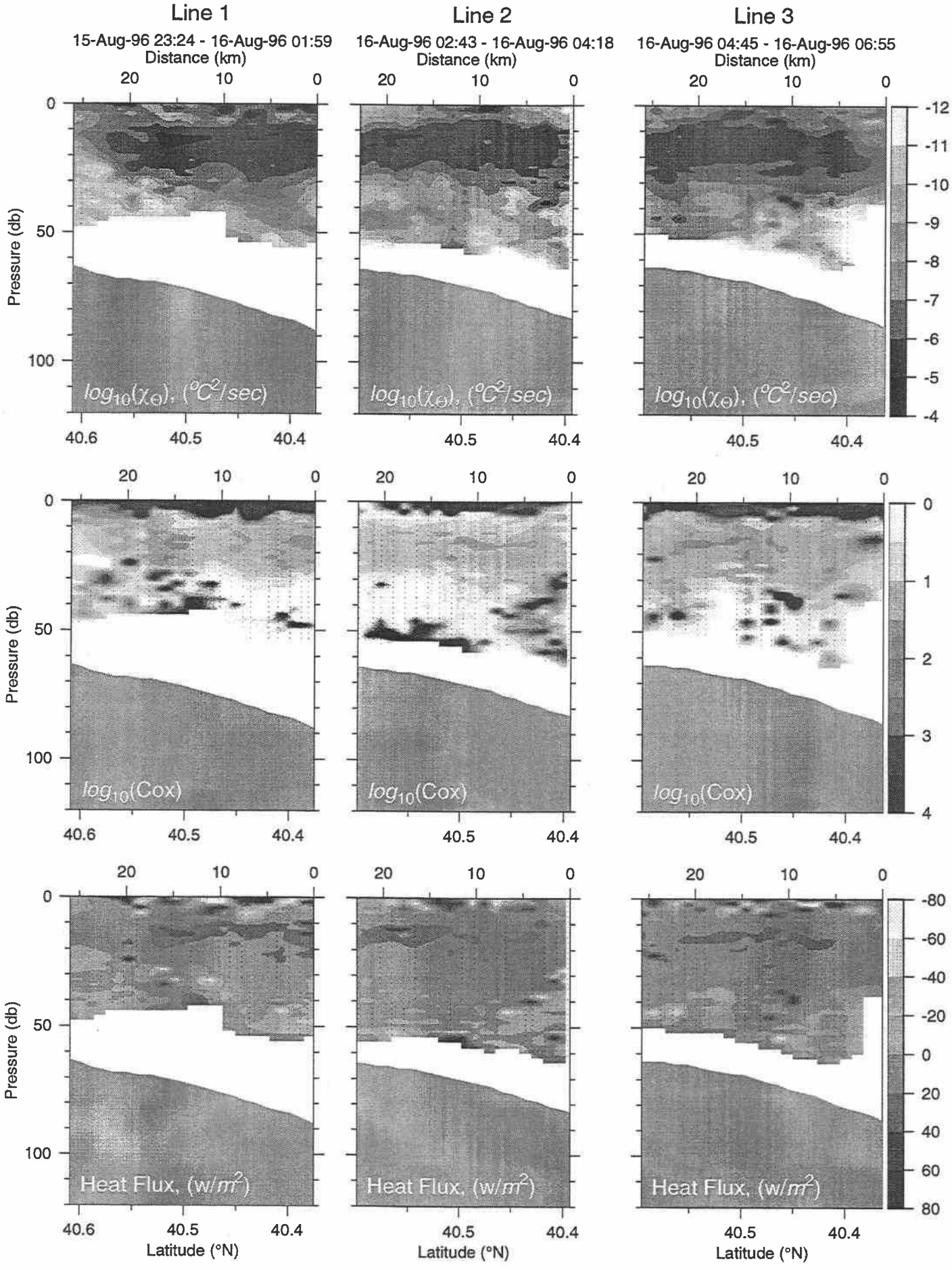

E9608 Small Box 1

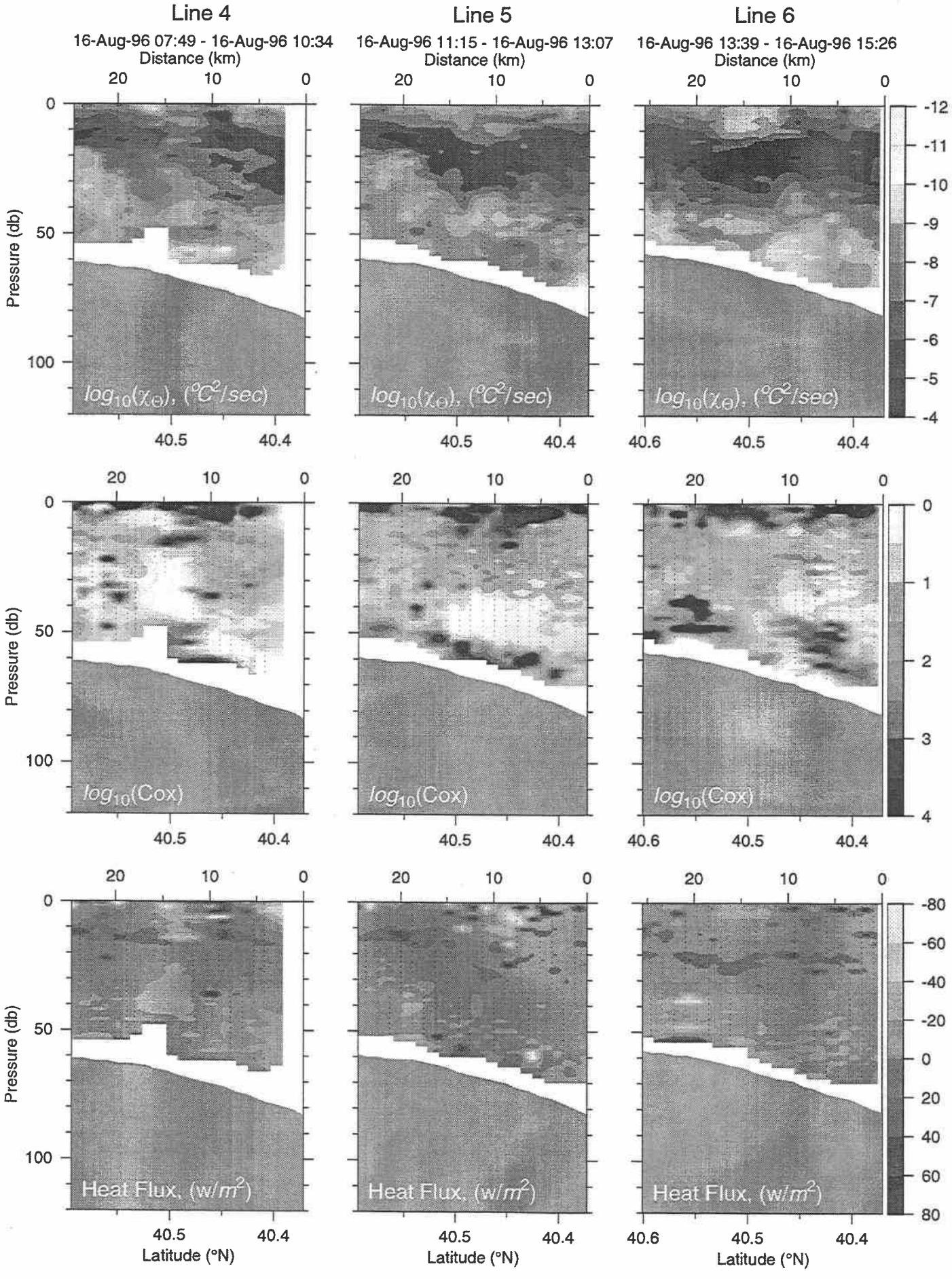

E9608 Small Box 3

19-Aug-96 01:49 - 19-Aug-96 03:08

Line sb2_sb3

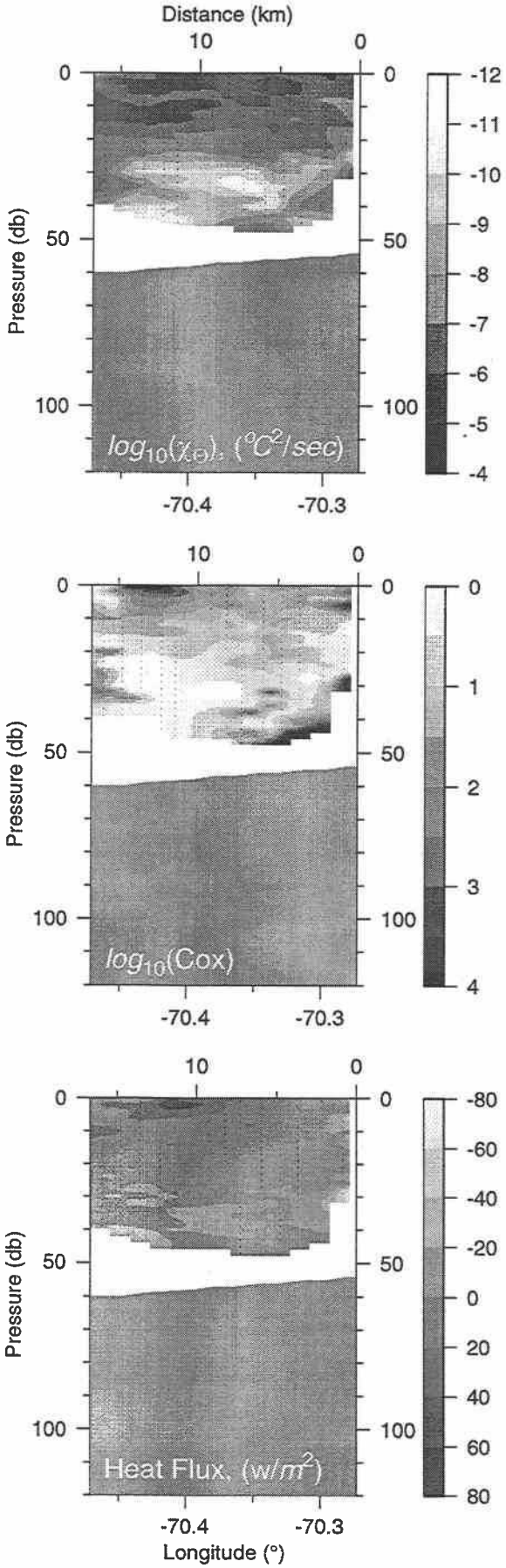

E9608 Small Box 2

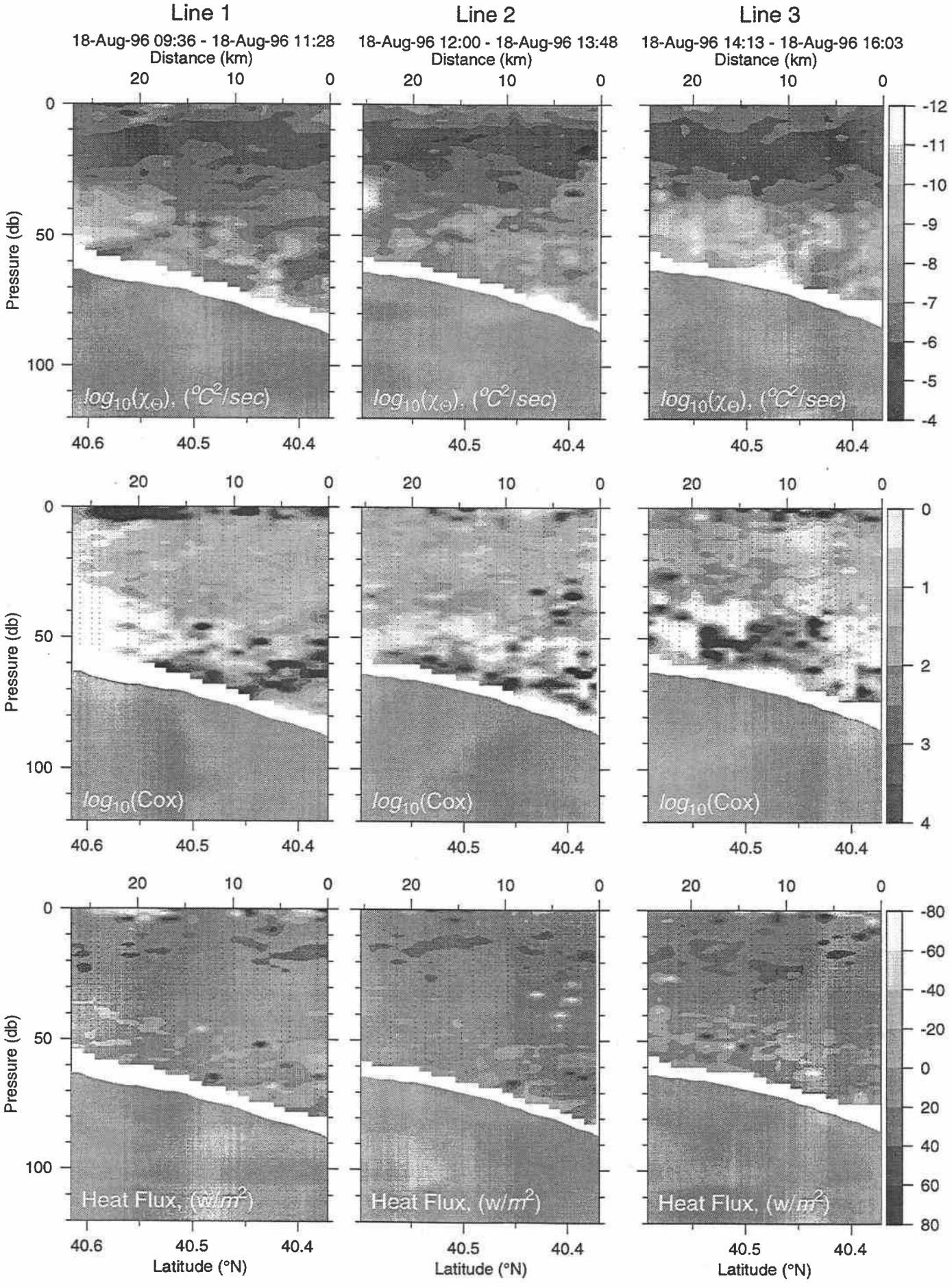

E9608 Small Box 2

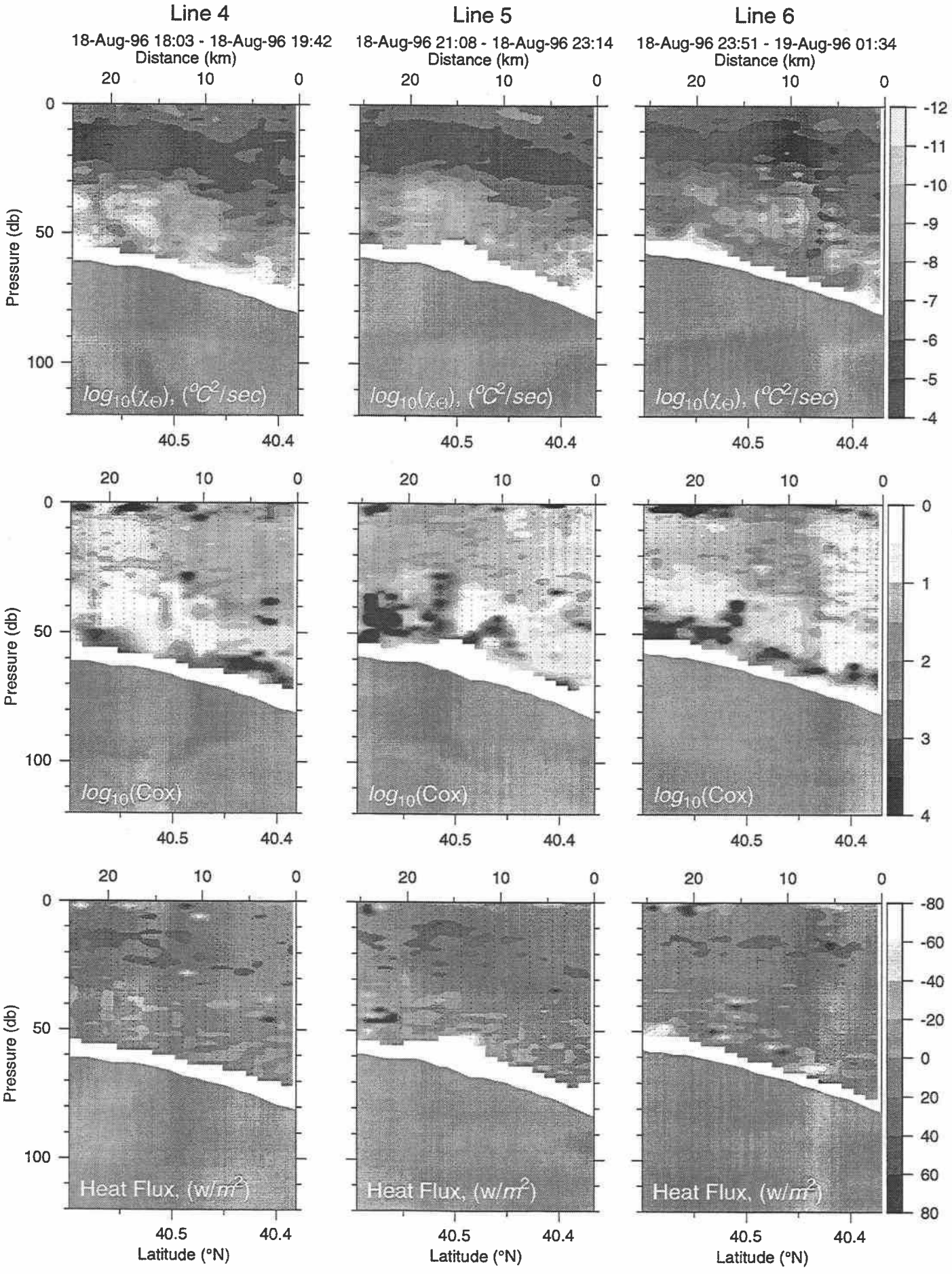

E9608 Small Box 3

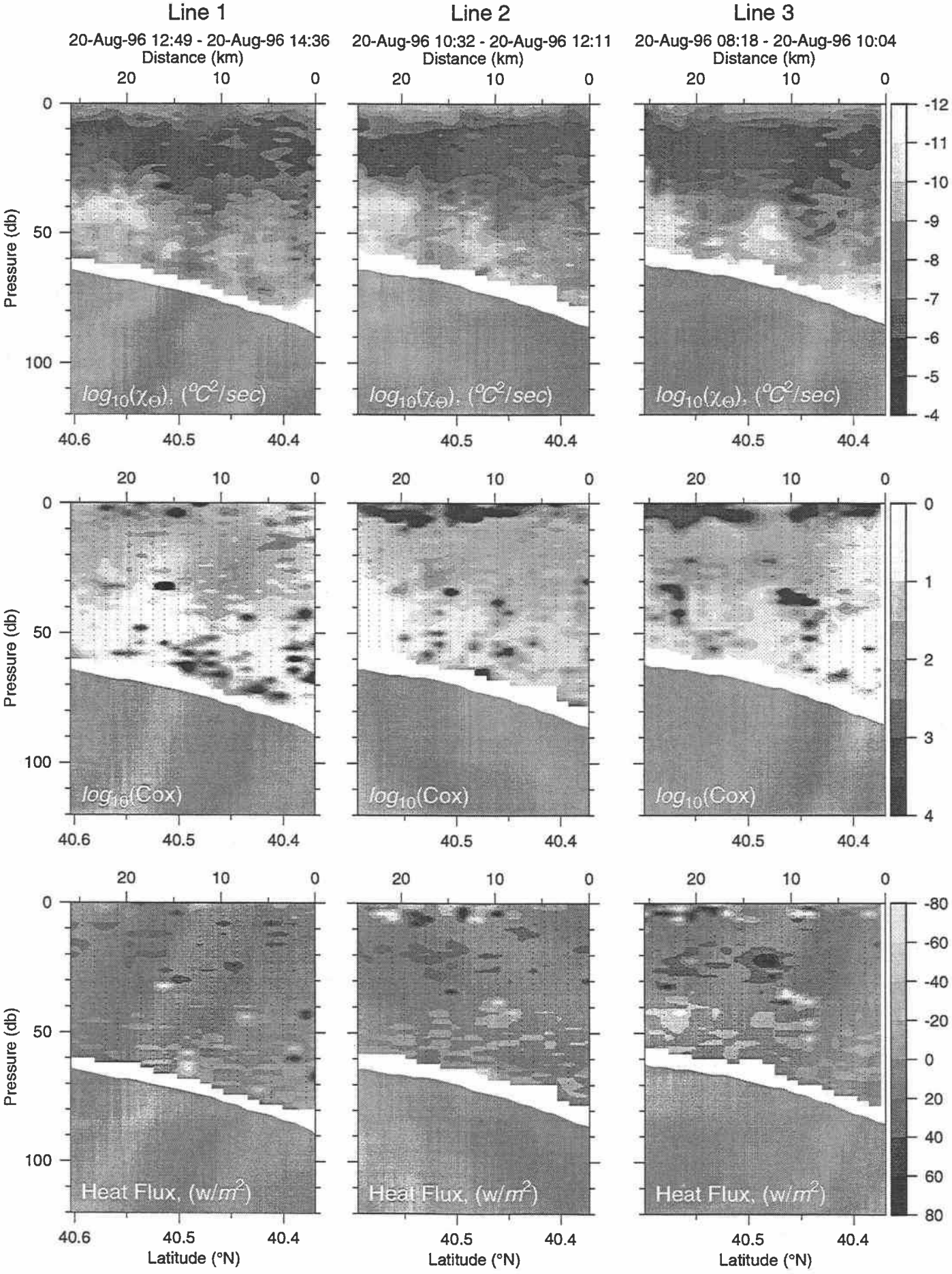

E9608 Small Box 3

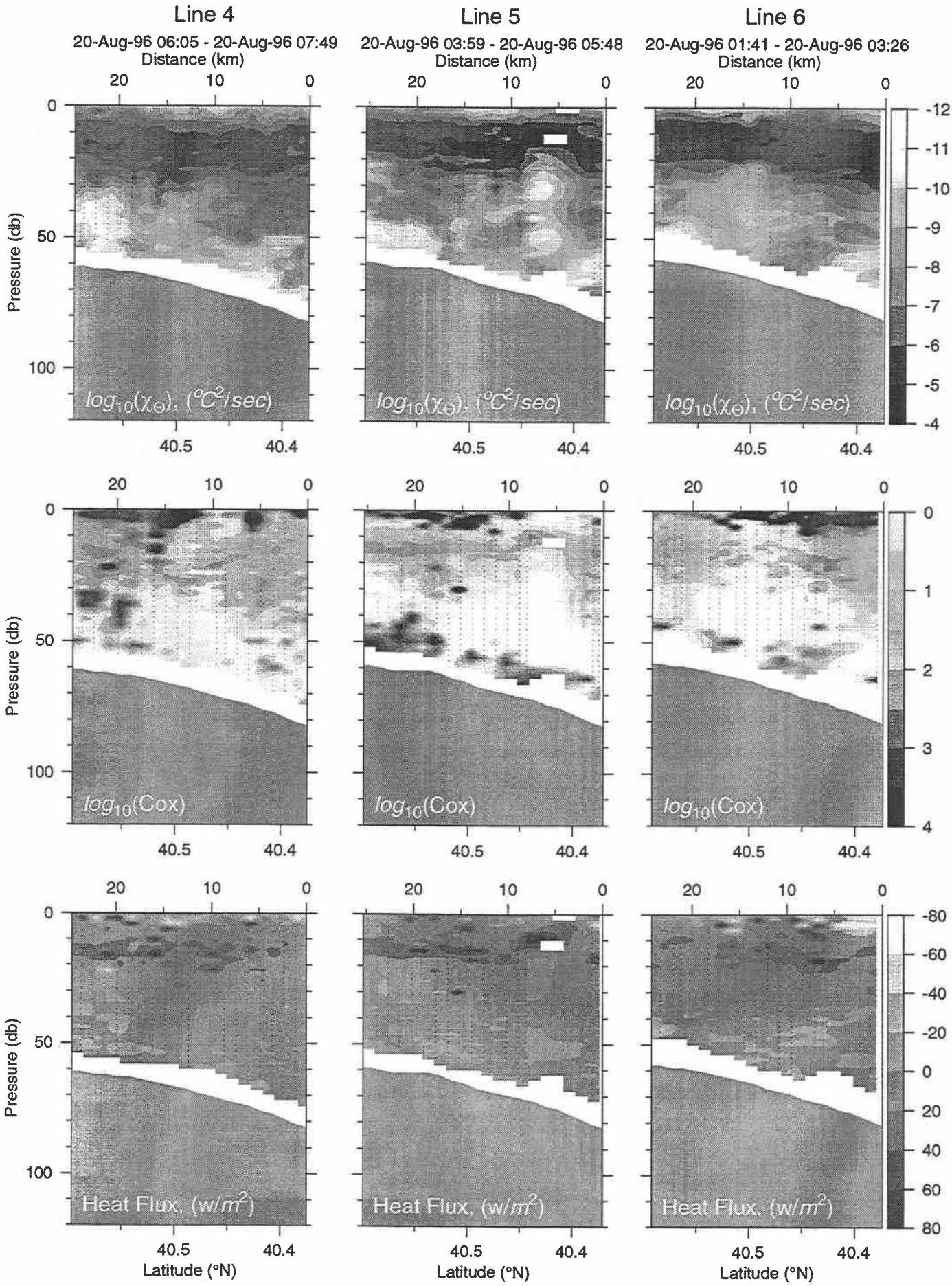

E9608 Small Box 7

16-Aug-96 04:45 - 16-Aug-96 06:55

Line 3

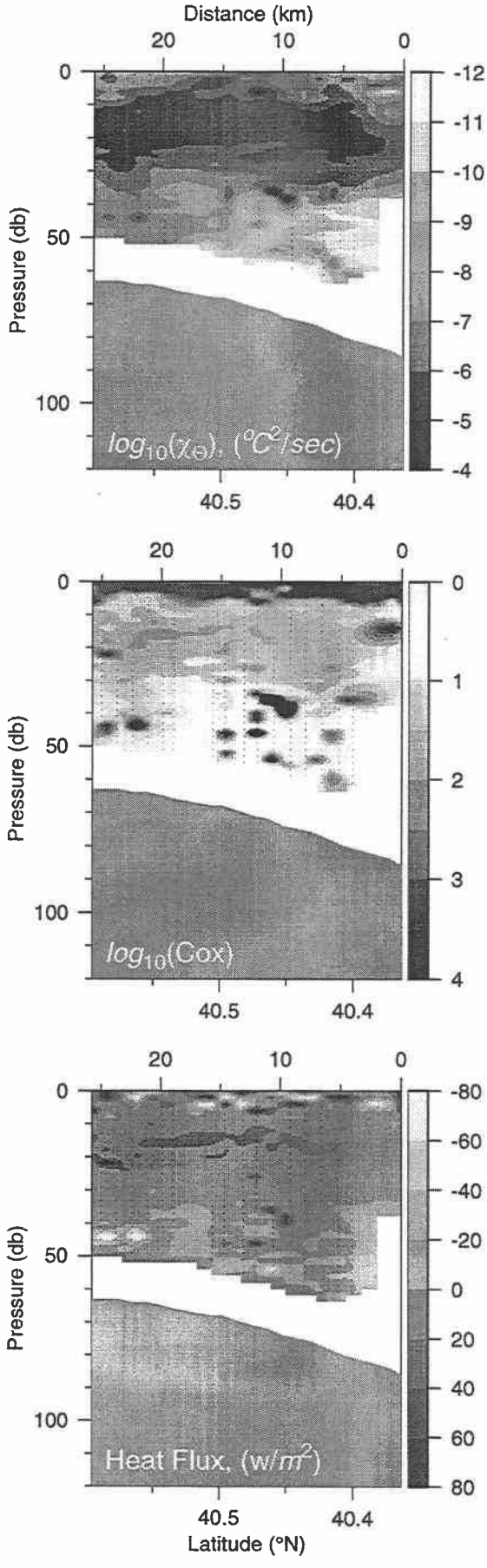

E9608 Small Box 7

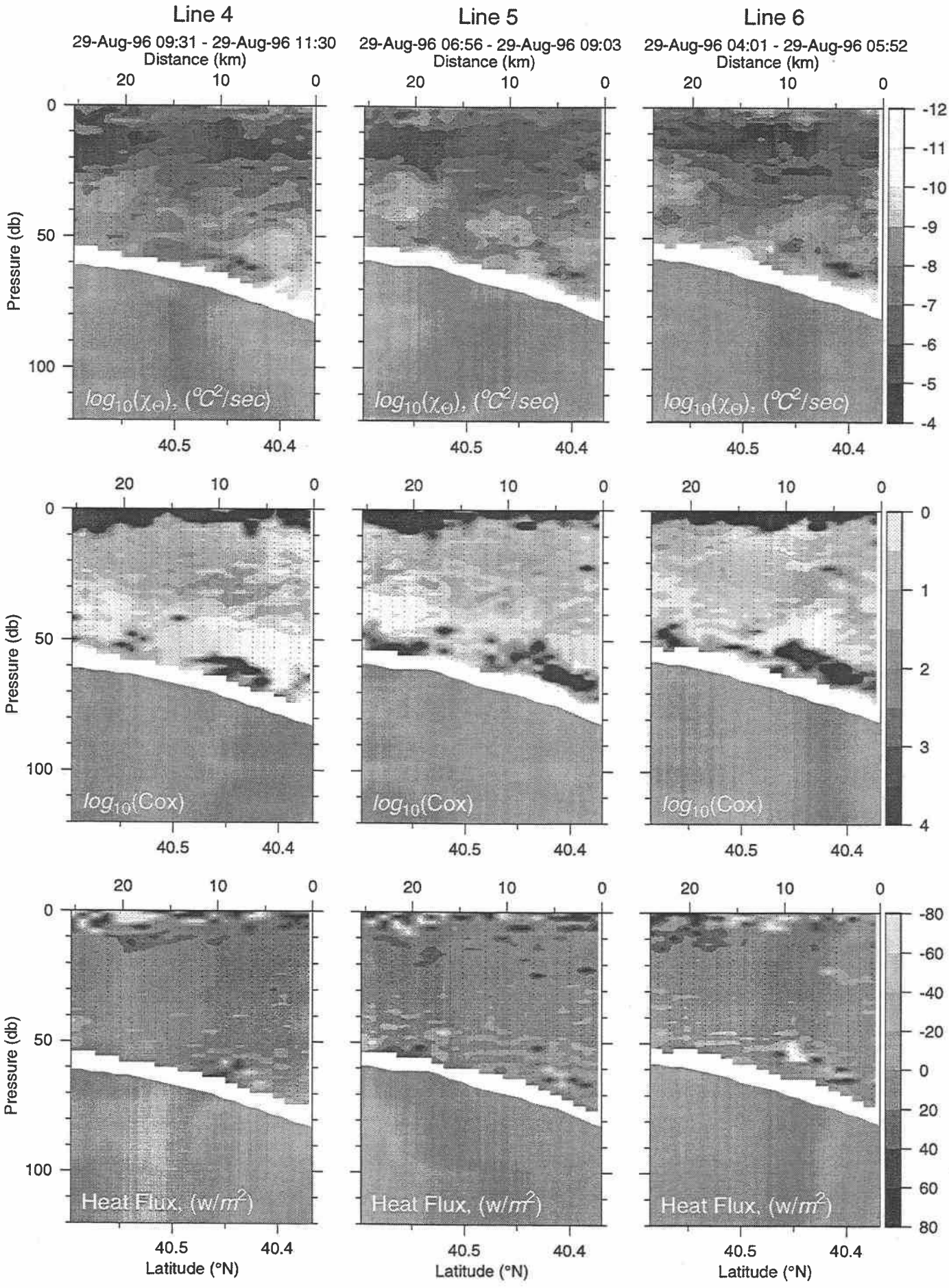

E9608 Big Box 3

31-Aug-96 05:00 - 31-Aug-96 05:48

Line sb9_bb3

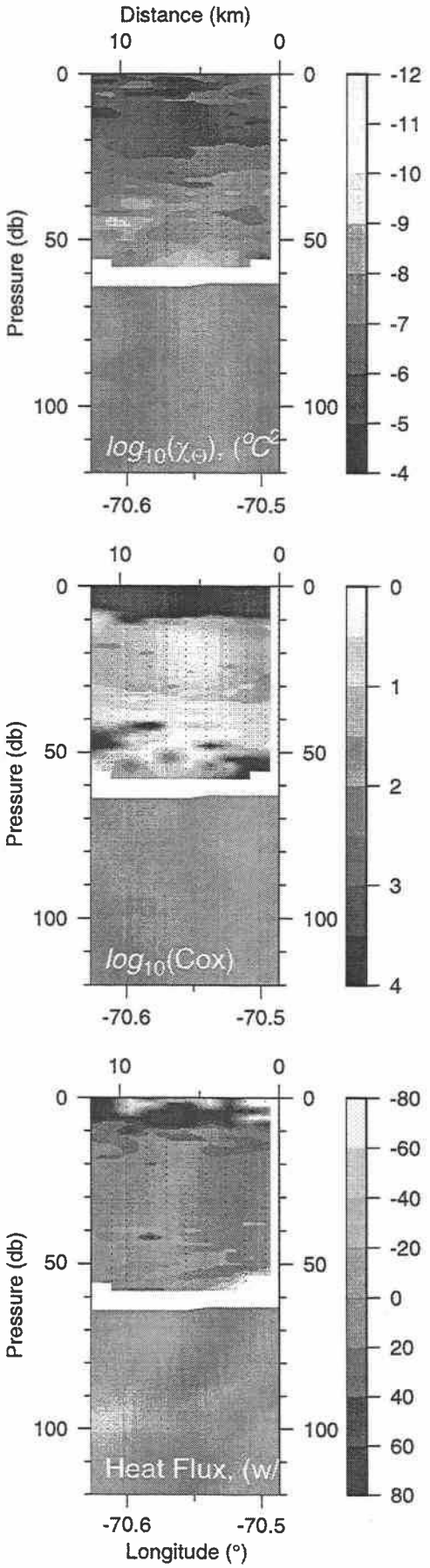

E9608 Small Box 9

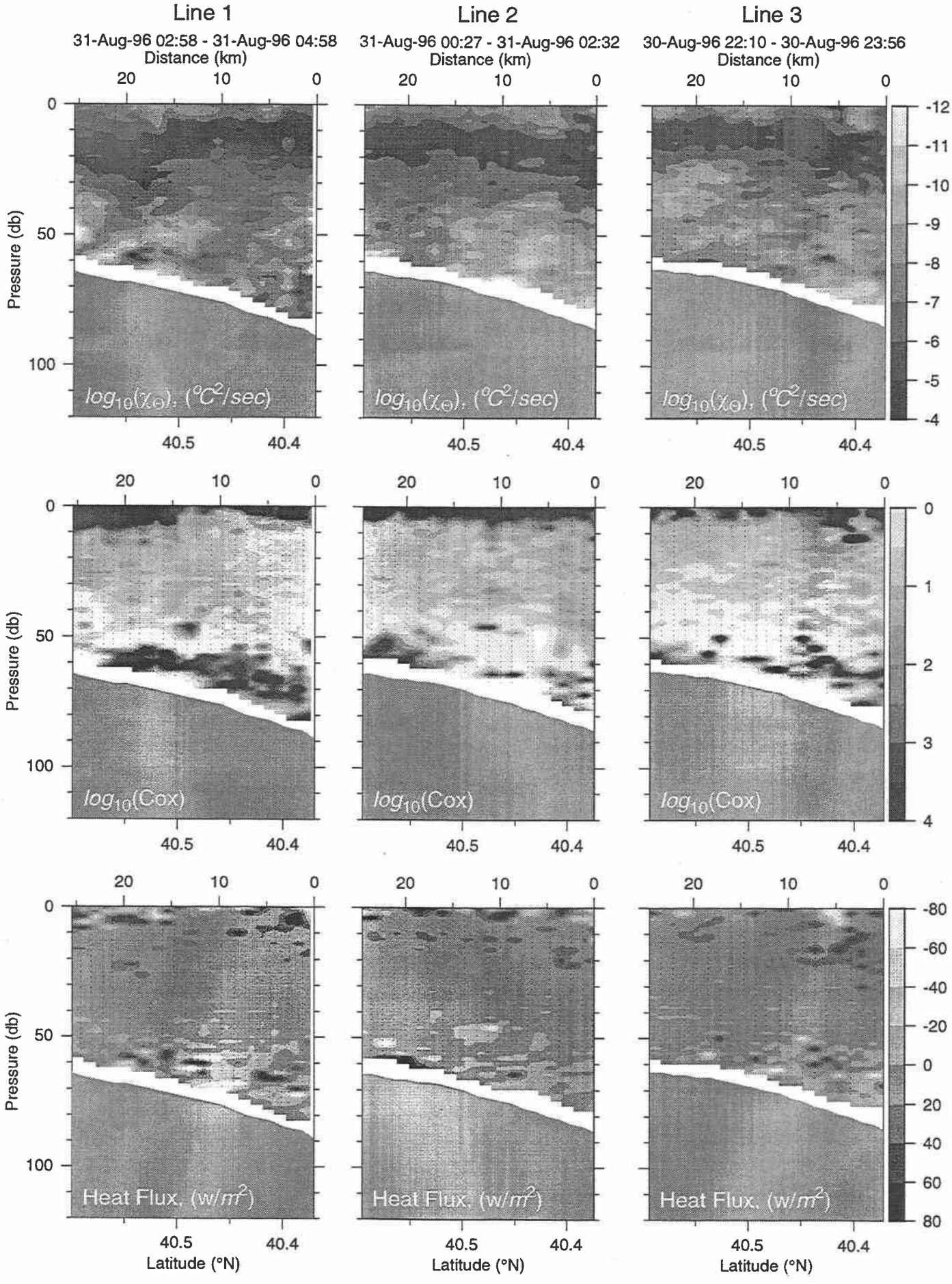

E9608 Small Box 9

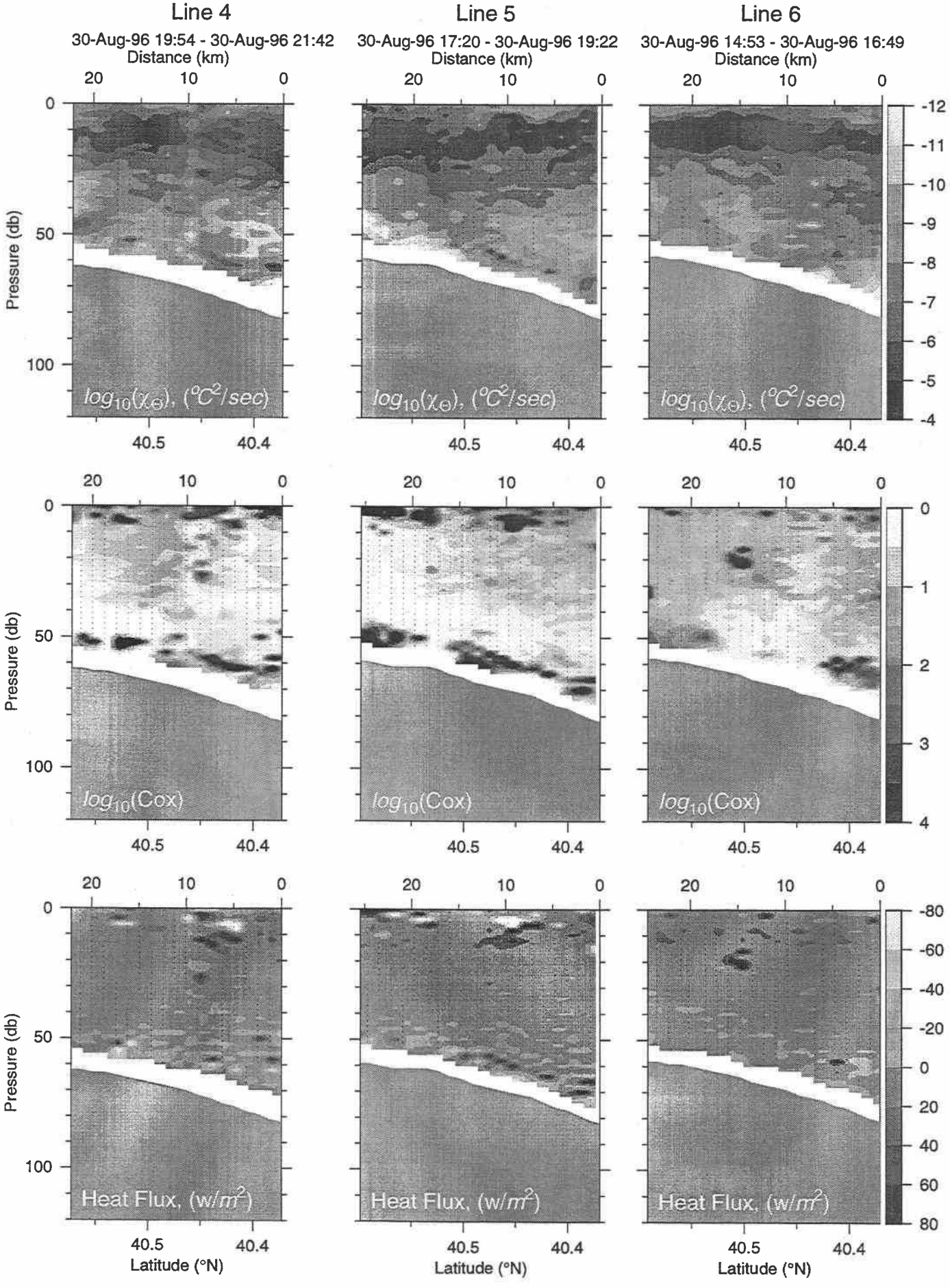

Maps of Temperature Variance Dissipation Rate, Cox number and Heat Flux

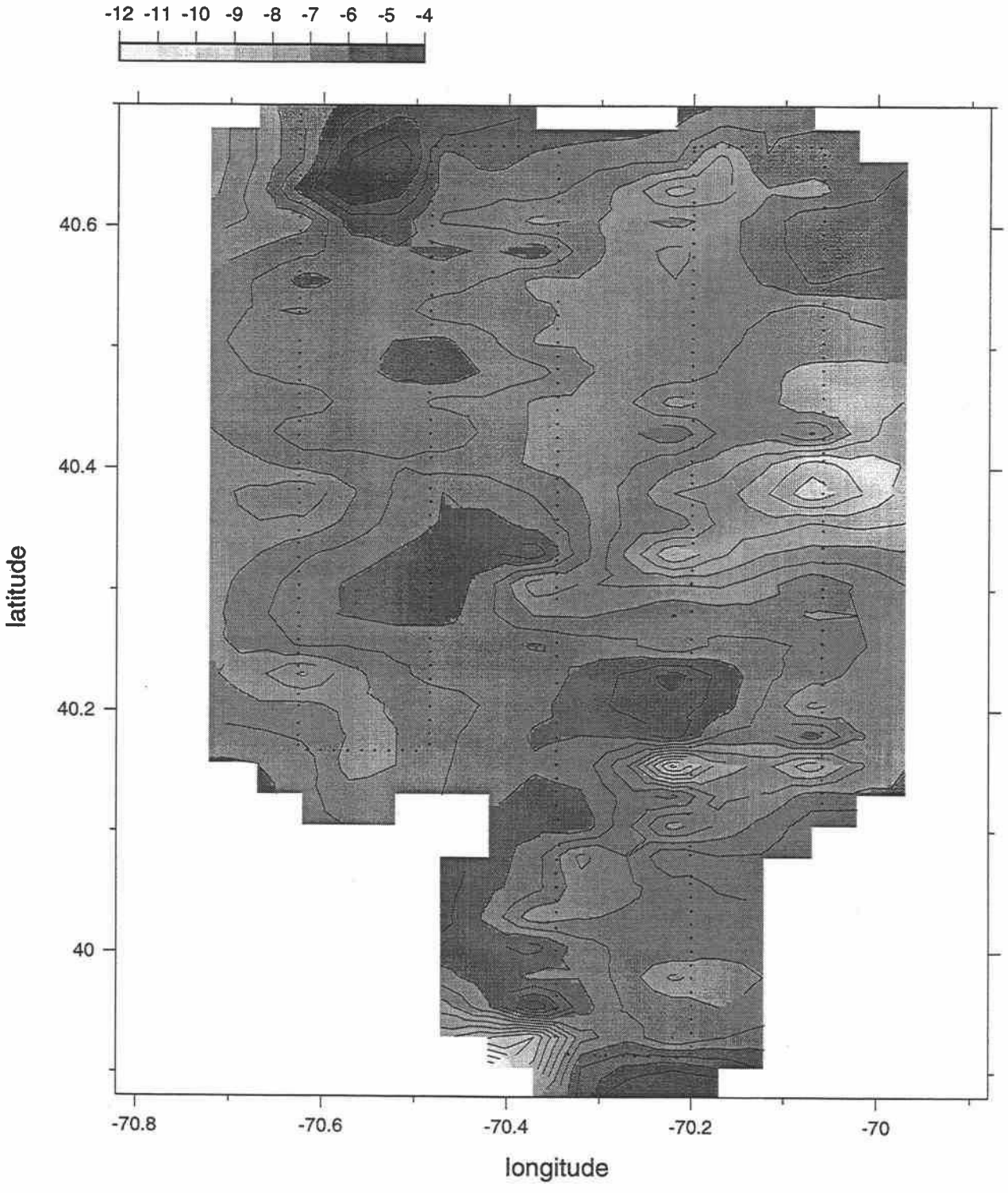
E9608 Big Box 1
17-Aug-96 02:09:20 - 18-Aug-96 09:07:04
Map View at 5 dbar
log10(χΘ), (°C²/ sec)
-12 -11 -10 -9 -8 -7 -6 -5 -4
40.6
40.4
40.2
40
latitude
-70.8
-70.6
-70.4
-70.2
-70
longitude

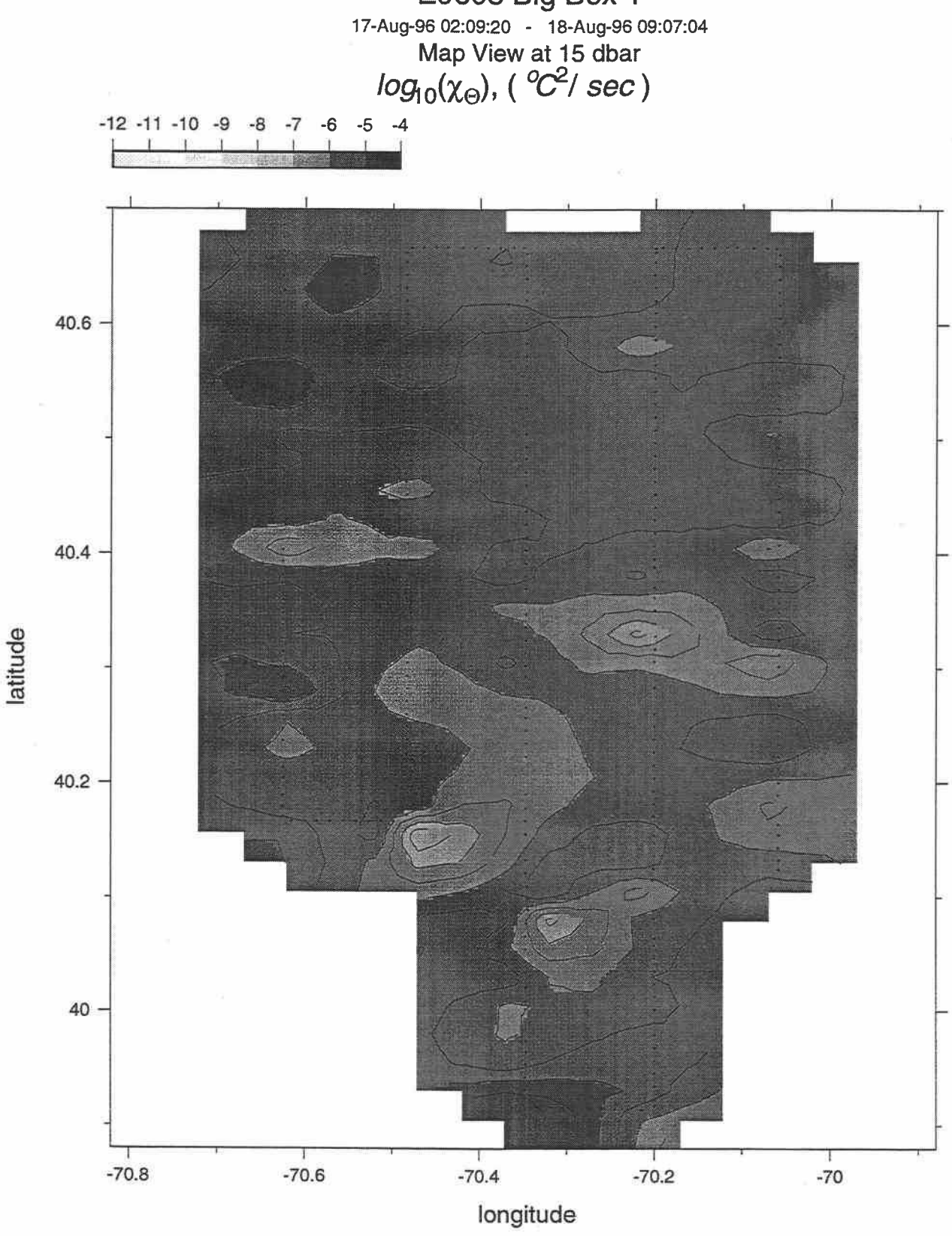
E9608 Big Box 1
17-Aug-96 02:09:20 - 18-Aug-96 09:07:04
Map View at 15 dbar
$log_{10}(\chi_\Theta)$, ($^oC^2$/ sec)
-12 -11 -10 -9 -8 -7 -6 -5 -4
40.6
40.4
40.2
40
latitude
-70.8
-70.6
-70.4
-70.2
-70
longitude

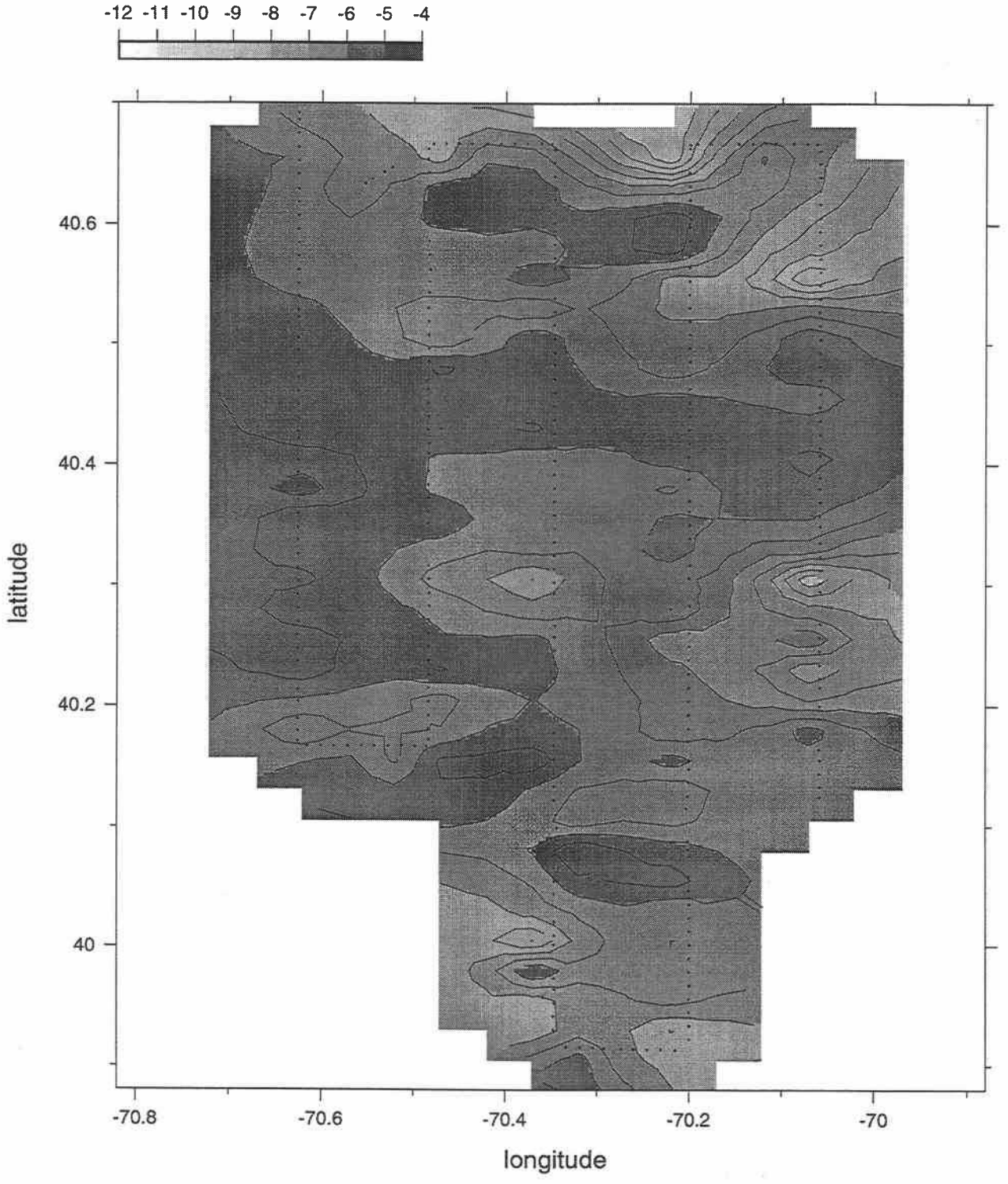
E9608 Big Box 1
17-Aug-96 02:09:20 - 18-Aug-96 09:07:04
Map View at 25 dbar
$log_{10}(\chi_\Theta)$, ($^oC^2/sec$)
-12 -11 -10 -9 -8 -7 -6 -5 -4
40.6
40.4
40.2
40
latitude
-70.8
-70.6
-70.4
-70.2
-70
longitude

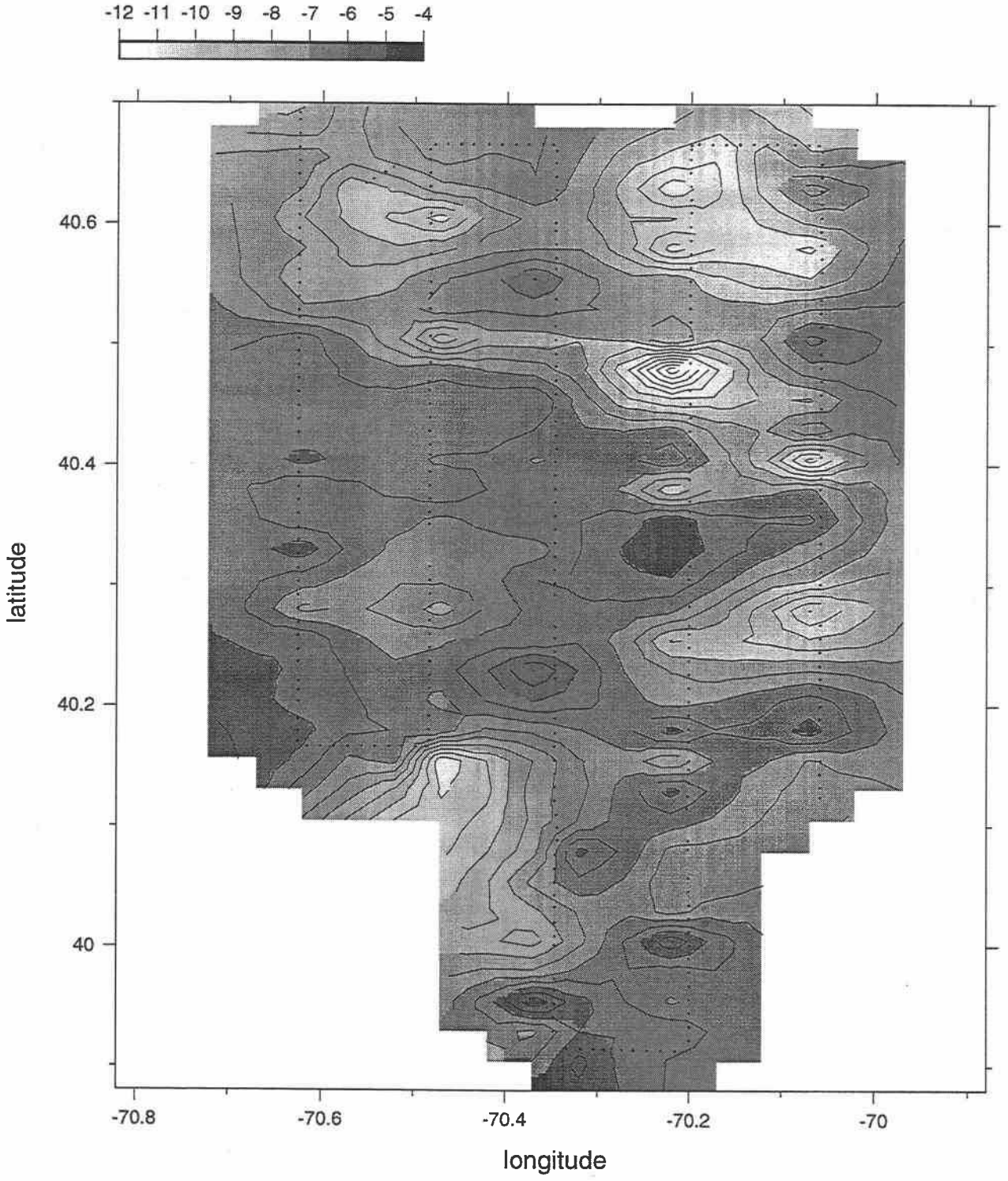
E9608 Big Box 1
17-Aug-96 02:09:20 - 18-Aug-96 09:07:04
Map View at 35 dbar
$log_{10}(\chi_\Theta)$, ($^oC^2/sec$)
-12 -11 -10 -9 -8 -7 -6 -5 -4
40.6
40.4
40.2
40
latitude
-70.8
-70.6
-70.4
-70.2
-70
longitude

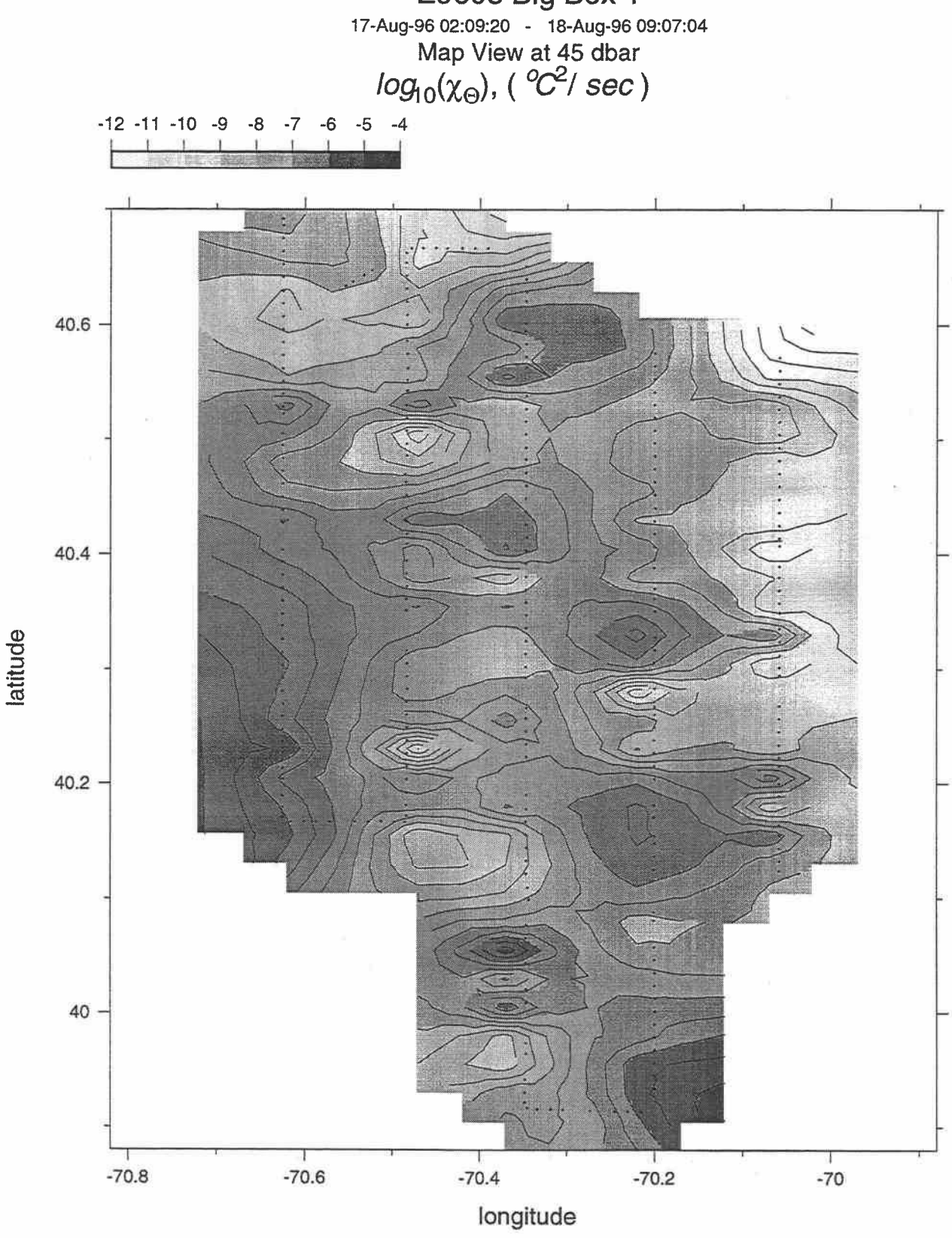
E9608 Big Box 1
17-Aug-96 02:09:20 - 18-Aug-96 09:07:04
Map View at 45 dbar
$log_{10}(\chi_\Theta)$, ($^oC^2$/ sec)
-12 -11 -10 -9 -8 -7 -6 -5 -4
40.6
40.4
40.2
40
latitude
-70.8
-70.6
-70.4
-70.2
-70
longitude

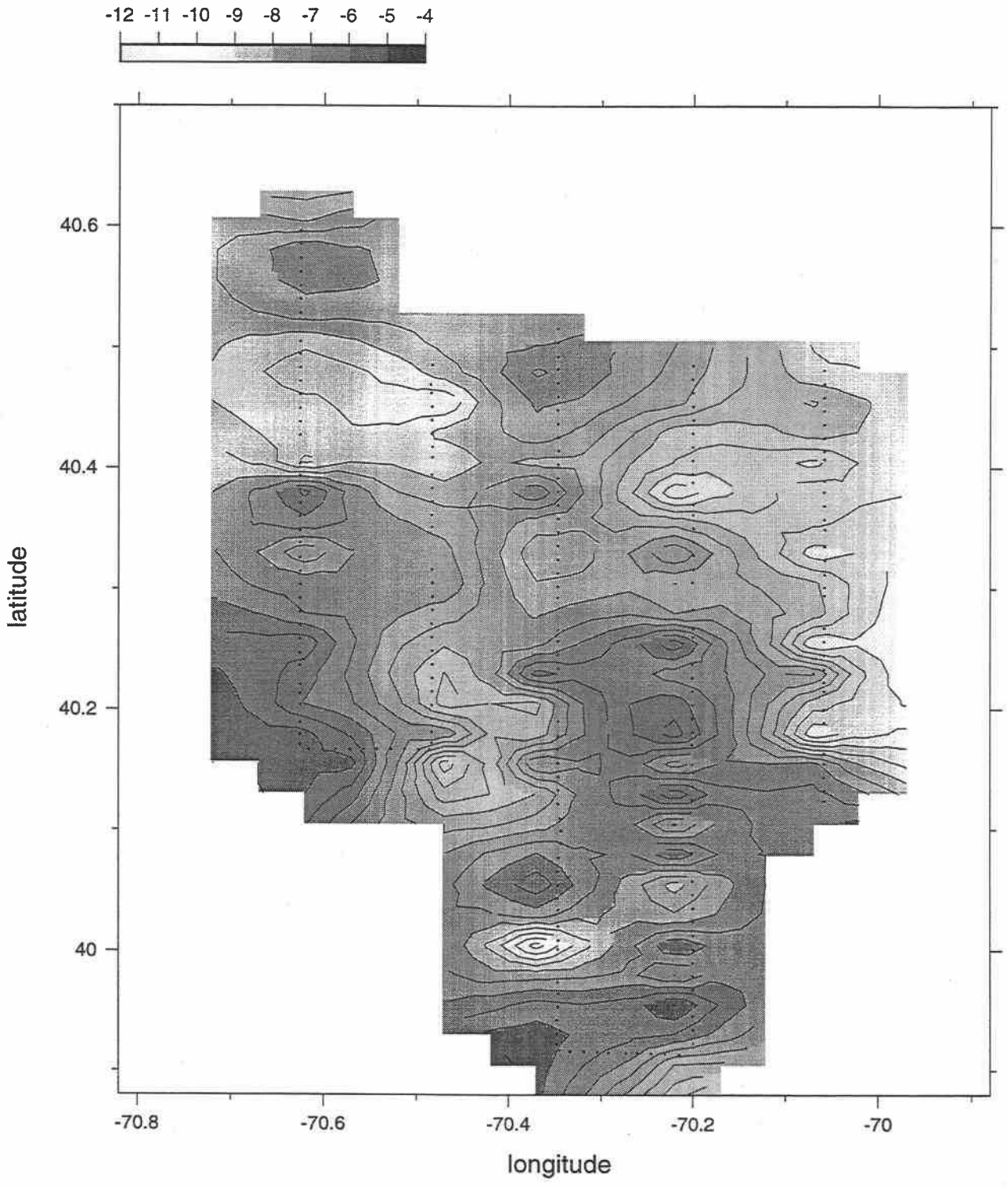
E9608 Big Box 1
17-Aug-96 02:09:20 - 18-Aug-96 09:07:04
Map View at 55 dbar
$log_{10}(\chi_\Theta)$, ($^oC^2$/ sec)
-12 -11 -10 -9 -8 -7 -6 -5 -4
40.6
40.4
40.2
40
latitude
-70.8
-70.6
-70.4
-70.2
-70
longitude

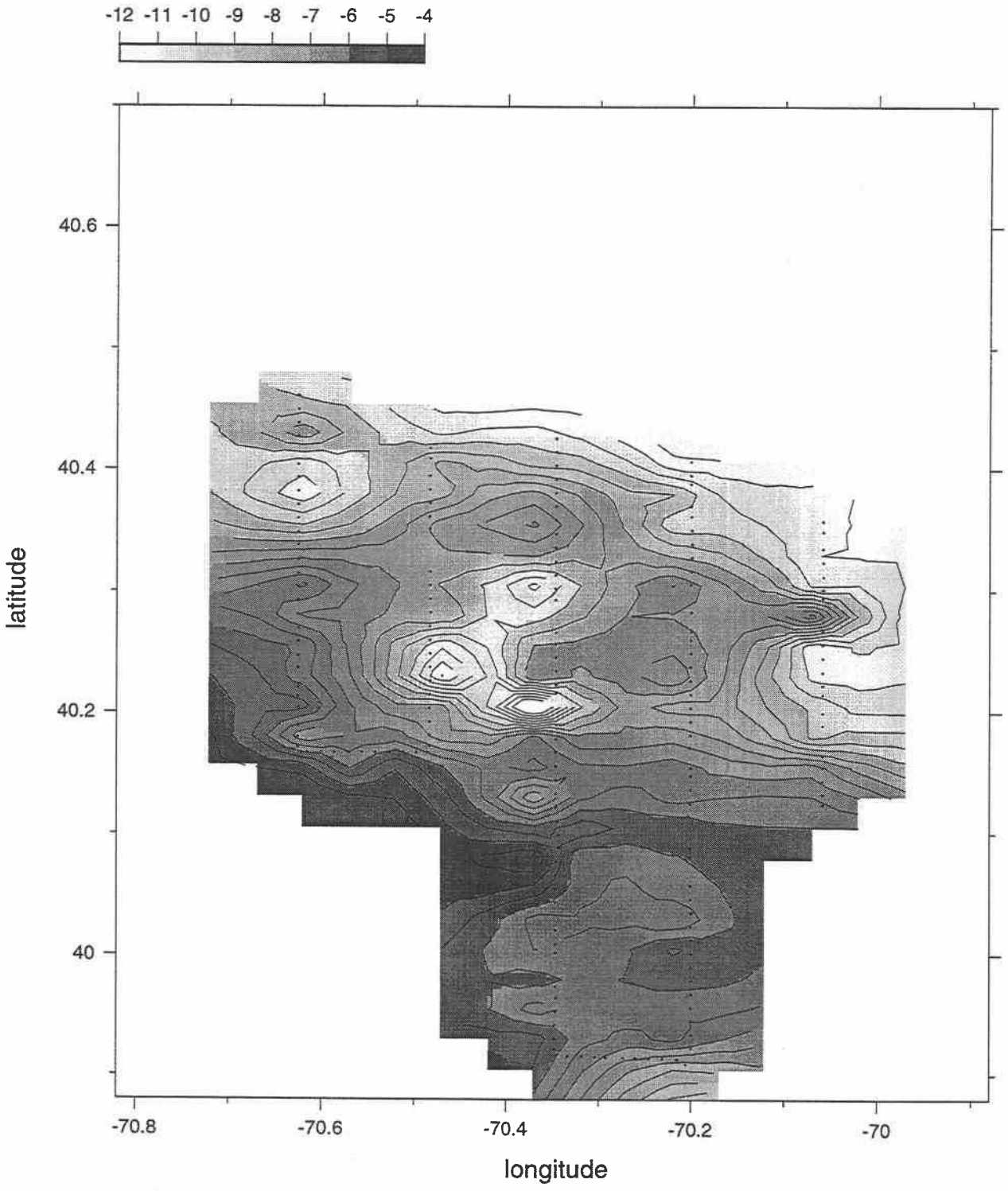
E9608 Big Box 1
17-Aug-96 02:09:20 - 18-Aug-96 09:07:04
Map View at 65 dbar
$log_{10}(\chi_\Theta)$, ($^oC^2$/ sec)
-12 -11 -10 -9 -8 -7 -6 -5 -4
40.6
40.4
40.2
40
latitude
-70.8
-70.6
-70.4
-70.2
-70
longitude

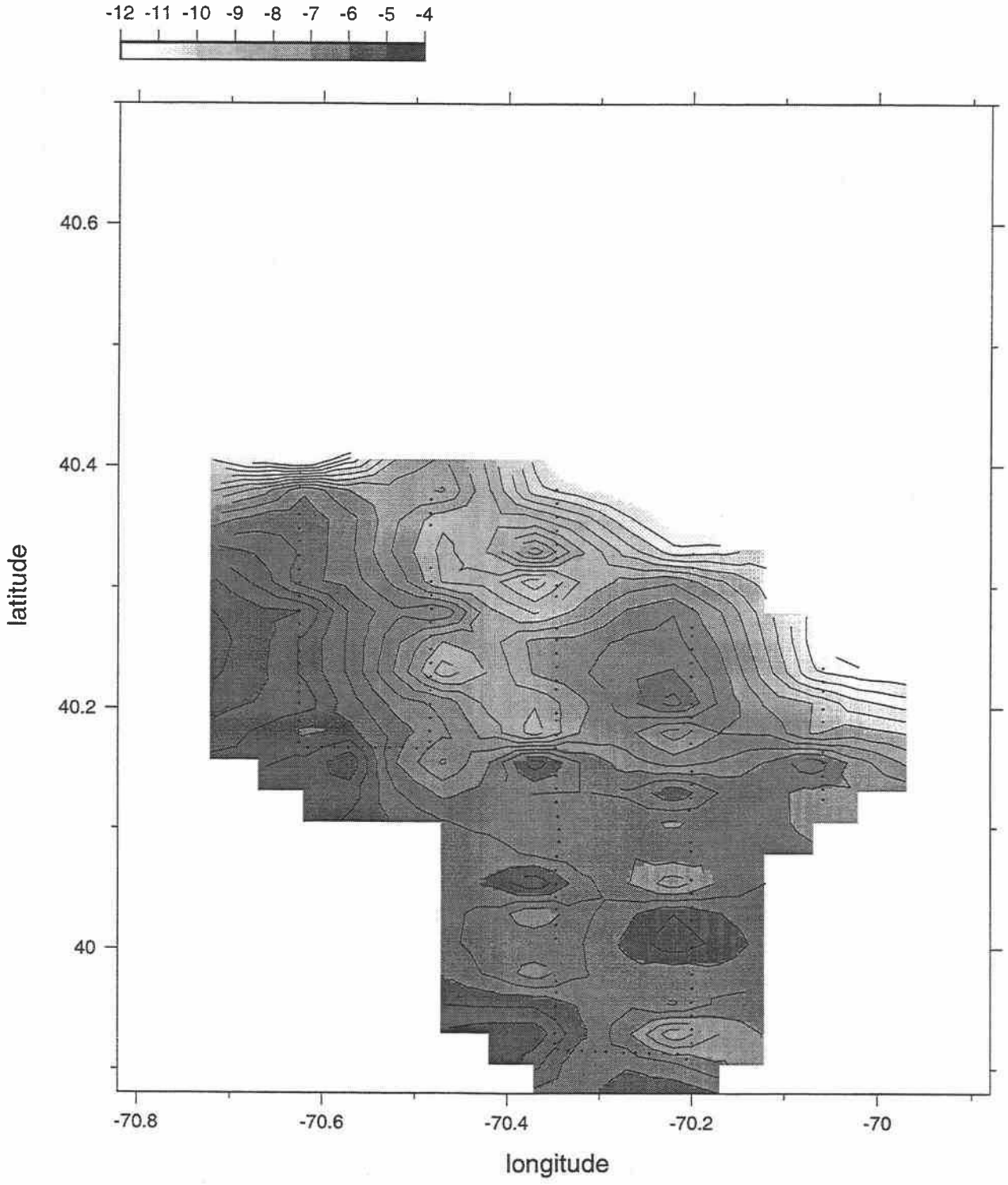
E9608 Big Box 1
17-Aug-96 02:09:20 - 18-Aug-96 09:07:04
Map View at 75 dbar
$log_{10}(\chi_\Theta)$, ($^oC^2/sec$)
-12 -11 -10 -9 -8 -7 -6 -5 -4
40.6
40.4
40.2
40
latitude
-70.8
-70.6
-70.4
-70.2
-70
longitude

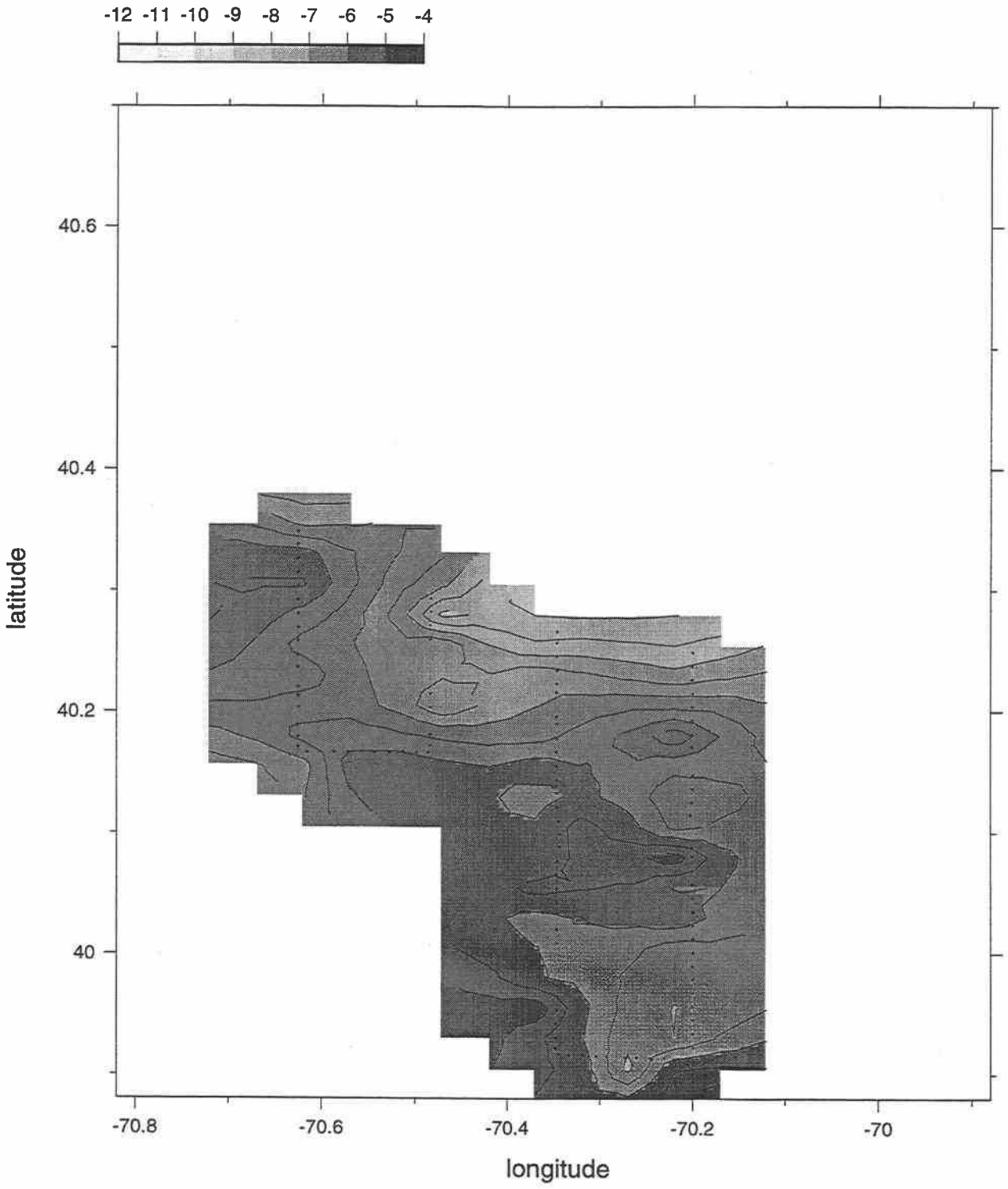
E9608 Big Box 1
17-Aug-96 02:09:20 - 18-Aug-96 09:07:04
Map View at 85 dbar
$log_{10}(\chi_\Theta)$, ($^oC^2/sec$)
-12 -11 -10 -9 -8 -7 -6 -5 -4
40.6
40.4
40.2
40
latitude
-70.8
-70.6
-70.4
-70.2
-70
longitude

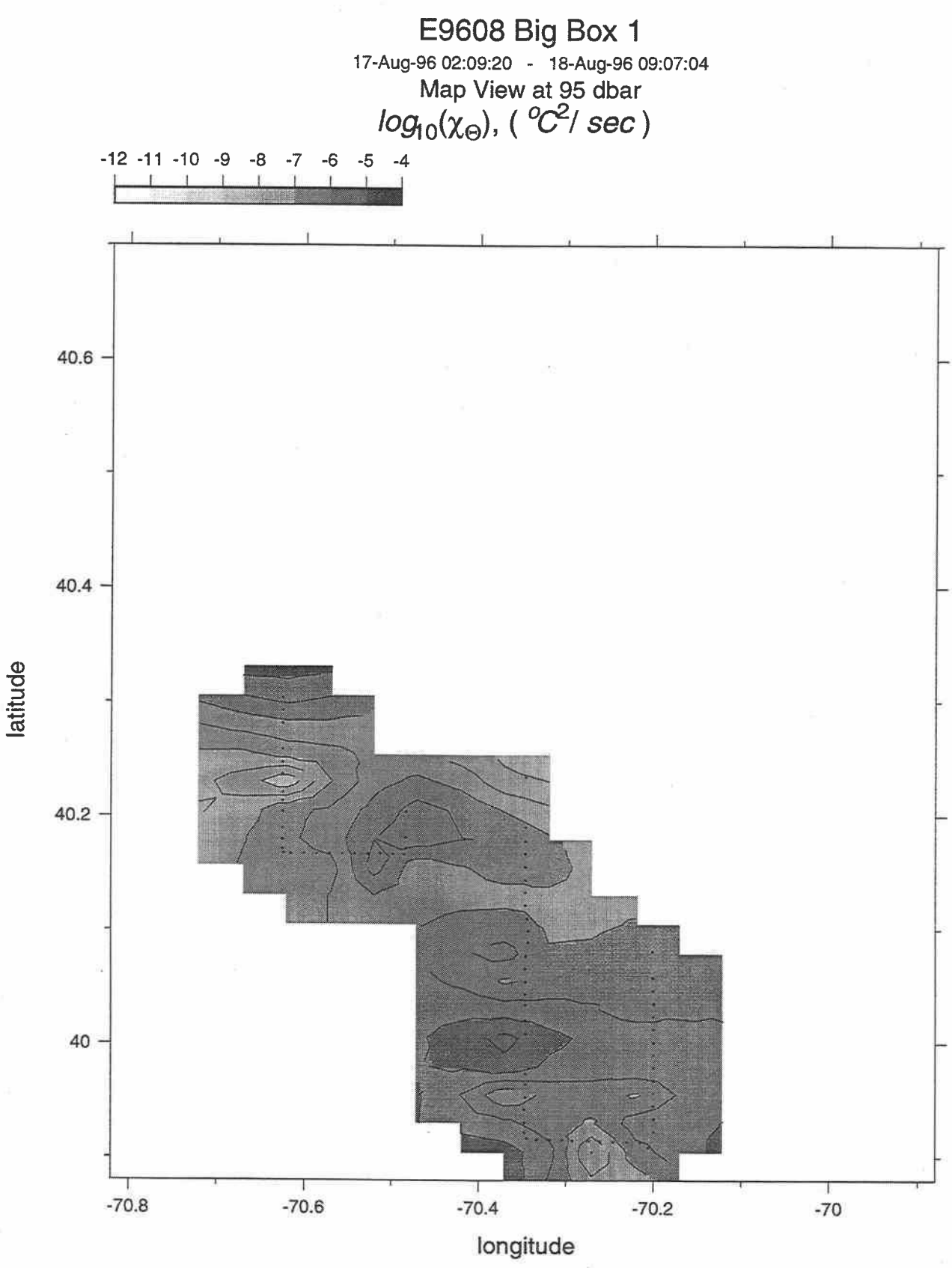
E9608 Big Box 1
17-Aug-96 02:09:20 - 18-Aug-96 09:07:04
Map View at 95 dbar
$log_{10}(\chi_\Theta)$, ($^oC^2$/ sec)
-12 -11 -10 -9 -8 -7 -6 -5 -4
40.6
40.4
40.2
40
latitude
-70.8
-70.6
-70.4
-70.2
-70
longitude

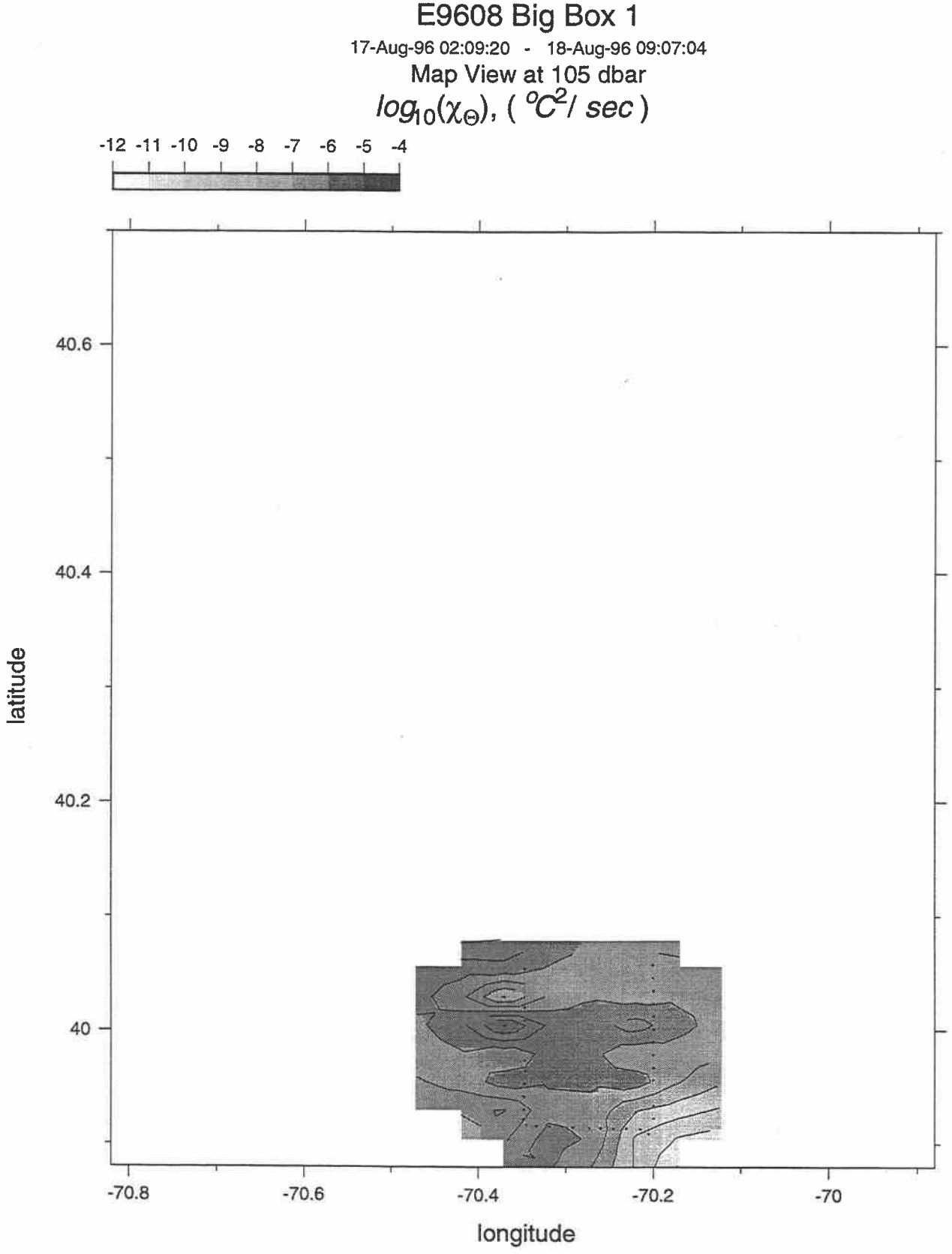
E9608 Big Box 1
17-Aug-96 02:09:20 - 18-Aug-96 09:07:04
Map View at 105 dbar
$log_{10}(\chi_\Theta)$, ($^oC^2/sec$)
-12 -11 -10 -9 -8 -7 -6 -5 -4
40.6
40.4
40.2
40
latitude
-70.8
-70.6
-70.4
-70.2
-70
longitude

E9608 Big Box 1

17-Aug-96 02:09:20 - 18-Aug-96 09:07:04

Map View at 5 dbar

log_{10}(Cox)

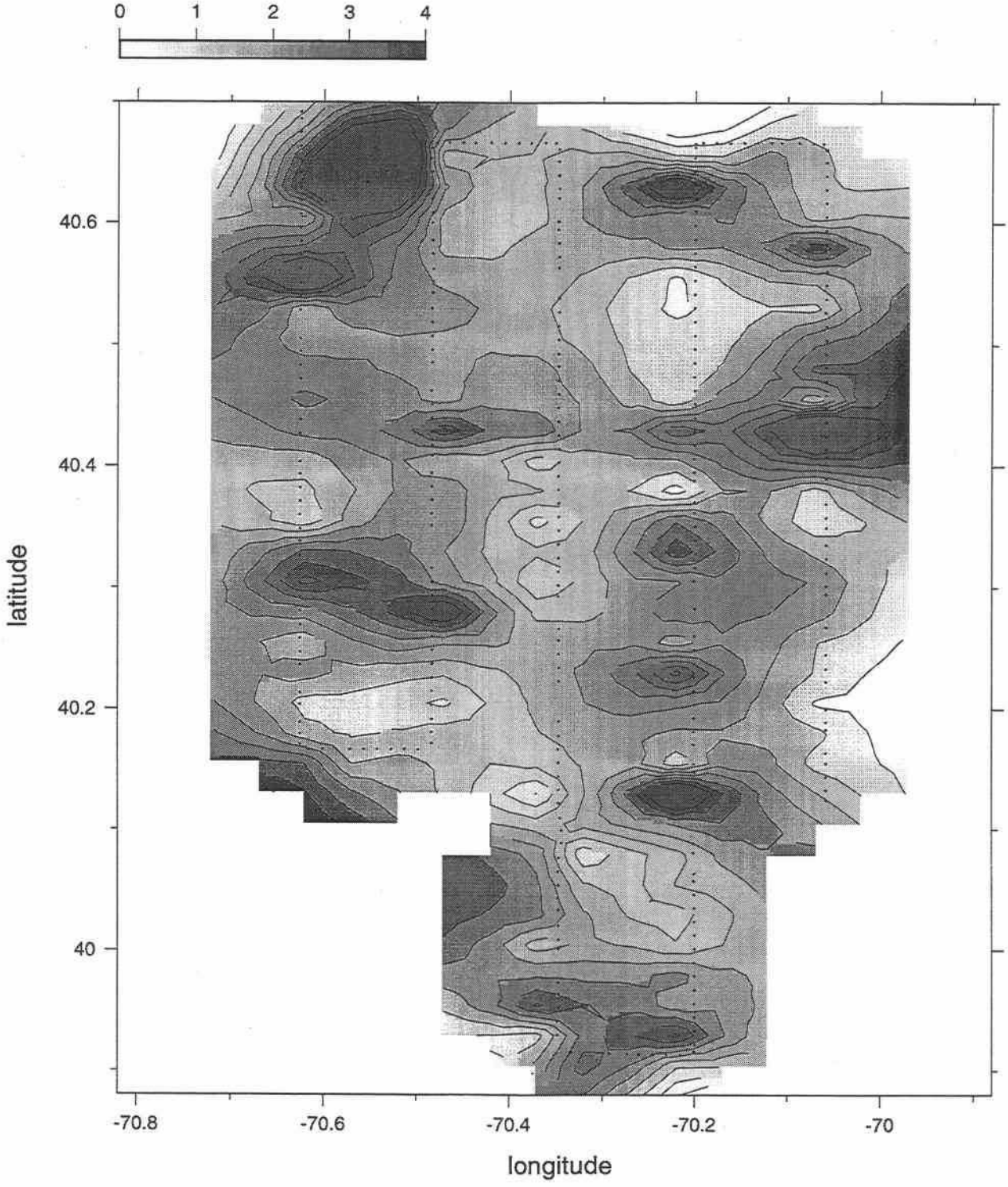

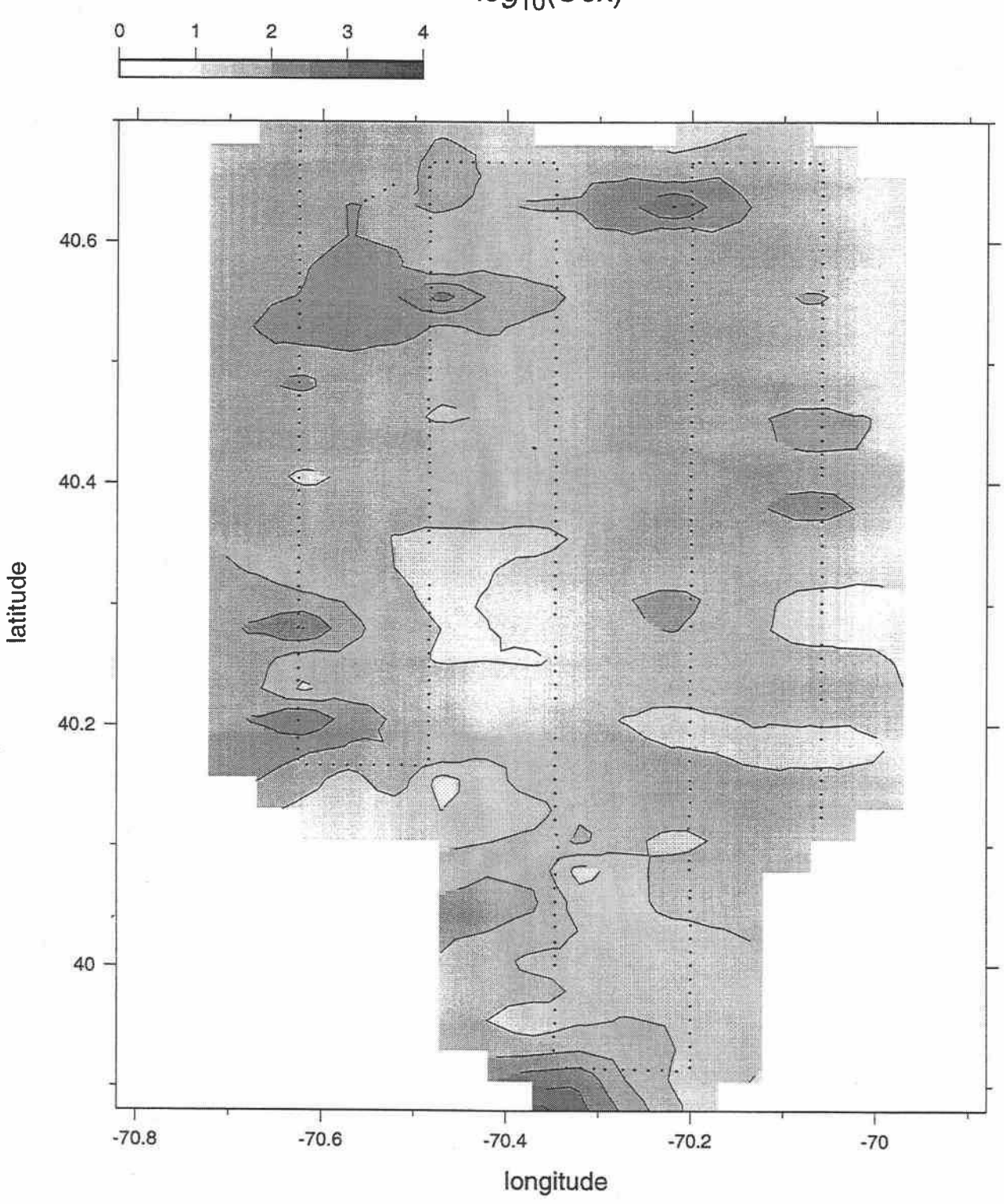
E9608 Big Box 1
17-Aug-96 02:09:20 - 18-Aug-96 09:07:04
Map View at 15 dbar
log10(Cox)
0
1
2
3
4
40.6
40.4
40.2
40
latitude
-70.8
-70.6
-70.4
-70.2
-70
longitude

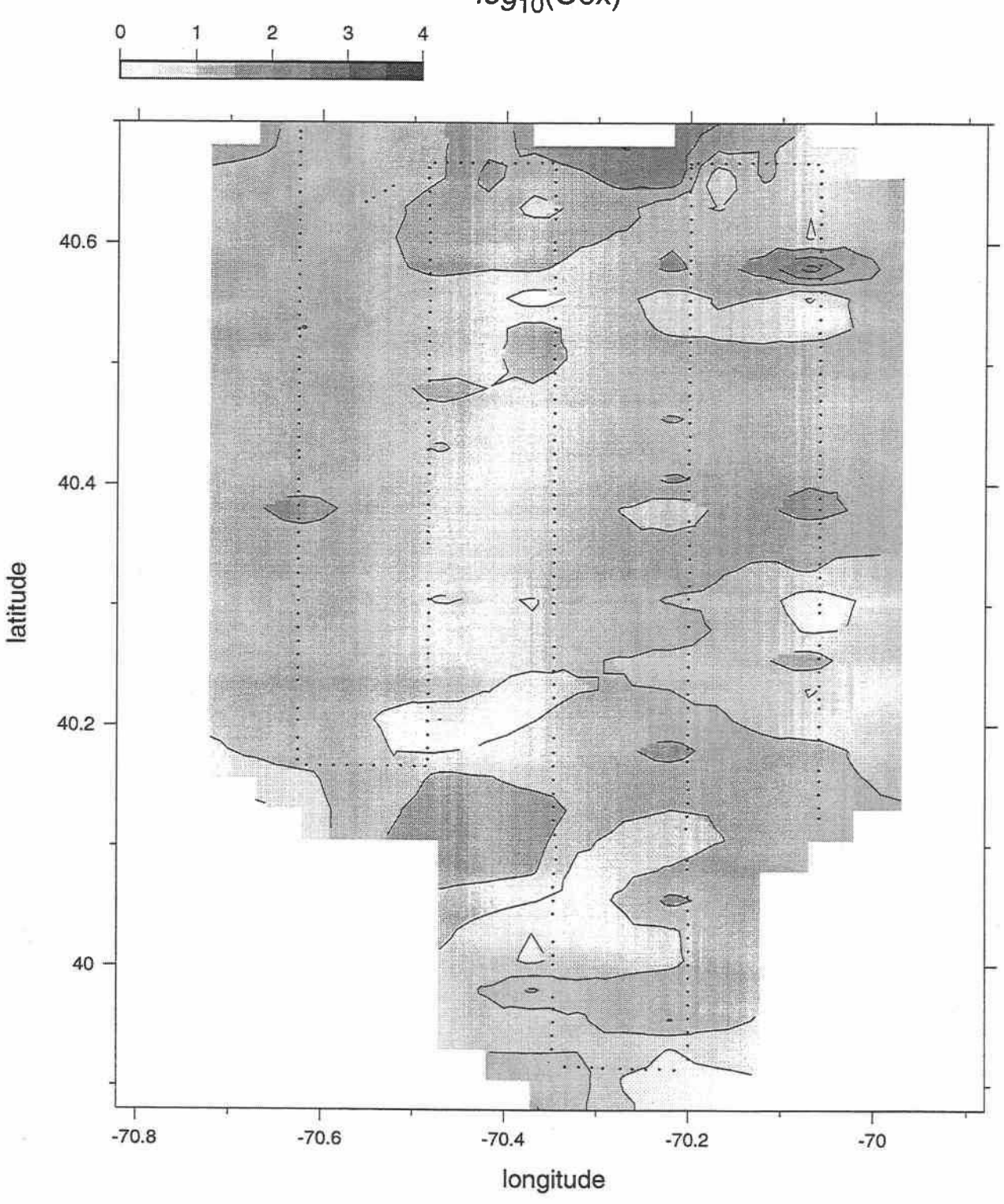
E9608 Big Box 1
17-Aug-96 02:09:20 - 18-Aug-96 09:07:04
Map View at 25 dbar
log10(Cox)
0
1
2
3
4
40.6
40.4
40.2
40
latitude
-70.8
-70.6
-70.4
-70.2
-70
longitude

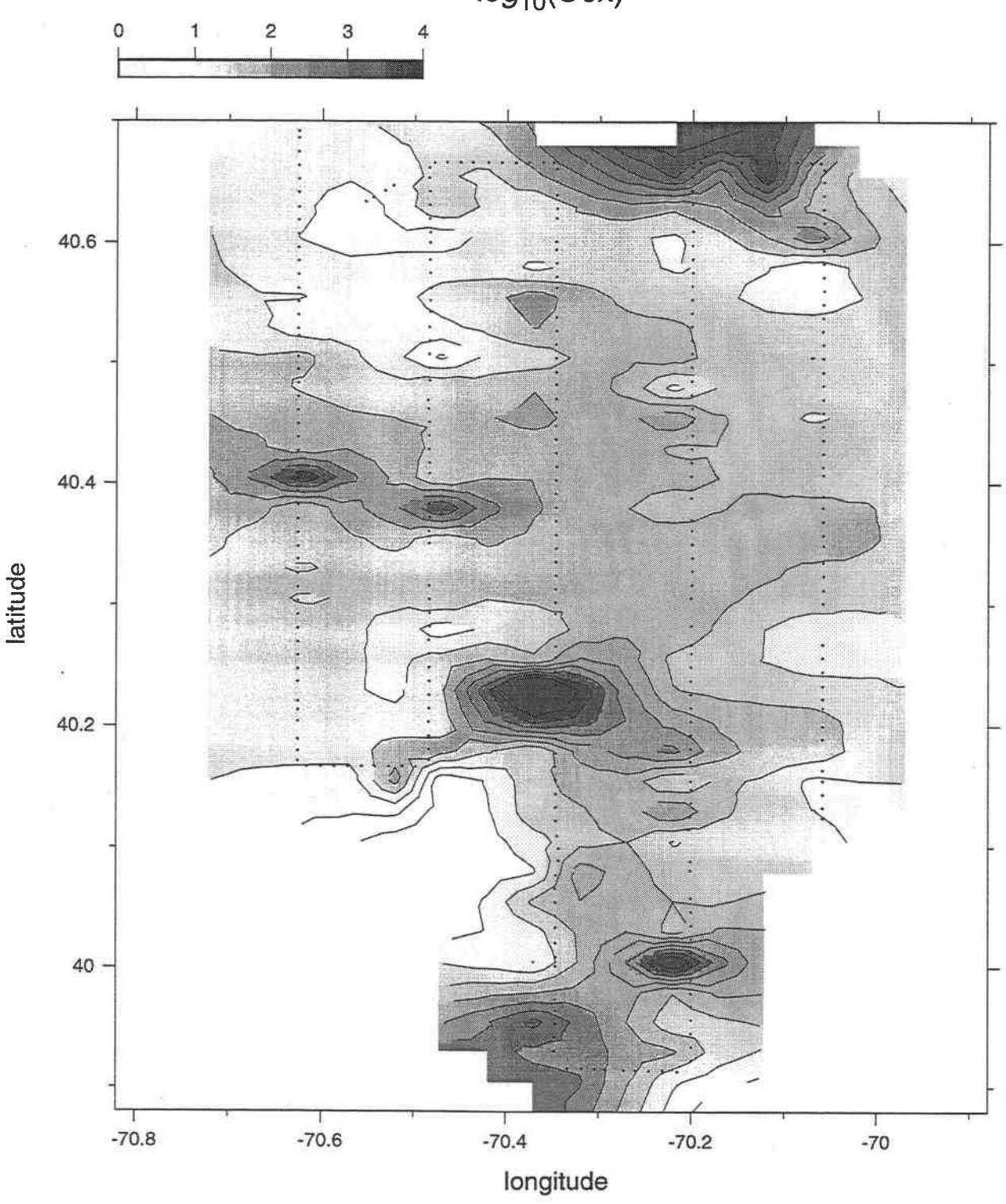
E9608 Big Box 1
17-Aug-96 02:09:20 - 18-Aug-96 09:07:04
Map View at 35 dbar
log10(Cox)
0
1
2
3
4
40.6
40.4
40.2
40
latitude
-70.8
-70.6
-70.4
-70.2
-70
longitude

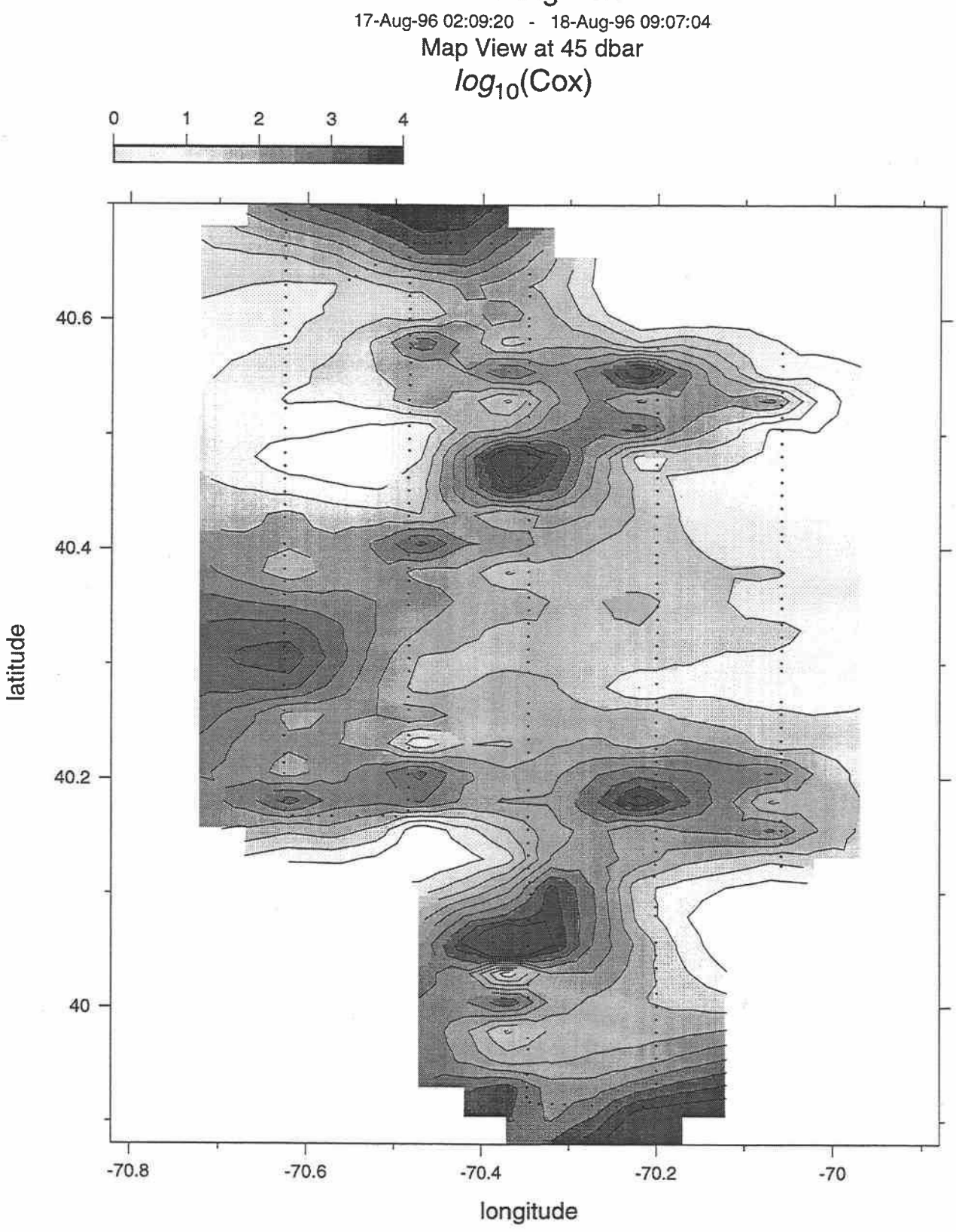
E9608 Big Box 1
17-Aug-96 02:09:20 - 18-Aug-96 09:07:04
Map View at 45 dbar
log_{10}(Cox)
0
1
2
3
4
40.6
40.4
40.2
40
latitude
-70.8
-70.6
-70.4
-70.2
-70
longitude

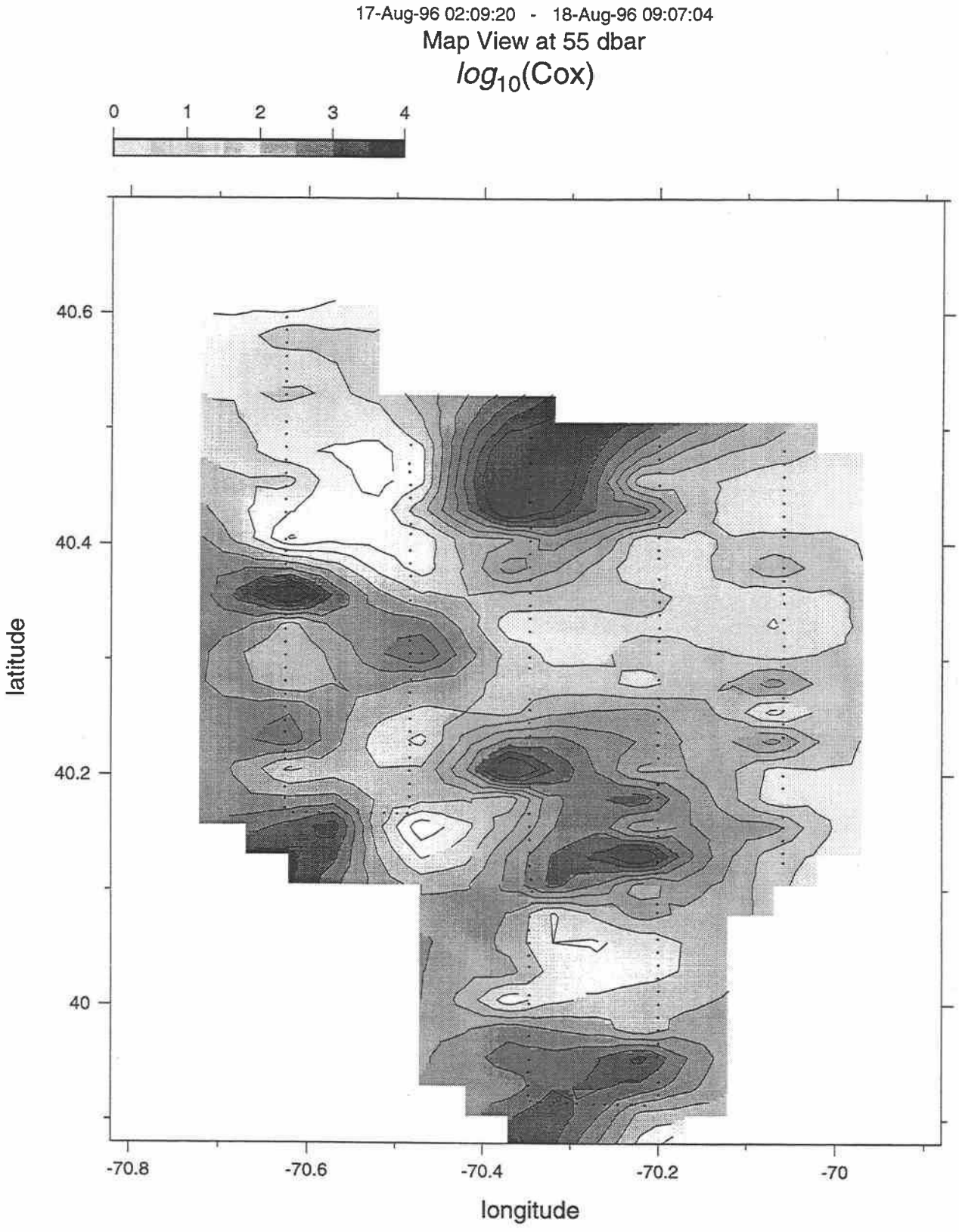
E9608 Big Box 1
17-Aug-96 02:09:20 - 18-Aug-96 09:07:04
Map View at 55 dbar
log_{10}(Cox)
0
1
2
3
4
40.6
40.4
40.2
40
latitude
-70.8
-70.6
-70.4
-70.2
-70
longitude

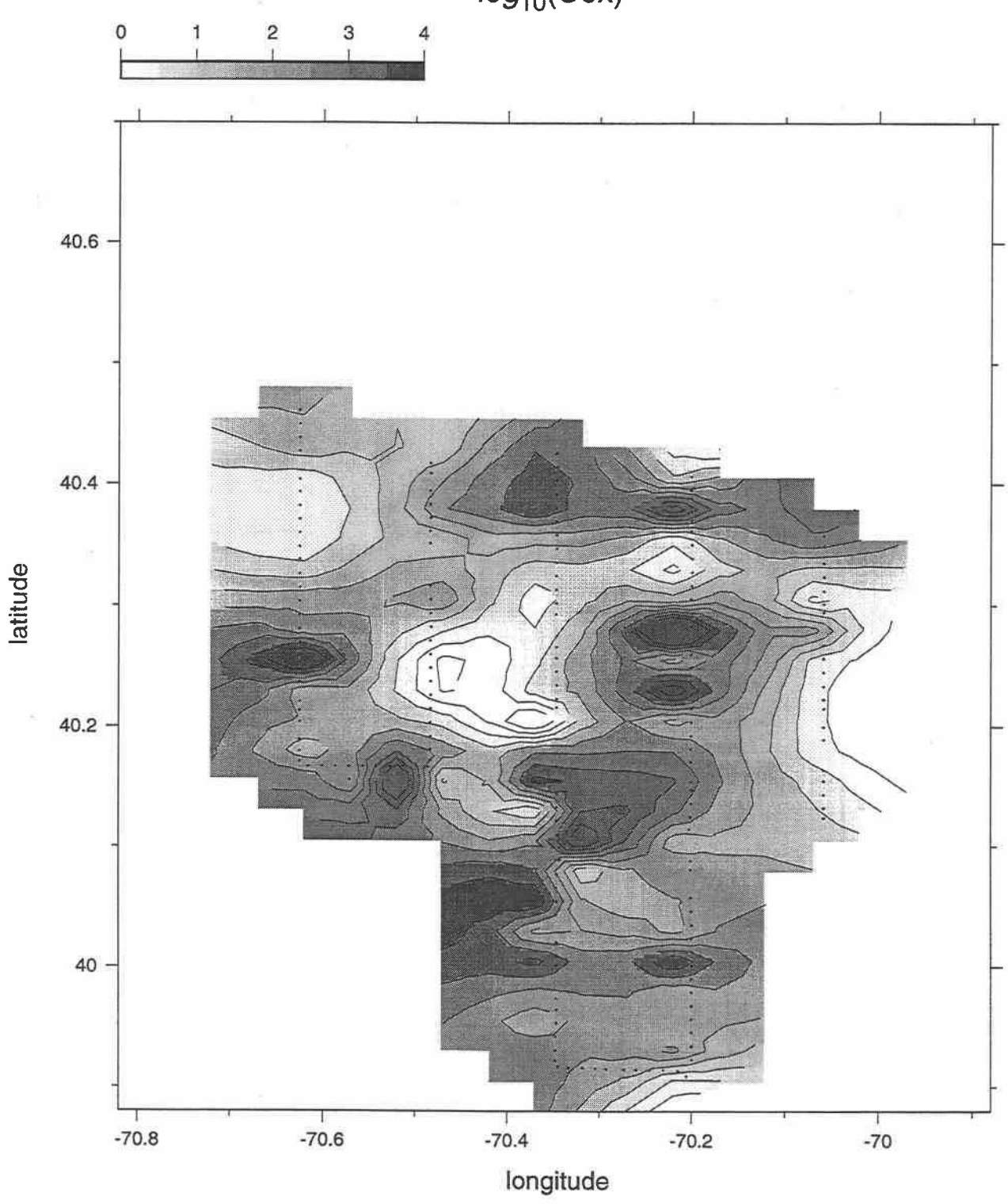
E9608 Big Box 1
17-Aug-96 02:09:20 - 18-Aug-96 09:07:04
Map View at 65 dbar
log_{10}(Cox)
0
1
2
3
4
40.6
40.4
40.2
40
latitude
-70.8
-70.6
-70.4
-70.2
-70
longitude

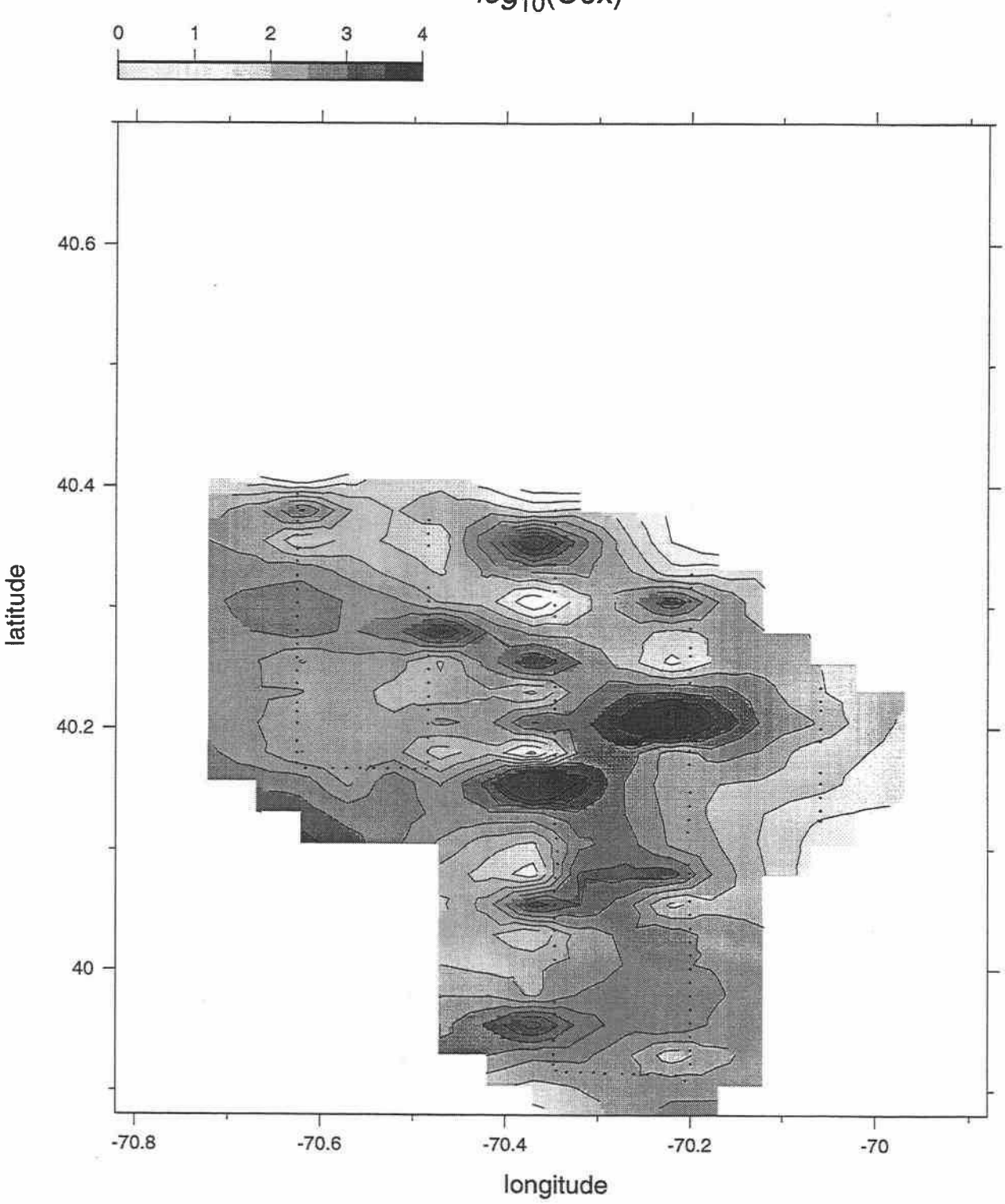
E9608 Big Box 1
17-Aug-96 02:09:20 - 18-Aug-96 09:07:04
Map View at 75 dbar
log10(Cox)
0
1
2
3
4
40.6
40.4
40.2
40
latitude
-70.8
-70.6
-70.4
-70.2
-70
longitude

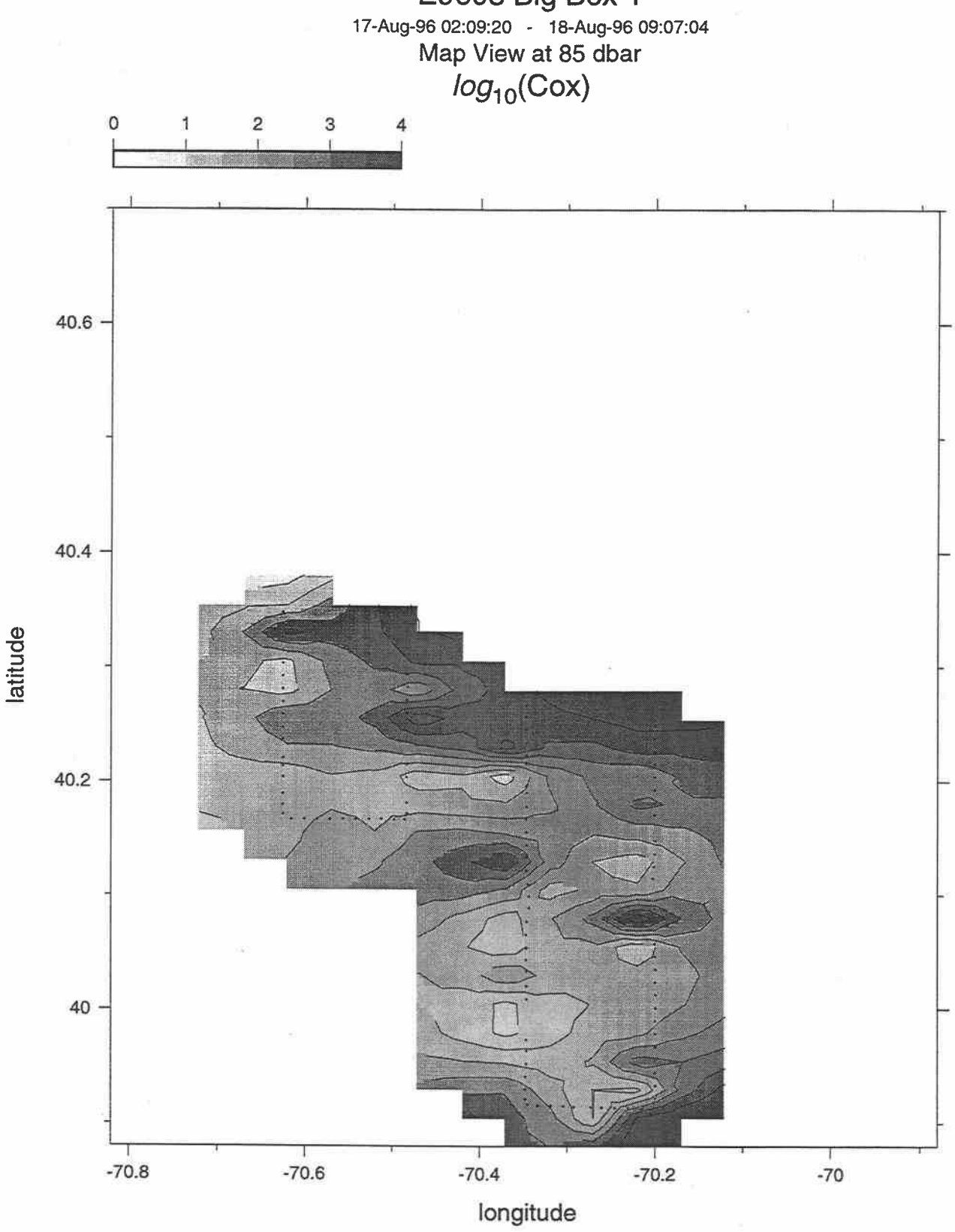
E9608 Big Box 1
17-Aug-96 02:09:20 - 18-Aug-96 09:07:04
Map View at 85 dbar
log10(Cox)
0
1
2
3
4
40.6
40.4
40.2
40
latitude
-70.8
-70.6
-70.4
-70.2
-70
longitude

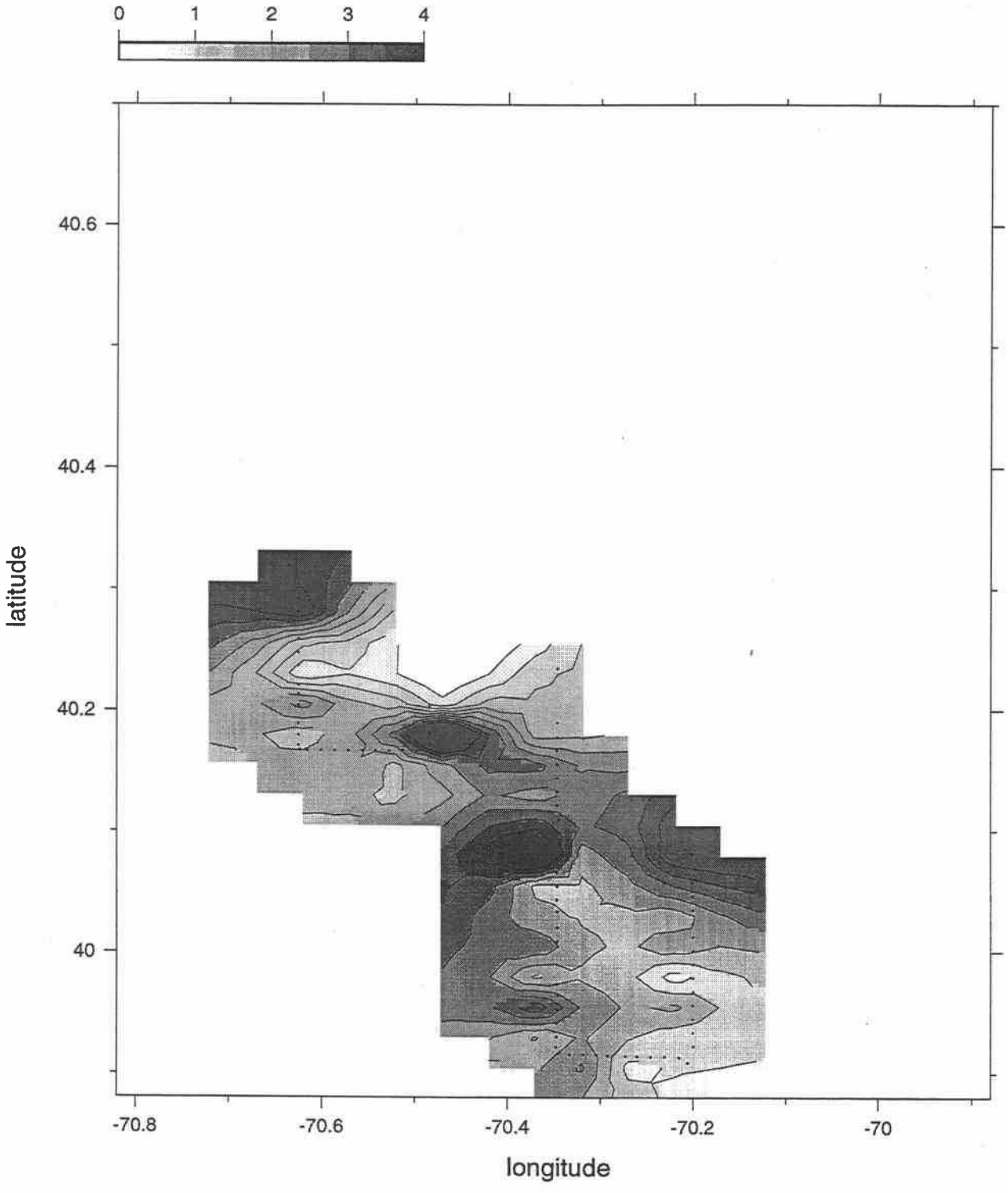
E9608 Big Box 1
17-Aug-96 02:09:20 - 18-Aug-96 09:07:04
Map View at 95 dbar
log_{10}(Cox)
0
1
2
3
4
40.6
40.4
40.2
40
latitude
-70.8
-70.6
-70.4
-70.2
-70
longitude

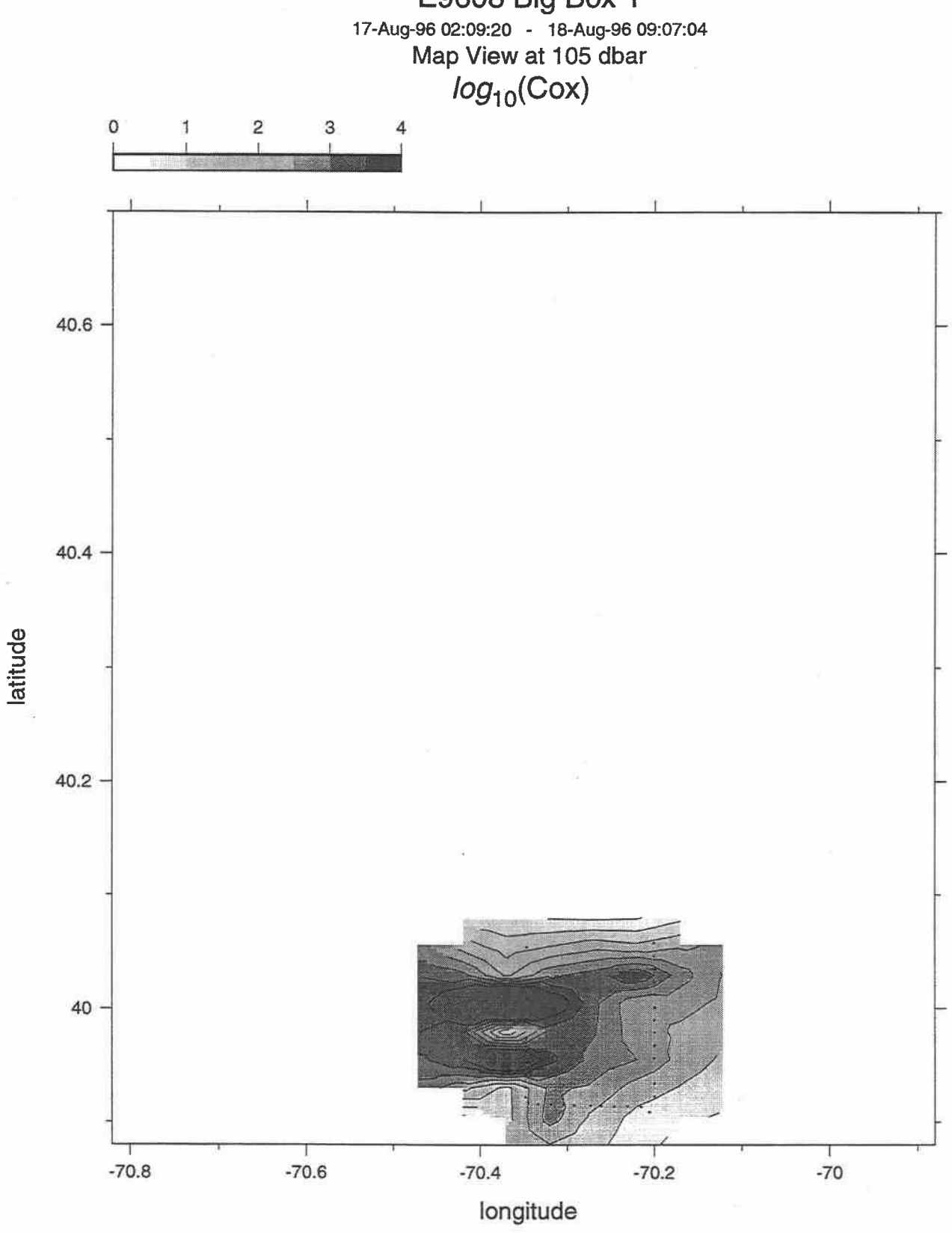
E9608 Big Box 1
17-Aug-96 02:09:20 - 18-Aug-96 09:07:04
Map View at 105 dbar
log10(Cox)
0
1
2
3
4
40.6
40.4
40.2
40
latitude
-70.8
-70.6
-70.4
-70.2
-70
longitude

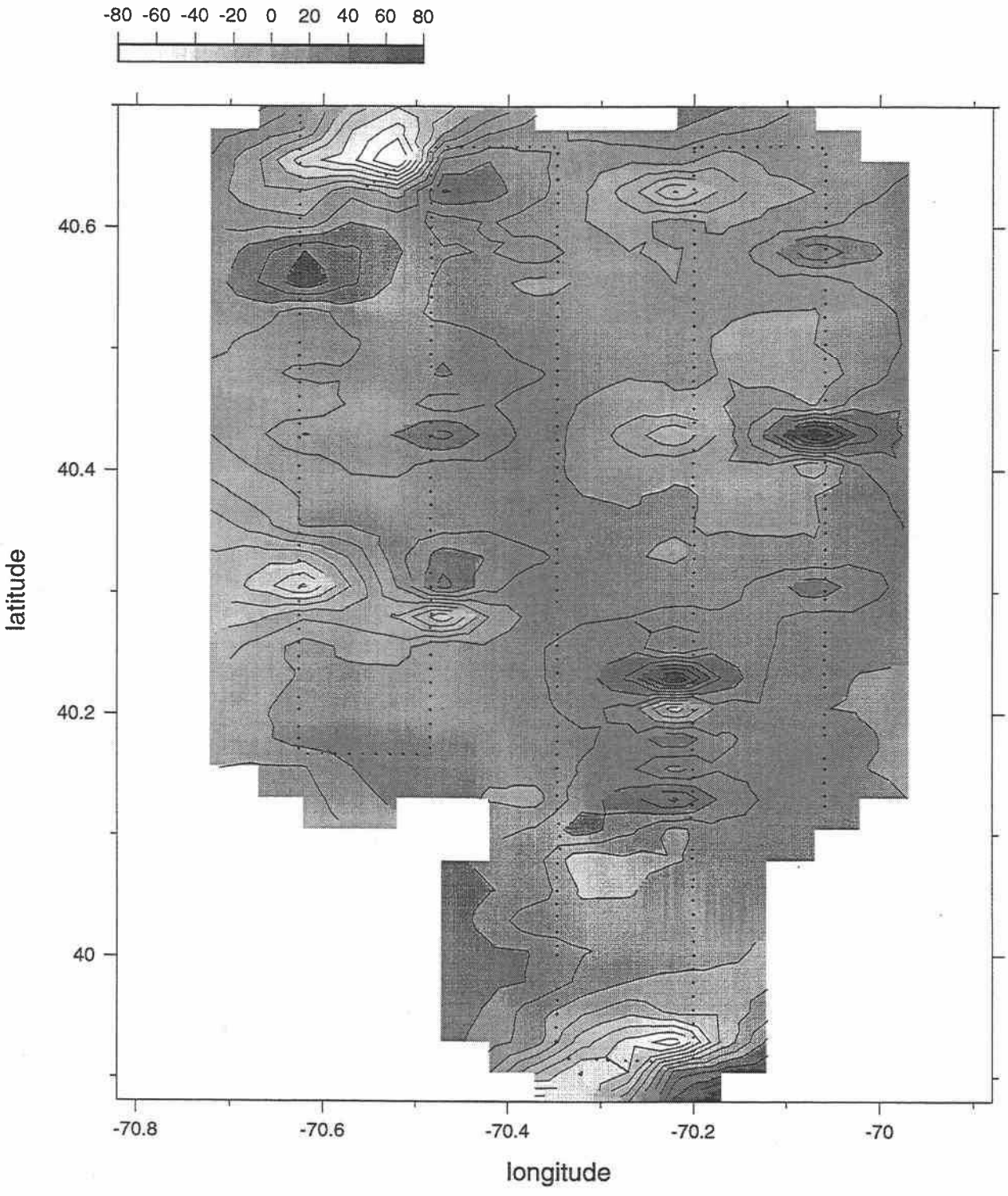
E9608 Big Box 1
17-Aug-96 02:09:20 - 18-Aug-96 09:07:04
Map View at 5 dbar
Heat Flux, (w/m^2)
-80 -60 -40 -20 0 20 40 60 80
40.6
40.4
40.2
40
latitude
-70.8
-70.6
-70.4
-70.2
-70
longitude

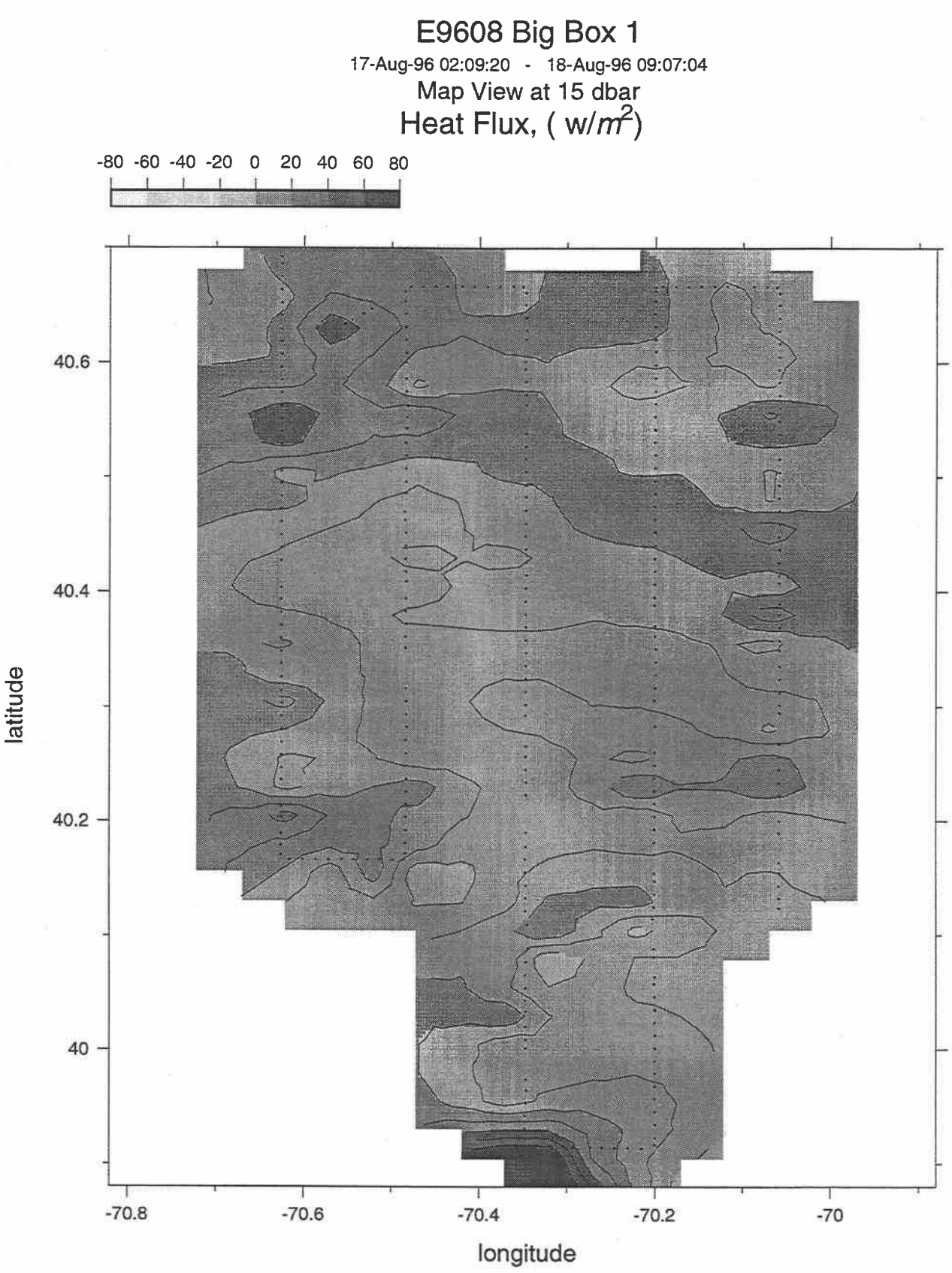
E9608 Big Box 1
17-Aug-96 02:09:20 - 18-Aug-96 09:07:04
Map View at 15 dbar
Heat Flux, (w/m^2)
-80 -60 -40 -20 0 20 40 60 80
40.6
40.4
40.2
40
latitude
-70.8
-70.6
-70.4
-70.2
-70
longitude

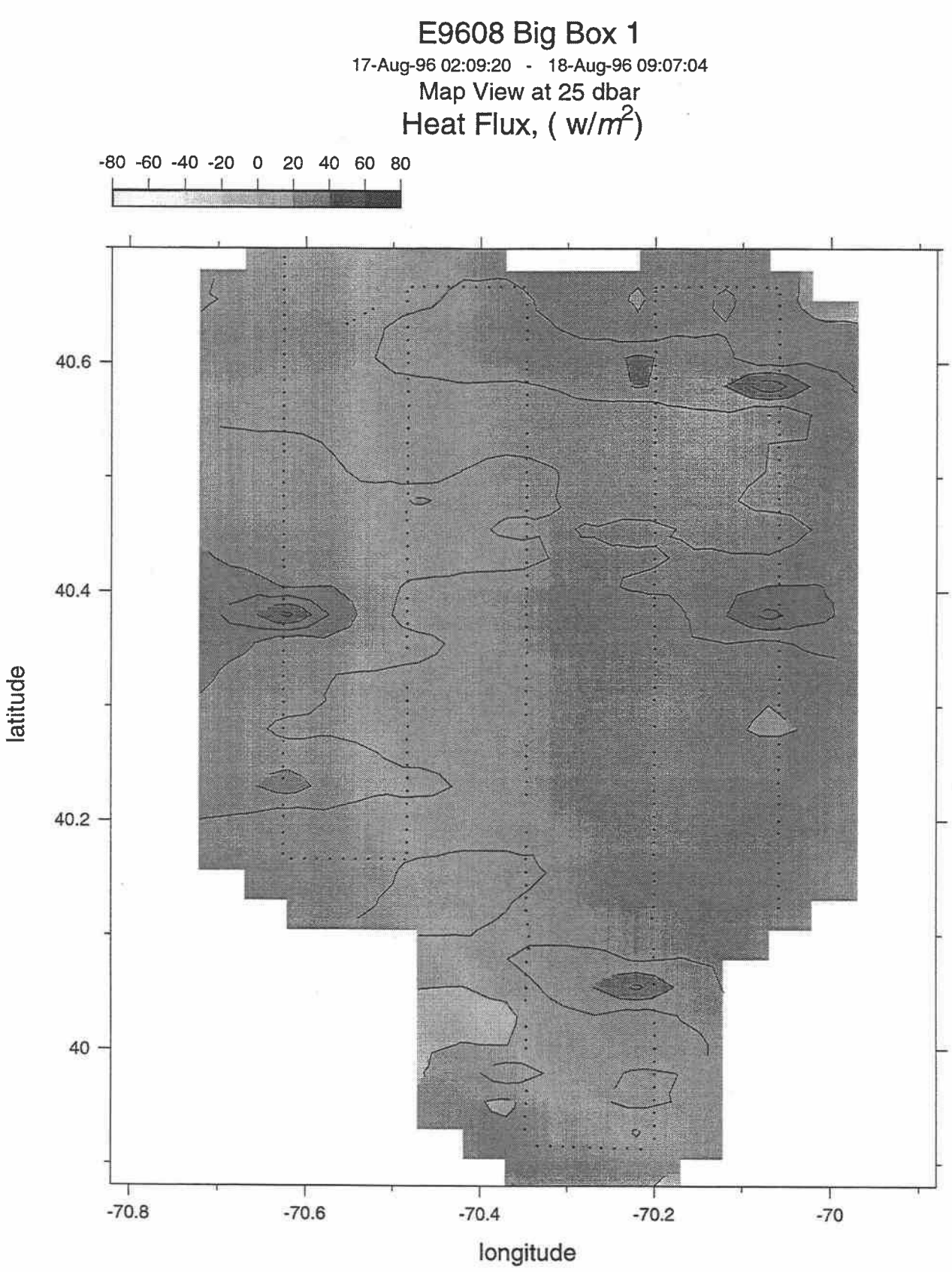
E9608 Big Box 1
17-Aug-96 02:09:20 - 18-Aug-96 09:07:04
Map View at 25 dbar
Heat Flux, (w/m^2)
-80 -60 -40 -20 0 20 40 60 80
40.6
40.4
40.2
40
latitude
-70.8
-70.6
-70.4
-70.2
-70
longitude

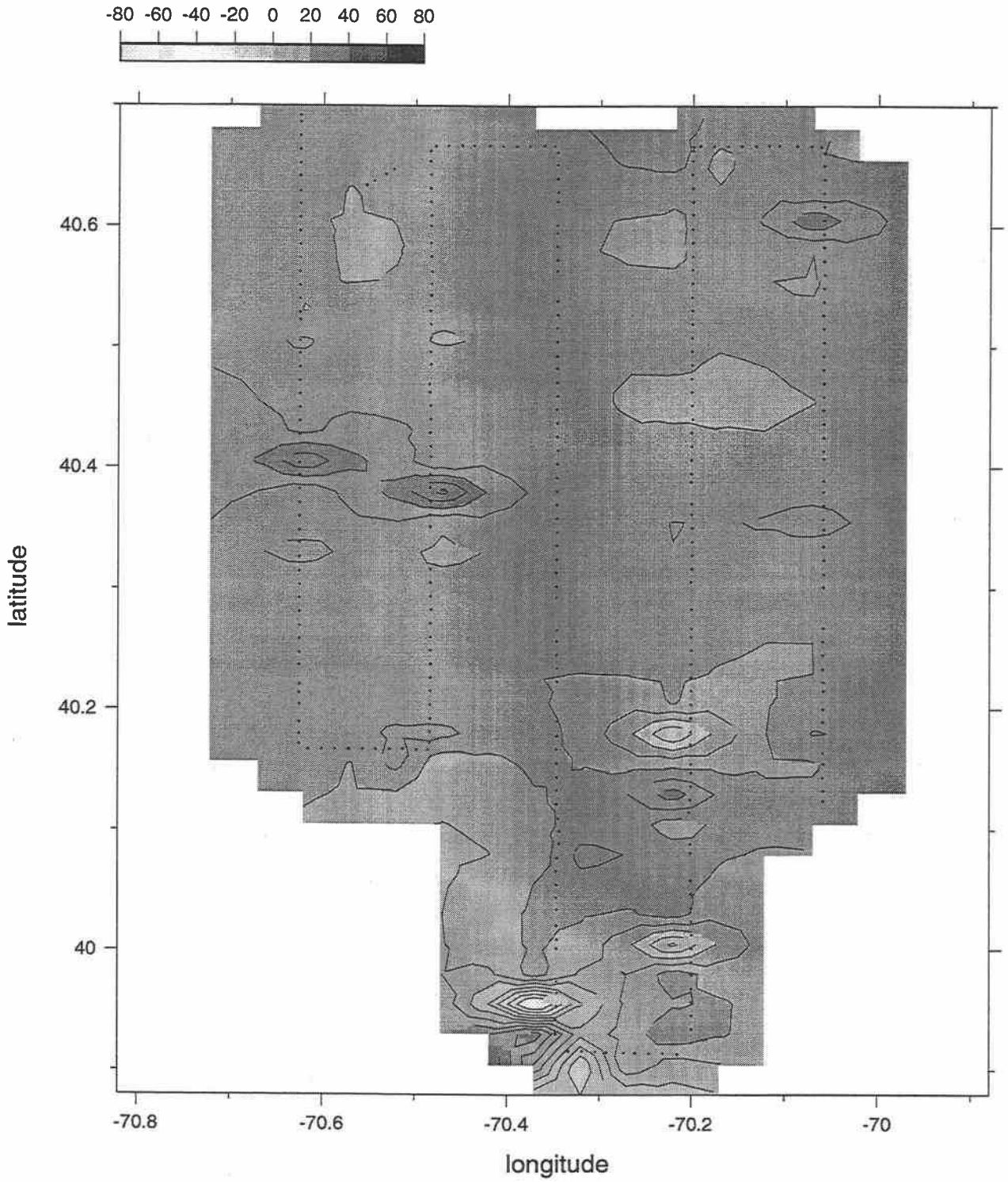
E9608 Big Box 1
17-Aug-96 02:09:20 - 18-Aug-96 09:07:04
Map View at 35 dbar
Heat Flux, (w/m^2)
-80 -60 -40 -20 0 20 40 60 80
40.6
40.4
40.2
40
latitude
-70.8
-70.6
-70.4
-70.2
-70
longitude

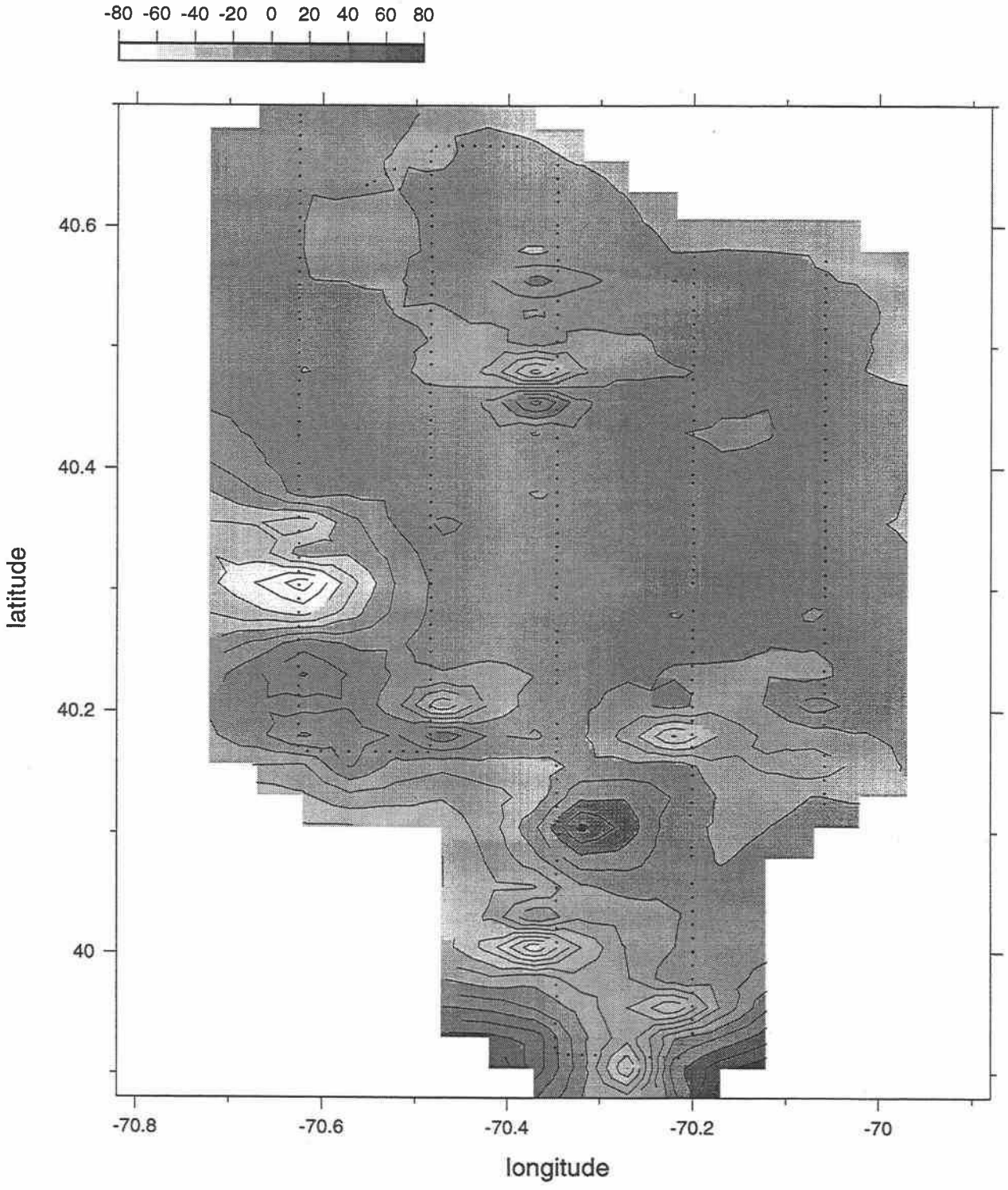
E9608 Big Box 1
17-Aug-96 02:09:20 - 18-Aug-96 09:07:04
Map View at 45 dbar
Heat Flux, (w/m^2)
-80 -60 -40 -20 0 20 40 60 80
40.6
40.4
40.2
40
latitude
-70.8
-70.6
-70.4
-70.2
-70
longitude

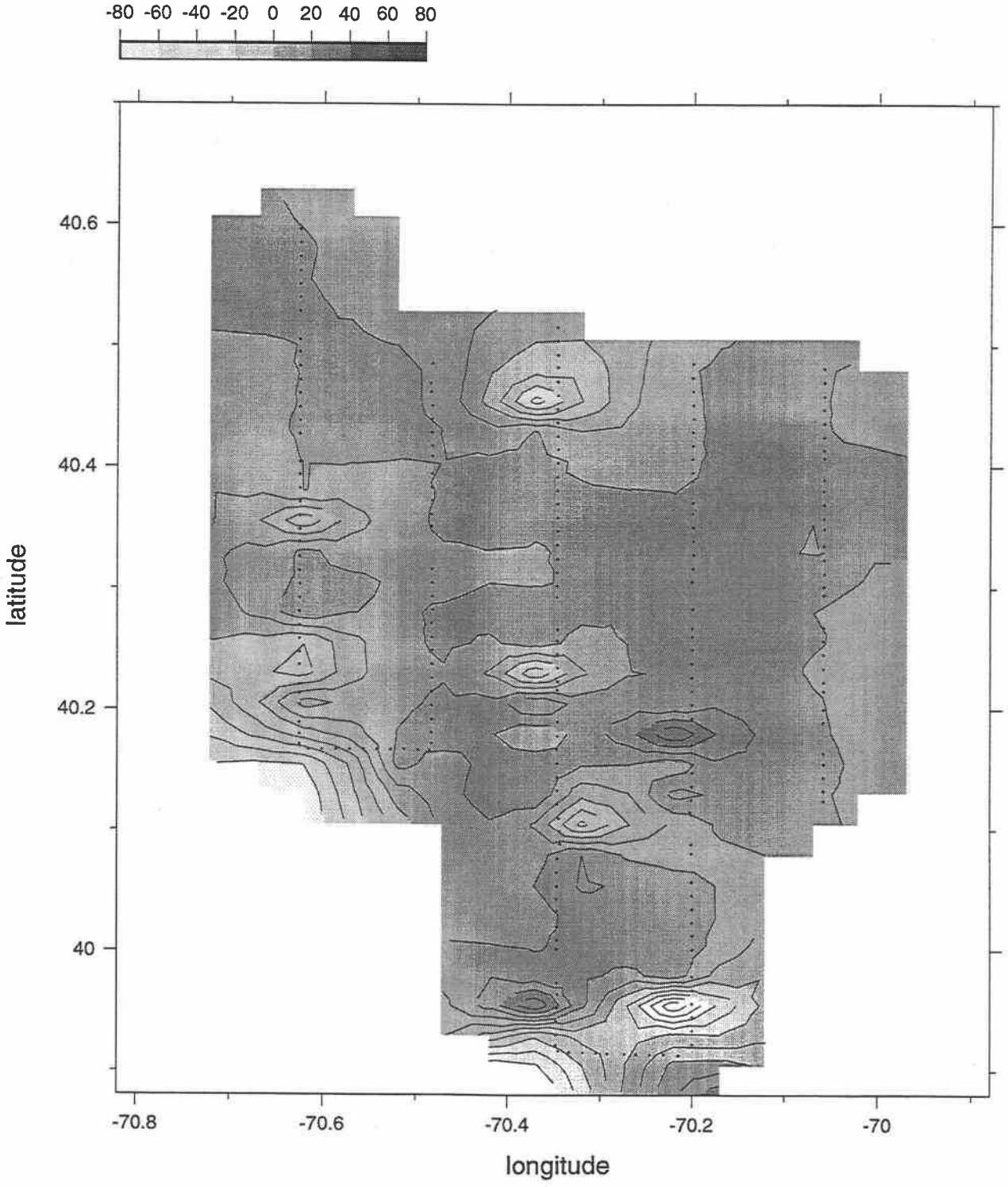
E9608 Big Box 1
17-Aug-96 02:09:20 - 18-Aug-96 09:07:04
Map View at 55 dbar
Heat Flux, (w/m^2)
-80 -60 -40 -20 0 20 40 60 80
40.6
40.4
40.2
40
latitude
-70.8
-70.6
-70.4
-70.2
-70
longitude

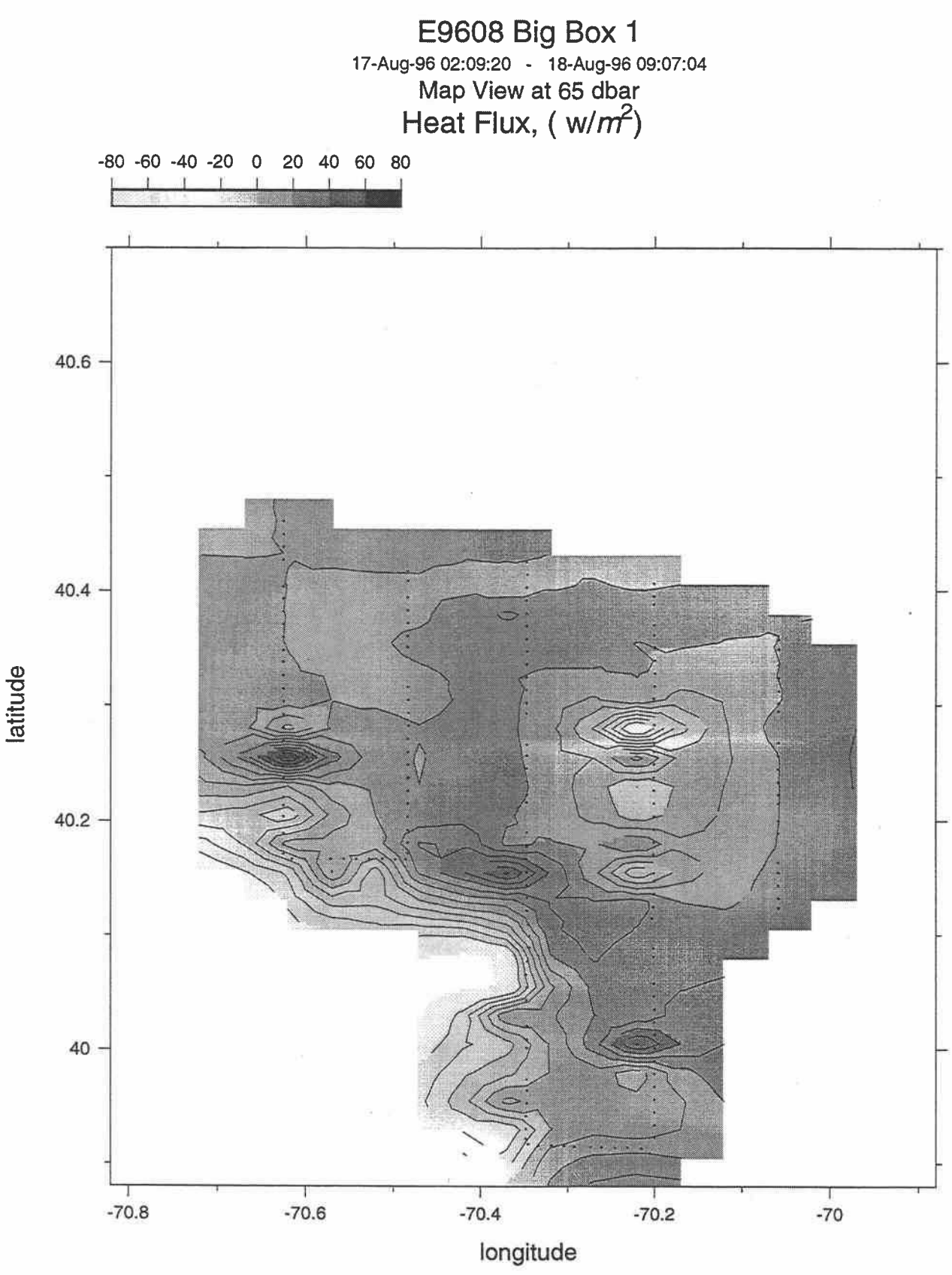
E9608 Big Box 1
17-Aug-96 02:09:20 - 18-Aug-96 09:07:04
Map View at 65 dbar
Heat Flux, (w/m^2)
-80 -60 -40 -20 0 20 40 60 80
40.6
40.4
40.2
40
latitude
-70.8
-70.6
-70.4
-70.2
-70
longitude

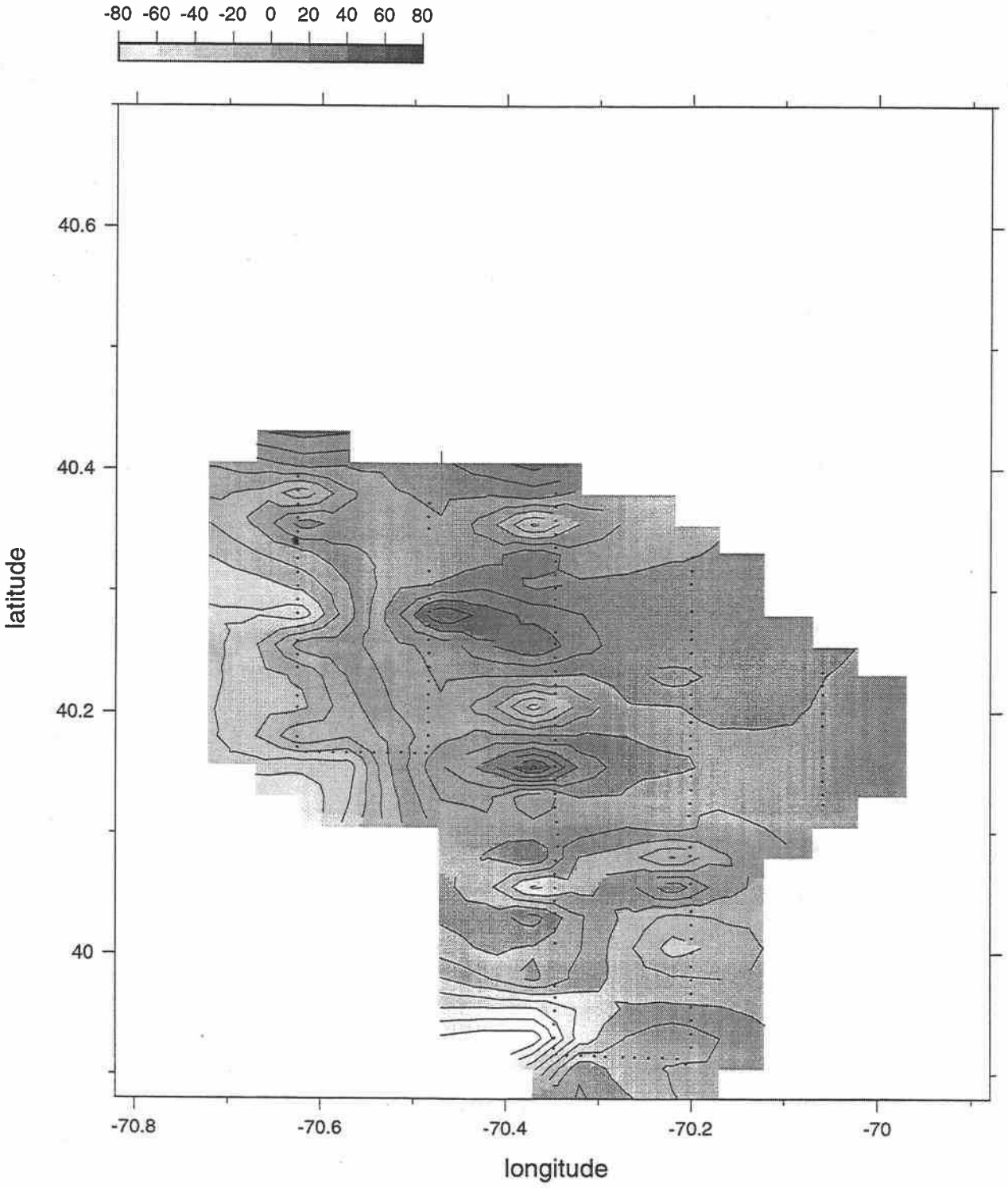
E9608 Big Box 1
17-Aug-96 02:09:20 - 18-Aug-96 09:07:04
Map View at 75 dbar
Heat Flux, (w/m2)
-80 -60 -40 -20 0 20 40 60 80
40.6
40.4
40.2
40
latitude
-70.8
-70.6
-70.4
-70.2
-70
longitude

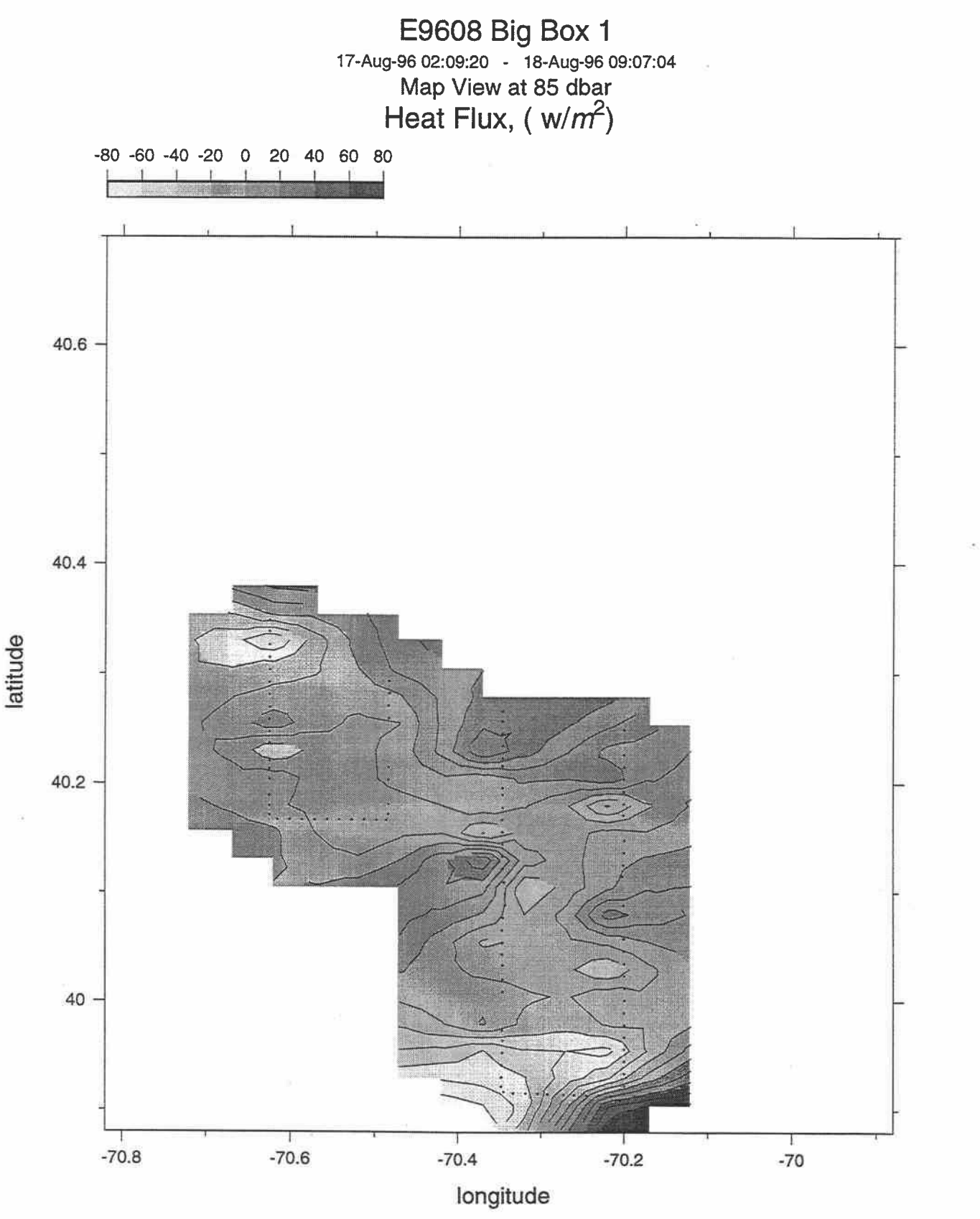
E9608 Big Box 1
17-Aug-96 02:09:20 - 18-Aug-96 09:07:04
Map View at 85 dbar
Heat Flux, (w/m^2)
-80 -60 -40 -20 0 20 40 60 80
40.6
40.4
40.2
40
latitude
-70.8
-70.6
-70.4
-70.2
-70
longitude

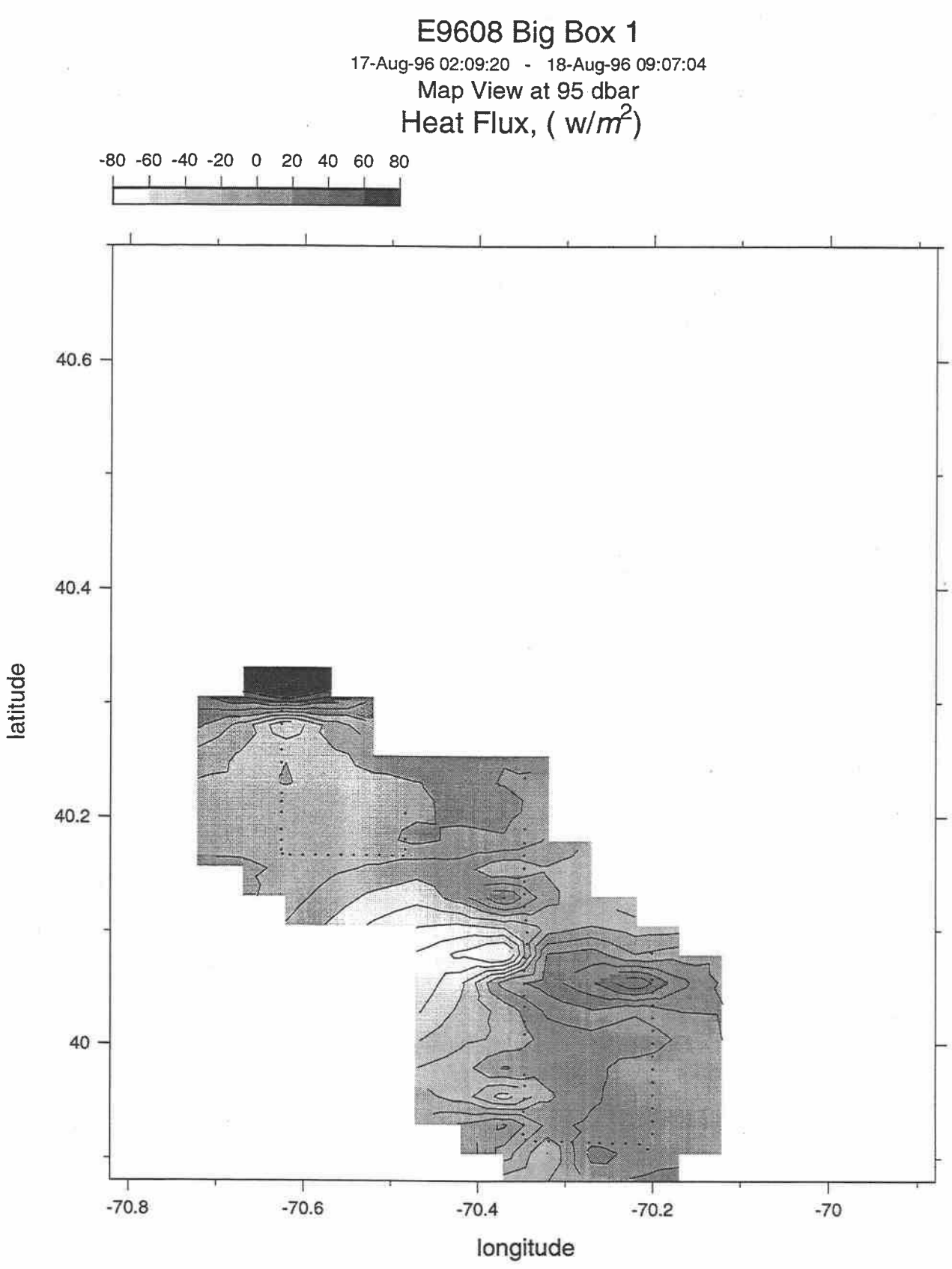
E9608 Big Box 1
17-Aug-96 02:09:20 - 18-Aug-96 09:07:04
Map View at 95 dbar
Heat Flux, (w/m^2)
-80 -60 -40 -20 0 20 40 60 80
40.6
40.4
40.2
40
latitude
-70.8
-70.6
-70.4
-70.2
-70
longitude

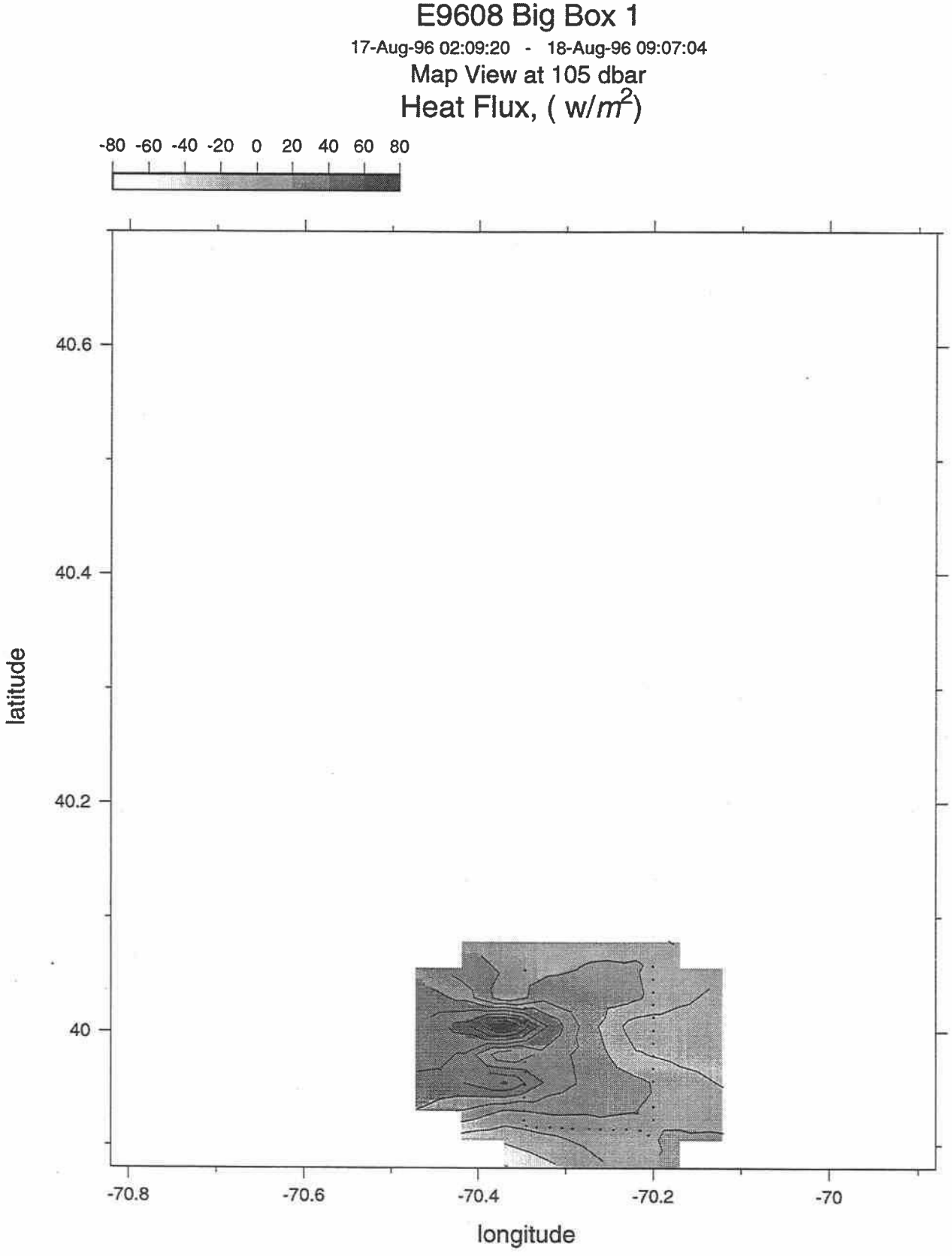
E9608 Big Box 1
17-Aug-96 02:09:20 - 18-Aug-96 09:07:04
Map View at 105 dbar
Heat Flux, (w/m^2)
-80 -60 -40 -20 0 20 40 60 80
40.6
40.4
40.2
40
latitude
-70.8
-70.6
-70.4
-70.2
-70
longitude